Surface Loop Dynamics of a Parvovirus

Nina DiPrimio

"A dissertation submitted to the faculty of the University of North Carolina at Chapel Hill in partial fulfillment of the requirements for the degree of Doctor of Philosophy in the Department of Pharmacology"

Chapel Hill
2009

Approved By:

Dr. Richard Jude Samulski

Dr. Lee Graves

Dr. Tal Kafri

Dr. Rudy Juliano

Dr. Mavis Agbandje-McKenna

ABSTRACT
Nina DiPrimio
Surface Loop Dynamics of a Parvovirus
"Under the direction of Dr. Richard Jude Samulski"

In order to understand Adeno-associated virus and its potential as a gene delivery vehicle, we are obligated to characterize virus structure-function relationships and their ability to be manipulated for efficient gene delivery. In this dissertation, multiple capsid surface loops were characterized in order to understand their roles in the virus life cycle and the potential for advancement of viral gene therapy.

Primarily, the HI loop, surrounding the five-fold pore on the capsid surface was characterized. Via domain swapping between serotypes, mutagenesis and biochemical analyses, it was determined that the HI loop is crucial for VP assembly. Specifically, a phenylalanine-proline interaction between subunits is necessary for maintaining full length VP1 incorporation into the intact particle during capsid assembly. From these studies, it was determined that the HI loop is highly plastic and certain amino acids are amenable to alteration. Therefore, the HI loop was substituted with alternative motifs including hexa-histidine. Not only did we generate vectors capable of metal ion affinity purification, but also conjugation to Ni-NTA nanogold beads for EM applications. Additionally, the hexa-histidine viruses display unique profiles *in vivo*, with tissue detargeting capabilities, modulated by altering the number of hexa-histidine tags on the surface. This alteration in

targeting may be due to capsid stability but the exact mechanism remains to be determined, however, this finding may add to the development of liver detargeting vectors for the treatment of specific genetic disorders.

Post characterization of the five-fold surface loop, interests expanded to amino acid position 265 within surface loop I between the five-fold and two-fold axes, deemed important in an alternative stage of the virus life cycle, infectivity. Upon AAV2 and AAV1 265 insertion and substitution, vectors display remarkable enhancements in liver and muscle transduction. Additionally, amino acid 265 substitution rescues infectivity of AAV2i8, a vector incapable of transducing the liver. Based on further characterization, mutation of position 265 enhances the ability of viral particles to enter cells, gaining tropism in multiple tissue types for potential use as gene therapy vectors. Therefore, the aforementioned data transcend virus biology to vectorology.

ACKNOWLEDGMENTS

Obtaining a Ph.D. is an experience like no other; something that one cannot prepare for or wrap one's head around. The best way to describe it is a rollercoaster ride, an adventure, and hopefully, if all goes well, the ride will end with excitement and you will want hop on another one just as thrilling. Graduate school is not solely about the science, but also emotional and intellectual growth. It is a way to get to know one's self, realize strengths and weaknesses, and gain confidence and most importantly, it helped me understand life's priorities.

Throughout this period of change, I was fortunate to have Dr. Richard Jude Samulski as a mentor. He allows us in the lab to agree to disagree with him and then disagree to often times find out that we were wrong. We have intellectual and scientific freedom, are allowed to work on what intrigues us, design our own experiments and progress our projects. From this, I have developed a valuable quality, independence. His scientific mentoring capabilities are astounding, and he has an ability to connect with and care for all of his "lab children" on a personal level.

Of course there are many more that are a part of this scientific family. I would not have been able to get through graduate school successfully without the support and guidance from those around me in the lab. It would not be a proper acknowledgment without mentioning three people, Dr. Mavis Agbandje-McKenna, Dr. Aravind Asokan and Julia Conway. Dr. Mavis Agbandje-McKenna, a member of my committee from afar, has been a huge support over the years, and I cannot say enough to thank her. She has been an

incredible scientific mentor and endulged my necessity for multiple therapy sessions. Aravind Asokan, sat at the desk next to me when I first joined the lab and listened to me vent and ramble and continues to do so in his new lab office. He has offered countless amounts of scientific and life related support and guidance. And Julia Conway, our undergraduate star, has aided in the completion of multiple projects and graciously lent a helping hand with constant enthusiasm.

Most importantly, I want to thank my family. To thank them like this is not enough, for there are no words, but I will give it a shot. My parents Elysa and John DiPrimio have given me unconditional love and support, supply me with some sanity in this life of insanity, believe in me and my ability to find my passions, and are proud of my achievements, no matter what they entail. My sister Olivia DiPrimio, is a beautiful, intelligent young lady, who is wise beyond her years and always there to make me smile and laugh and give me advice, from a teenager's perspective. And of course my grandparents, Herb and Lee Miller. They are strong, wise and unsurpassable in the amount of love, support, and motivation they supply. My successes are my family's successes and theirs mine. I am truly blessed.

TABLE OF CONTENTS

LIST OF TABLES

LIST OF FIGURES

LIST OF ABBREVIATIONS

AAV	Adeno-associated virus
BSA	Bovine Serum Albumin
$CaCl_2$	Calcium chloride
CBA	Chicken Beta Actin
CMV	Cytomegalovirus
CPV	Canine Parvovirus
CsCl	Cesium Chloride
DMEM	Dulbecco's Modified Eagles Medium
E	Elution
EDTA	Ethylenediaminetretraacetic acid
EM	Electron Microscopy
FGFR	Fetal Growth Factor Receptor
FPV	Feline Panleukopenia virus
FT	Flowthrough
GFP	Green Fluorescent Protein
HI6xHis	HI loop substituted with hexa-histidine motif
FPLC	Fast Protein Liquid Chromatography
HUVEC	Human Umbilical Vein Endothelial Cells
IFWB	Immunofluorescence Wash Buffer
IM	Intramuscular
IP	Intraperitoneal
IV	Intravascular

MEC	Myocardial endothelial cells
$MgCl_2$	Magnesium chloride
m-lam	Mouse Lamin Gene
MVM	Minute Virus of Mice
Ni	Nickel
NPC	Nonparenchymal Cells
NTA	Nitrilotriacetic acid
RLU	Relative Light Unit
RT	Room Temperature
PAGE	Polyacrylamide Gel Electrophoresis
PBS	Phosphate Buffered Saline
PC	Parenchymal Cells
PDB	Protein DataBank
PDGFR	Platelet Derived Growth Factor Receptor
PI	Post Injection/Infection
PPV	Porcine Parvovirus
q-PCR	Quantitative Polymerase Chain Reaction
SDS	Sodium Dodecyl Sulfate
TEM	Transmission Electron Microscopy
TR	Terminal Repeat
VG	Vector Genomes
VP	Viral Protein
W	Wash

CHAPTER I

Introduction

Viruses are intelligent nanoparticles completely reliant on a host for persistence but can undergo evolutionary change to outsmart obstacles in their path. Our interest in viruses spans many genres. We study them to defeat them in the case of those causing disease, utilize them for vaccinations, or exploit their endogenous properties as genome containing particles to deliver payloads. In our laboratory we perform the latter, by utilizing an already known non-pathogenic virus, adeno-associated virus (AAV), as a vehicle to deliver genes of interest to a specific tissue target. In the process we aim to understand the virus life cycle in order to generate the best possible medium to accomplish the task. The following introduction will give an in depth background on AAV as a virus and a vector.

1. T=1 Isocahedral Viruses

An icosahedral virus is composed of identical protein subunits ordered in a 2-3-5 symmetry rotation pattern. The two-fold, three-fold and five-fold symmetries are located through the center of each edge, face and corner, respectively. T=1 icosahedral symmetry is generated from 60 identical viral protein subunits, T being the triangulation number or the square of the distance between two adjacent five-fold vertices. Generally, viruses are classified into four groups: helical, icosahedral, enveloped or complex. Helical viruses, like tobacco mosaic virus (21), are viruses comprised of a single protein repeatedly stacked to form a hollow tube around a central axis and are identifiable by their rod like structures. Enveloped viruses, such as influenza (129), utilize the cell lipid bilayer post budding from the infected cell as an outer shell protecting the capsid protein layer. As the virus assembles inside the host cell, matrix proteins attach themselves to the lipid bilayer and bud off the cell surface containing glycoproteins and transport channels. These viruses use their outer lipid

bilayer consisting of specific glycoproteins. When the virus enters another cell, the lipid envelope fuses with the host cell surface to deliver the capsid, making viral entry an easier process. Complex viruses (95), like bacteriophages, structurally appear to be a combination of helical and icosahedral viruses with additional features to the icosahedral head and helical tail such as protein tail fibers. These unique fibers are structures necessary for the docking of bacteriophages to a host bacterial cell and ejecting the viral genome. There are obviously a vast range of viruses with different structures, however, our focus is on a parvovirus, AAV, a T=1 icosahedral virus, which has many homologous partners, some of which have been researched for potential utilization in gene therapy.

2. Subfamily Parvovirinae genus Dependovirus

Parvoviruses are of the smallest non-enveloped viruses known, whose members include, canine parvovirus (CPV) (111, 161), minute virus of mice (MVM) (15, 78), porcine parvovirus (PPV) (109, 122), adeno-associated virus (AAV) (114, 163), feline parvovirus (FPV) (1, 99), B19 (63, 167) and many more. These viruses have a single-stranded DNA (ssDNA) genome averaging 5kb in length, which is flanked by short palindromic sequences, generating inverted terminal repeats (ITRs). Part of the Parvorinae subfamily, is the genus dependovirus, comprised only of AAV serotypes, being dependent on other viruses for genome replication. AAV2, being the main player in this family, will be discussed in more detail below.

3. Adeno-associated Virus Life Cycle

The AAV life cycle is similar to all parvovirus cell infection mechanisms, beginning with host cell recognition. AAVs interacts with the host cell via primary receptor recognition (heparan sulfate proteoglycan for AAV2) and internalizes via co-receptor interactions (integrin, FGFR and C-Met for AAV2) (5, 62, 105). The interactions between different serotypes and their specific host cell receptor accounts for the variances in tissue tropism. From what has been determined to date, AAV serotypes bind initially to a carbohydrate on the cell surface, which adds to the tropism variability since there are a wide array of carbohydrate variants on multiple tissue types. For instance, AAV1, 4, 5 and 6 have been shown to bind sialic acid (142), and receptors such as FGFR (105), PDGFR (20) and laminin (3) have been shown to play a role in the attachment of various serotypes. Primarily amino acids present at the three-fold axis of symmetry are responsible for receptor recognition (75, 94, 96, 157), which will be discussed in more detail when describing capsid structure-function relationships.

Post cellular attachment and virus internalization, are the intracellular trafficking steps (23, 25). It has been shown that AAV2 enters cells via clathrin-coated pits and blocking the endosome or changing endosomal pH inhibits AAV2 infection. Specifically for AAV2, once cell surface binding occurs, the Rac1 PI3 Kinase cascade is activated (115), which could aid in the translocation of AAV2 to the nucleus. It is not known whether the virus releases the viral genome perinuclearly, in the nucleus or the nucleolus. But recent data from our lab (59) has shown that the AAV capsid remains intact upon entry and can translocate to the nucleus and the nucleolus, and has been determined that the viral genome is

released in both of these locations, the importance of which is yet to be determined. However, this may not be the case for other serotypes, since they interact with different receptors and cell lines, which could dictate the pathway of viral infection. Our knowledge of AAV trafficking comes from studies on AAV2 and AAV5. AAV5 follows a similar infectious life cycle utilizing receptor-mediated endocytosis for cellular entry (6) and endosomal escape for nuclear translocation. There is also evidence that both AAV2 and AAV5 traffic to the trans-Golgi network (6, 98).

AAV only replicates in the presence of a helper such as adenovirus or herpesvirus as previously mentioned (33). Post infection, the Rep proteins are located in the nucleus along with the viral genome (52), then the Cap proteins are generated and detected near Rep proteins in the nucleoplasm. Replication centers have been shown to form where adenovirus helper proteins are present (147), such as E1a which activates the AAV promoters and then E1b and E4 which aid in AAV messenger RNA accumulation. When there are no factors driving AAV replication, AAV2 can persist as a latent infection (8), where it can integrate into chromosome 19 with help from the Rep protein or remain episomally (45, 103). Once replication is induced, the viral genome is packaged into the capsid in the nucleoplasm (151). However, empty capsids can assemble intracellularly in the nucleolus without the presence of viral DNA (152). It is important to note that the viral proteins cannot self assemble and are reliant on the presence of cellular factors for assembly (126).

4. AAV Genome Replication and Site-specific Integration

AAV does not contain its own replication machinery, and can only replicate in the presence of a helper virus. Being a ssDNA genome, second strand synthesis has to occur for

viral DNA replication (28). The genome is flanked by inverted terminal repeats that are 145bp in length and form T shaped hairpin structures (143). During replication a 3' duplex is formed and Rep 68 or 78 nick the hairpin, which is then unwound and extended, and refolded to form the hairpin. Generated is a duplex and a ssDNA genome both of which can serve as templates for further replication (90). The genome has the option of maintaining persistence via episomal formations or integrating into host chromosome 19 (34, 104). However, the viral genome most often remains in an episomal conformation post infection.

5. Adeno-associated Virus rep Gene and Proteins

Directly following the left hand ITR is the rep gene driven by the p5 and p19 promoters generating two transcripts that are differentially spliced at the 3' end leading to four different messages. The messages are translated to Rep78, Rep68, Rep52 and Rep40 named according to kilodalton size. Each Rep protein has a different function in the virus life cycle. Rep78 and 68 are endonucleases (49), which can cleave the AAV ITR at the designated terminal resolution site at nucleotide 124 and aid in replication and site specific integration into chromosome 19 of the human genome. Rep52 and 40 are necessary for the generation of ssDNA genomes during replication (66, 133). All Rep proteins have the ability to bind ATP and act as helicases to unwind the viral genome during packaging, additionally, they have been shown to upregulate the p40 promoter which drives cap gene expression and downregulate or inhibit p5 and p19 driven expression of the Rep proteins (93, 146).

6. Adeno-associated Virus capsid Gene and Proteins

The capsid gene is to the left of the right ITR driven by p40 promoter. The gene encodes three viral proteins from a single transcript. VP1 is the full-length transcript with its own start site, VP2 is a splice variant of VP1 with a threonine start site, and VP3 has a methionine start site internal to the VP2 start. Therefore, VP1 has a unique N-terminal extension, and VP1 and VP2 contain the VP3 amino acid sequence within them. These three viral proteins come together to assemble the intact capsid particle.

The AAV icosahedral capsid is 26nm in diameter (163), being one of the smallest viruses in nature. The capsid surrounding the viral genome is made up of three viral proteins, VP1, VP2 and VP3 in a 1:1:10 ratio. VP1 and VP2 unique N-terminal extensions remain internal to the intact capsid until triggered by a stage in the virus life cycle for externalization (71, 125). Based on the crystal structure, the viral proteins come together to form the 2-fold, 3-fold and 5-fold axes of symmetry. The 2-fold axes is the weakest part of the capsid with the lowest contact energies, and the 3-fold is the most highly interdigitated region of the capsid with the largest contact energies. Since the symmetry axes go through the capsid, from point to point, there are twenty-eight 2-fold, twenty 3-fold and twelve 5-fold axes (163).

The capsid proteins of the multiple serotypes dictate the variances in serotype functionality. Each serotype is known for its ability to transduce different tissue types based on their amino acid sequence. AAV1 infects the lung and muscle (46), AAV2 liver and neurons (51), AAV3 nothing, AAV4 heart, lung eye and astrocytes (77), AAV5 eye (80) and brain, AAV6 muscle and lung, AAV7 muscle and liver, AAV8 systemically but abundantly liver, and AAV9 systemically (169). This is all based on the fact that the amino acids in each capsid protein for each serotype recognize different receptors on various tissue types. Now

that we know that each individual serotype has unique qualities affecting their phenotypes, we can use our knowledge of the crystal structure combined with mutagenesis studies in order to discern which capsid domains on each serotype are responsible for different functionalities.

7. AAV Crystal Structures

Knowing the crystal structure for AAV2 has been extremely beneficial to the field of AAV gene therapy (163). For it has allowed us to understand the capsid topology and amino acid composition and their implications in the virus life cycle. Additionally, with the resolution of crystal structures from multiple AAV serotypes we have been able to characterize and understand specific functions of other AAV variants (McKenna unpublished, Asokan unpublished).

There are key structural elements present within the AAV capsid that all parvoviral capsids contain based on the crystal structures. One consistency is that the VP1 unique N-terminus has not been crystallized since it is present in low copy number and potentially incorporated in different amounts within each capsid or in a heterogeneous fashion. Also, the genome has not been crystallized with the capsid since it does not seem to be ordered symmetrically. Assembly of the viral protein subunits, is primarily based on hydrophobic interactions between the amino acids at the interfaces. However, it is not known how the viral protein subunits come together, whether they form trimers or pentamers first. When the VPs do assemble, a 5-fold pore is formed, twelve of which are present on the capsid and the 3-fold peaks are formed, twenty of which are present.

From the AAV2 crystal structure alone, surface loops and beta sheets have been named and assigned, and with the resolution of other serotypes and autonomous parvoviruses are seemingly conserved structural regions. In the AAV monomer, a jelly-roll beta barrel is conserved connected by long loops. The most variable parts of the monomers are the loops connecting beta strands, making up many of the unique variable surface topologies. Protruding off of the AAV capsid are the three-fold peaks, which are formed from neighboring interdigitated VP subunits. A subloop resides in the center of each loop, forming the GH loop, named from the beta strands in which the loop begins and ends. At the five-fold axis resides the HI loop, comprising amino acids 655-667, interacting with a neighboring underlying subunit at the BC and EF loops (163).

Crystal structures for AAV1 (84), 4 (38), 5 (22, 140), 6 (162) and 8 (92) have been solved and others are on the way (Dr. Mavis Agbandje-McKenna personal communication). From these structures, differences in topology have been noted. AAV1 x-ray crystallographic studies are preliminary but do show that this particle is topologically similar to AAV2. AAV4 and 5 differ the most structurally. The variation between the AAV serotypes is most likely due to the differences in amino acid sequence and structure between the surface loops. The loops are responsible for host cell interactions, receptor recognition and antigenicity (137), which will be discussed in the next section in further detail. AAV4 and 5 based on the crystal structure are missing the basic regions that are necessary for AAV2 heparan recognition, and they also differ significantly topologically in this region, resulting in blunted three-fold protrusions. Therefore, the surface loop amino acid sequence and structure differences observed in AAV4 and 5 may account for their disparate receptor recognition, and in conjunction it has been determined that these two serotypes bind sialic

acid and not heparan sulfate (117, 141, 142). Recently, co-crystals of AAV5 with sialic acid have been resolved determining that amino acids at the three-fold on the capsid surface interact with this receptor (McKenna unpublished), and similar studies have been executed for AAV2 and its primary receptor heparan sulfate proteoglycan (75, 94). However, in order to confirm that the surface loops are potentiating variances in receptor recognition between the serotypes, further co-crystallization and mutagenesis studies must be performed.

Not only are AAV4 and 5 the most variant in overall amino acid sequence and surface loop topology, but they are also extremely different from AAV2 antigenically. The known A20 antibody used to detect intact AAV2 particles via a conformational epitope does not recognize (153) AAV4 and 5 which is confirmed by the crystal structure since the variable loops that A20 recognizes in AAV2 are different structurally and sequentially than in AAV4 and 5.

The AAV8 crystal structure (92) has revealed many similarities to AAV2 in topology unlike AAV4 and 5. There are only three variable region differences in structure as compared to AAV2, whereas AAV4 and 5 had differences in all nine designated variable regions. One of which is variable region I, a surface loop spanning amino acids 263-271 (AAV8 numbering), present at the between two-fold and five-fold axes of symmetry. Variable region II, another area of disparity between AAV8 and AAV2, is the loop that generates the channel for the five-fold pore. And the last variable region between the two serotypes is the GH loop, responsible for heparan sulfate binding of the AAV2 capsid. It is known that AAV8 does not bind heparan sulfate, but it is not know which receptor it does bind, therefore there are strong implications based on the structure and sequence information

that the inability of this serotype to bind heparan leads to its ability to transduce systemically (Asokan unpublished).

8. Adeno-associated Virus Structure-function

8.1 *Two-fold axis of symmetry including proximal dead zone*

This axis of the capsid is the weakest based on amino acid interactions determined by the crystal structure (160) but has recently gained attention in multiple research studies due to a region in close proximity. The region between this axis and the five-fold has been termed the dead zone (79, 96), for it has fallen victim to multiple mutagenesis studies not affecting heparan sulfate binding, or primary receptor interactions, but virus transduction. This region covers 15% of the capsid surface and was proposed to play a role in receptor binding based on its proximity to the heparan binding site and lack of mutational toleration (79), for many of these mutants were unable to infect cells but still bound heparin. Recent cryo-EM analysis has further substantiated this fact via capsid-heparin footprint analysis, however, it is does not rule out the possibility of this region interacting with co-receptors on the cell surface (94).

One mutagenesis study demonstrated that mutation of the surface loop I within the dead zone on this axis led to increased viral transduction (79). Specifically, mutation of S267 to A or T increased transduction four-fold to nine-fold, respectively. Other mutations to the dead zone decreased virus transduction without affecting heparan binding (79). Additionally, another mutagenesis study on this surface loop on the capsid, led to non-infectious particles, or particles that were partially defective in infectivity and lacking A20 antibody recognition (156).

A recent study named this region a hot spot on the capsid (168). The authors mutated all surface tyrosine residues to phenylalanines, due to the possibility of capsid tyrosine phosphorylation leading to capsid degradation. Specifically tyrosine 730 in close proximity to the 265 surface loop (168), played a role in virus transduction upon mutagenesis. Alteration of this single amino acid led to increased virus transduction in specific tissue types and further research is being performed to determine the mechanism causing this phenotype.

Additionally, research from our lab by Dawn Bowles (unpublished) determined that 5 residues in the AAV1 capsid along this region were necessary for the increased muscle transduction as compared to AAV2. The amino acids from AAV1 were put into the AAV2 backbone, increasing AAV2 muscle transduction *in vivo* and decreasing AAV2 neutralizing antibody recognition. This mutant was deemed AAV2.5 and is currently in clinical trial for muscular dystrophy. One of the five amino acids is located at position 265 in surface loop I of the AAV1 capsid, in the dead zone, and was shown alone to potentiate an increase in viral transduction when inserted into the AAV2 capsid at the corresponding position (Bowles unpublished). **Due to the research mentioned above and the research that will be presented in Chapter IV of this dissertation, this region of the capsid is no longer the "dead zone," but a proposed hot zone that upon mutagenesis results in remarkable levels of increased virus transduction in multiple AAV backgrounds.**

8.2 *Three-fold axis of symmetry*

Over the past decade advances in resolving the crystal structures of multiple AAV serotypes has allowed (92, 97, 140, 160) the AAV community to gain further insight in AAV structural elements and their functional correlates. AAV2 being the first cloned AAV

serotype, has been the most characterized and was therefore the first AAV serotype to be crystallized. Instead of visualizing the capsid protein linearly, we are able to place approximately 530 of the amino acids three dimensionally, and begin to assess key functions of structural domains. Mutagenesis studies took place prior to understanding the capsid protein structure (156), which shed some light on amino acids that are crucial for stages in the AAV life cycle. From these experiments residues necessary for primary receptor binding were resolved and later located to the three-fold axis of symmetry (64, 96). The three-fold axis of symmetry receives a significant amount of attention in the AAV community due to the topology of this region of the capsid and its implications in AAV biology. Since the AAV2 crystal structure has been solved, it has easily been the most characterized serotype, specifically with regards to receptor recognition (3, 5, 64, 96).

At the three-fold axis of symmetry, three viral protein subunits assemble and two VPs form each protrusion, being the most interdigitated region of the capsid and completely accessible to cell surface receptors of target tissues. These three-fold peaks are located at every three-fold axis of symmetry, totaling 60 peaks on the capsid surface. Each peak contains a subloop at its center stemming from the GH loop of a single VP subunit and is located between two subloops from the neighboring VP GH loop.

Interestingly, as mentioned previously prior to resolution of the AAV2 crystal structure, it was determined that heparan sulfate proteoglycan is the primary receptor for AAV2 (128). Further mutagenesis to the capsid revealed that mutations at the three-fold axis of symmetry, specifically an alanine substitution at 585-RGNR-588 and an epitope insertion at position 591 disrupted heparin binding affinity (156). Once data aligned this region of the capsid with dictating virus tissue tropism, it was determined that the exact

heparin binding motif is comprised of positively charged amino acids at the three-fold R585-R588, R484-R487 and K532 (64). These residues form a basic patch on the surface of the three-fold, however, they lie in the valleys between the peaks, creating a perfect location for the negatively charged heparin molecule to dock itself on the AAV2 surface.

Once the AAV2 capsid docks to the cell surface utilizing the heparan sulfate binding motif, it then internalizes using co-receptors (3, 5, 62, 105). At amino acid positions 511-513 on the AAV2 capsid near the three-fold axis resides an NGR domain, which recognizes alpha5beta1 integrin coreceptor for virus internalization (5). Integrin is not the only proposed coreceptor for AAV2 but also the laminin receptor (3), thought to bind at the three-fold axis, and FGFR (105). The laminin receptor is also reported to be utilized by serotypes AAV3, 8 and 9 (3).

Not all AAV serotypes bind to the same receptors. For instance, AAV1, 5 and 6 and AAV4 bind N-linked and O-linked sialic acid, respectively (61, 142) and AAV5 PDGFR as a coreceptor (20). However, it is still not known which residues these receptors interact with on the AAV4 capsid surface, but due to the compelling amount of data on AAV2 and receptor binding and recent data on AAV5 (unpublished), it is assumed that most serotypes use the three-fold as the site for receptor binding. Interestingly, knowing that this region of the capsid is a hotspot for receptor binding, the tissue tropism of the capsid could potentially be altered by mutating this region.

For instance, Asokan et al. replaced the heparin binding residues in AAV2 with the corresponding residues from AAV8 as determined by the amino acid sequence and crystal structure, which does not bind heparan sulfate. In doing so, the AAV2 capsid with AAV8

amino acids (AAV2i8) detargeted the liver and transduced all tissues including the skeletal and heart muscle (Asokan unpublished).

With regards to AAV1 and 6 (84, 162), they are homologous in amino acid sequence, but it has been shown that AAV6 can bind heparin, even though it does not contain the basic patch seen in the AAV2 crystal structure responsible for heparin binding recognition. What AAV6 does have in this region that AAV1 does not, is a lysine at position 531 (157), where upon mutation, heparin binding capabilities are ablated. This residue lies within its own basic patch of lysines and an arginine, contributing to receptor recognition and further demonstrating this region of the capsid plays an enormous role in receptor recognition of other AAV serotypes. Interestingly, a study attempted to uncover the amino responsible for AAV1 tissue tropism and the amino acid stretch was narrowed down to approximately 100 (aa350-430) within VP3 (46) at the three-fold peaks.

In addition to receptor interaction, the AAV2 heparan binding site at the three-fold has been named as an antigenic site on the capsid based on the ability of the RXXR motif to induce T cell activation (137). Therefore, the three-fold axis and its involvement in receptor recognition and host immunity activation has been extremely important for gene therapy applications due to our ability to alter the capsid and affect tissue tropism for disease specificity. With the addition of the crystal structures from AAV1, 4, 5, 6 and 8, it has increased capsid rational mutagenesis and characterization of tropic and antigenic determinants or has shed light on previous mutagenesis studies (46, 118).

8.3 *Five-fold axis of symmetry*

The five-fold axis of symmetry has yet to be implicated in receptor recognition like the three-fold axis, but partakes in many other stages of the virus life cycle. The five-fold axis of symmetry is formed when five viral protein subunits assemble generating the pentamer. In the center of the pentamer is the five-fold pore, twelve of which are on the capsid surface. Surrounding the five-fold pore is the HI loop, extending from one viral protein subunit to the next, being the primary contacts at the five-fold axis. Both the pore and the HI loop have been implicated as key players in the AAV life cycle (10, 24, 75).

In 2000, Muzyczka's group performed gross mutagenesis on the AAV2 capsid in hopes of determining multiple regions of importance (156). In doing so, it was determined that inserting an HA tag at amino acid position 328 in the five-fold pore, ablated virus particle infectivity and vector genome packaging. However, HA tag insertion into the HI loop surrounding the five-fold pore at position 664 did not affect viral infectivity or vector genome packaging. From this study, it was not understood why the five-fold mutations affected the capsid properties, but was determined that specific changes to certain regions of the capsid can have a huge impact on stages in the life cycle.

Following this study, a more in depth investigation was performed on the role of the five-fold pore (10). Mutation of residues in conserved regions led to packaging and infectivity defects, and interestingly, the decrease in infectivity was due to an inability to expose the VP1 unique N terminal phospholipase activity. This led to the conclusion that the five-fold pore is not only important for DNA packaging, as implied by the previous study, but also in VP1 N –terminal extrusion for infectivity. Additional research from Kleinschmidt's lab, following the work on the five-fold pore, further corroborated the

importance of the five-fold pore in DNA packaging. In 2006 Bleker et al. (9) demonstrated that a specific amino acid at the pentamer interface R432, previously shown to have ablated viral packaging capabilities when mutated to an alanine (156), had increased Rep protein binding to the capsid. This further suggested the role of the five-fold axis in viral genome packaging and potential Rep protein interactions. In the case of VP1 N-terminal externalization, Kronenberg et al. has suggested the five-fold pore as the potential site for VP1 extrusion based on electron microscopy density analysis (71). Therefore the five-fold pore is an important capsid structure in viral genome packaging and infectivity.

As for the HI loop surrounding the five-fold pore, it has the potential to participate in all of the functions mentioned above. **Up until this point there has been little characterization of this region of the capsid, however, based on studies explored in this dissertation, it has been determined that this loop plays a crucial role in viral capsid assembly also affecting viral genome packaging and infectivity. This region of the capsid will be discussed further in Chapter II.**

9. AAV Gene Therapy

Advancements in the past 25years have led to the development of vectors for gene therapy, however where we are today would be impossible without the work accomplished in 1982 (114). With the cloning of AAV2, researchers have been able to utilize this virus for efficient gene delivery taken from bench top to bedside (145). AAV2, was initially cloned with the intention of understanding the viral life cycle. In turn, it was determined that this unique virus is dependent upon helper viruses such as adenovirus or herpes virus for lytic

infection. Additionally the genome of this virus can integrate into chromosome 19 site specifically, and/or remain episomally post host cell infection.

The dependency on a helper virus for viral genome replication and completion of the lytic cycle made AAV an obvious reagent for gene delivery, being able to treat patients without the fear of viral replication post delivery. In addition, AAV is a non-pathogenic virus with the capability of packaging a transgene of choice, further validating its attractiveness as a vector. The TRs flanking the ssDNA genome allows for the packaging of a desired transgene, as long as it meets the size requirements and is flanked by TRs. The ability to package a transgene is one of the utilization limitations since the virus cannot package a gene over a certain size (41). One other limitation is post viral genome entry into a cell, the ssDNA genome has to convert to a double strand in order to express the transgene. Both of these issues are currently being tackled in AAV gene therapy with the development of vectors with increased packaging size, size optimized transgenes (73), and double stranded (ds) DNA vector genomes to circumvent genome conversion (4, 57).

AAV gene therapy is in preclinical or clinical trial primarily for genetic diseases like cystic fibrosis, duchenne muscular dystrophy, hemophilia, alpha-1 antitrypsin deficiency and rheumatoid arthritis, and also for tumors, neurological disorders, ocular and cardiovascular diseases (145). These trials began due to compelling evidence that the virus could be used safely. Two large areas of interest were and are cystic fibrosis and hemophilia, both genetic disorders resulting in the inability to incorporate the cystic fibrosis transmembrane conductance regulator or produce blood clotting factors, respectively. In the case of CFTR, the CFTR DNA was packaged into an AAV2 capsid and delivered intranasally and endobronchially to patients (29). Gene transfer was accomplished with minimal side effects,

however, the duration of correction was limited and the patient immune response was stimulated, generating antibodies against the AAV2 capsid (87, 139). For Hemophilia B, the studies were also promising, displaying gene transfer post hepatic delivery, however, there seemed to be an elimination of AAV2 capsids due to a correlative decrease in vector expression (14, 89). Due to these findings, there was a research focus on the ability to generate vectors that would not be recognized by the immune system (53, 67, 76, 79, 164), understand the immunity observed in patients (Li et al. 2009 submitted) and or transduce specific cell types *in vivo* necessary for specific transgene expression.

Recently, retinal gene therapy has succeeded via supplementation of the RPE65 gene, which is mutated in congenital amaurosis leading to blindness. AAV2 carrying the RPE transgene was injected into three patients. Two to three weeks post injection the patients' vision improved significantly (81).

Along with the promising ocular studies, there have been equally promising results with neurodegenerative diseases such as Canavan's (55, 82), Parkinson's (130) and Alzheimer's (30). In the case of Canavan's disease, a neurodegenerative disease caused by a defective aspartoacyclase enzyme necessary for breaking down building blocks for myelin, much progress has been made. In 1996 the first Canavan's patient was treated and since then not only has this patient's degeneration halted, but also all patients have shown clinical improvement.

The first Parkinson's study was funded and started by Neurologix in 2005, supplying the glutamic acid decarboxylase gene, which is responsible for synthesizing gamma aminobutyric acid, an inhibitory neurotransmitter in the brain. Post treatment, patients

displayed improvement in motor function and a decrease in Parkinson's severity and brain abnormalities.

Even though there have been great advances in gene therapy there are still some reservations as to the safety and efficacy of the vector. Currently, there is a research effort to characterize the immune response to the virus capsid and/or delivered transgene. Recent reports have indicated a potential immune response to AAV2 transduced hepatocytes during Factor IX delivery for hemophilia (89). However, this response may be due to the transgene products from multiple open reading frames (Li et al. unpublished). Recently, a commentary published in Gene Therapy (44) demonstrates that it is not the capsid or transgene alone that elicits an immune response. It may be the combination of the transgene supplied and what its impact is on the immune system for it to trigger a response against capsid proteins. For instance, when targeting the TNF receptor in baboon hearts, using AAV TNFRII-Fc, myocarditis developed (83). Through multiple studies it was determined that blocking TNF prevented the development of T cells that tolerate the AAV capsid which subsequently triggered the immune response again the AAV capsid leading to myocarditis. In order to determine the cause of the immune response generated post AAV gene therapy, more work has to be done, but it is promising and researchers are getting a better feel for which transgenes and capsids to utilize for specific therapies to minimize the response, and are also considering treatments such as immunosuppressants (58).

There has been an effort to understand the amino acids responsible for T cell or antibody recognition in the host post administration. Currently, we and others are working on generating capsid mutants that will not be recognized by the immune system. Besides controlling the immune response there is a strong effort to modulate the capsid in order to

generate increased vectors for gene deliver to specific tissue types. This has been accomplished via capsid mutagenesis to find the determinants of tissue tropism (Asokan et al. unpublished) and enhanced vector transduction (Bowles et al. unpublished) and also through insertion of targeting peptides onto the capsid surface to redirect the virus to specific tissue types (35, 101, 119, 120, 154).

To date 22 clinical trials have been completed, are currently active or recruiting. Not all of the AAV serotypes are approved for clinical trial, only AAV1, AAV2, AAV6 and AAV8. Currently, AAV1 packaging the SERCA2a transgene is being used to treat heart failure and is also being used to treat Limb Girdle Muscular dystrophy (NIAMS). In this case AAV1 is used because it transduces the myocardium and the skeletal muscle more efficiently than AAV2. AAV2 and variants of AAV2 are being used in multiple clinical trials specifically involving AAV-RPE65 for Leber Congenital Amaurosis (OHSU, UMASS), AAV-CFTR for Cystic Fibrosis (UFl), AAV-NGF for Alzheimers (Ceregene) and AAV2-hFIX16 for Hemophilia (CHOP). Additional to the AAV1 heart failure trial, researchers at Imperial College London are using AAV6-SERCA2a for heart failure (http://www.clinicaltrials.gov).

10. Vector Purity for Clinical Use

As mentioned above, multiple serotypes are utilized for various clinical trials. In order to use these AAV vectors, they have to be produced in large amounts and purified properly for optimal prep cleanliness and infectivity. Currently there is no universal method for purification of all AAV serotypes, however, there are many techniques that are being

utilized for multiple serotypes and are necessary for the development of clinical vectors, which will be discussed in further detail.

The triple transfection method (159) is most commonly used while producing virus. This technique involves the triple transfection of 293 cells with a helper plasmid carrying the cap and rep genes, a TR plasmid containing the transgene (i.e. TR-CMV/CBA-luciferase) and a plasmid carrying the adenovirus helper genes for viral production as mentioned previously, pXX6-80. In addition to 293 cells transfection, insect cells are being optimized for AAV production using the baculovirus system (124, 135). Post virus harvesting from the cells there are multiple paths one can take in order to purify the vector preparation. In the case of AAV2 the preferred purification method is separating empty particles from genome containing particles via iodixanol gradient and then purification on a heparin column to remove cellular protein post gradient centrifugation (39). AAV2 can be purified on a heparin column since it binds heparan sulfate as a primary receptor however, the other AAV serotypes do not bind heparin sulfate as a primary receptor, or their primary receptors are not yet known.

Currently, most techniques for purification involve a gradient to separate empty particles from genome containing particles followed by a column for cleanup. There have been many advances in AAV purification post-production in recent years. A few researchers have put tags on the virus surface, specifically a six-histidine tag at the VP3 N-terminus (165) and also at the 3-fold loops at amino acid position 585 (68). These techniques will be expounded upon in chapter 2.

Additional to the metal affinity column purification, there have been advances in chromatography. Recently Smith et al 2008 (123) described a technique involving

polyethylene-glycol purification, anion-exchange chromatography and gel filtration. Additionally, authors report using a POROS 50HS for cation-exchange followed by anion exchange resin Q-sepharose XL (106) in order to separate empty from genome containing capsids. All techniques have their advantages and disadvantages but have yet to be expanded and applied to all serotypes and their variants. However, without these advances in purification, clinical grade vectors would not be producible.

In Chapter III of this dissertation, I will discuss my findings on the utilization of the HI loop as a potential domain for placing a hexa-histidine tag for purification of all AAV serotypes. Additionally, this tag not only aids in the universal purification of virus particles, but also a domain for nanogold particle conjugation for EM applications. Furthermore, the hexa-histidine motif can be utilized as a domain to modulate muscle and liver targeting.

In the following dissertation multiple topics will be discussed including the HI loop at the five-fold axis and its role in viral assembly, the utilization of this loop as a novel site for hexa-histidine tag incorporation and its implications, and the analysis of surface loop I in the dead zone between the two-fold and five-fold axes and its role in virus infectivity.

CHAPTER II

Surface Loop Dynamics in AAV Capsid Assembly

Abstract

The HI loop is a prominent domain on the AAV capsid surface that extends from each VP subunit overlapping the neighboring five-fold VP. Despite the highly conserved nature of the residues at the five-fold pore, the HI loops surrounding this critical region vary significantly in amino acid sequence between the AAV serotypes. In order to understand the role of this unique capsid domain, we ablated side chain interactions between the HI loop and the underlying EF loop in the neighboring VP subunit by generating a collection of deletion, insertion and substitution mutants. A mutant lacking the HI loop was unable to assemble particles while a substitution mutant (ten glycine residues) assembled particles but was unable to package viral genomes. Substitution mutants carrying corresponding regions from AAV1, AAV4, AAV5 and AAV8 yielded; a) particles with titers and infectivity identical to AAV2 (AAV2 HI1 & HI8), b) particles with decreased virus titer (one log), but normal infectivity (HI4), and c) particles that synthesized VPs but were unable to assemble into intact capsids (HI5). AAV5 HI is shorter than all other HI loops by one amino acid. Replacing the missing residue (threonine) in AAV2 HI5 resulted in a moderate particle assembly rescue. In addition, we substituted the HI loop with peptides varying in length and amino acid sequence. This region tolerated seven-amino acid peptide substitutions, unless spanning a conserved phenylalanine at amino acid position 661. Mutation of this highly conserved phenylalanine to a glycine resulted in a modest decrease in virus titer, but a substantial decrease (one log order) in infectivity. Subsequently, confocal studies revealed that AAV2 F661G is incapable of efficiently completing a key step in the infectious pathway, nuclear entry, hinting at a possible perturbation of VP1 phospholipase activity. Molecular

modeling studies with the F661G mutant suggest that disruption of interactions between F661 and an underlying P373 residue in the EF loop of the neighboring subunit might adversely affect incorporation of the VP1 subunit at the five-fold axis. Western blot analysis confirmed inefficient incorporation of full length VP1 as well as a proteolytically processed VP1 subunit that could account for the markedly reduced infectivity. This phenomenon is most likely caused by the unstable interaction between the HI loop and the neighboring subunit upon mutation of F661, leading to an exposed VP1 unique N-terminus amenable to protease digestion post viral capsid assembly. In summary, our studies show that the HI loop, while flexible in amino acid sequence, is critical for AAV capsid assembly, proper VP1 subunit incorporation, and viral genome packaging all of which implicate a potential role for this unique surface domain in viral infectivity.

Introduction

Adeno-associated virus (AAV), a 26nm nonpathogenic human parvovirus, is distinct from most viruses due to the dependence on a helper virus for productive infection (Ad or HSV) (8). In light of the rapidly growing applications of AAV as a gene therapy vector (145, 158), several efforts to understand events in the infectious pathway including host cell recognition (3, 20, 64, 105, 142), intracellular trafficking (7, 23) and uncoating (131) in the absence of helper are currently underway. Within this context, a thorough understanding of the structural correlates of the AAV capsid and how they contribute to steps during viral transduction is necessary (156). The determination of crystal structures of several AAV

serotypes (97, 140, 163) and related parvoviruses (2, 63) over the past few years has been critical in this regard.

With respect to AAV, the capsid is encoded by three overlapping viral proteins (VPs) VP1, VP2 and VP3 (112), which are incorporated into a 60 subunit capsid in a 1:1:10 ratio. VP1 has a unique N-terminus containing a phospholipase (PLA2) domain (36) and nuclear localization sequences (42, 125) thought to be necessary for endosomal escape (27) and possibly nuclear entry (138). VP2 also has an extended N-terminus (compared to VP3) that remains internal to the capsid similar to VP1 until exposed to experimental conditions involving low pH or heat (71). Although this protein has been suggested to be nonessential for viral assembly and infectivity (144) the exact role remains unknown (42). VP3 is the primary capsid protein (contained within VP1 and VP2) that constitutes the surface topology of the AAV capsid, which in turn dictates antigenicity (48, 79) and tropism (3, 5, 96). Based on crystal structures of AAV, the VP amino acids involved in forming the icosahedral five-fold (Figure 1B), three-fold (5) and two-fold symmetry interfaces have been visualized. The three-fold axis has the largest amount of buried surface area and the highest contact energy, being the most interdigitated region of the capsid (163). The surface loops at the three-fold axis of symmetry are thought to be involved in host cell receptor binding (5, 64) and has been the target of several mutagenesis studies (79, 96, 121, 156, 157). In addition, recent data has shown that a single amino acid change K531E located at the base of the three-fold loops has the ability to alter the phenotypes of multiple AAV serotypes (157) suggesting an incomplete understanding of this critical region. The two-fold axis of symmetry has the weakest amino acid interactions and the lowest contact energy, while the five-fold symmetry axis is thought to have intermediate interactions (163). As mentioned above there have been many studies

on the three-fold axis of symmetry, however, the role of surface loops that form the interactions at the five-fold and two-fold symmetry axes remains to be determined.

The pentameric assembly of VP3 subunits results in the formation of twelve pores at the five-fold axis of symmetry (Figure 1B), which have been the focus of several recent investigations. Mutagenesis of residues that constitute the pore has suggested a critical role in assembly and packaging (10, 40, 156). Therefore, it is likely that the five-fold pore is necessary for DNA packaging including Rep protein binding, capsid assembly, and VP1 N-terminus exposure. Surrounding this pore at the five-fold axis of symmetry is a prominent region of the AAV capsid - the HI loop located between the β strands βH and βI, which spans residues 653 to 669 (VP1 numbering) and extends to overlap each adjacent subunit (Figure 1). Recent data has shown that the HI loop conformationally changes upon capsid interaction with the primary receptor heparan sulfate proteoglycan (75) eluding to an important capsid conformational change for subsequent stages in the AAV life cycle. In this study, we have carried out a thorough characterization of the HI loop through deletion and substitution mutagenesis as well as a battery of biochemical assays to assess the role of this surface feature in the AAV life cycle. Our results help demonstrate the plasticity of the HI loop and implicate a potential role in viral genome packaging. Simultaneously, we identified a critical residue within the HI loop that dictates proper incorporation of VP1 in the viral capsid.

Materials and Methods

Generation of mutants

All constructs were generated in the pXR2 (108) backbone using primers and restriction sites for PCR or oligo insertion, respectively. PCR was used to generate AAV2 poly-glycine and AAV2 HI-/- mutants. PCR was performed using the Expand Long Template PCR kit from Roche. All other mutants generated were the result of enzyme digests and oligo insert ligations. Restriction sites were placed downstream and upstream of the HI loop, Sbf1 and Afe1 (pXSA), respectively. The HI loops from AAV4 and AAV5 were amplified with these restriction sites on the 5' and 3' ends, digested and inserted into the digested pXSA backbone. pXR1 and pXR8 were digested with Sbf1 and Afe1, removing the HI loop, which was then ligated into pXSA. Restriction enzyme sites were generated at amino acid position 648 (Age1) and 666 (Nhe1) surrounding the HI loop in order to insert oligos into this region. Oligos were ordered with corresponding restriction sites at the 5' and 3' ends, digested, and ligated into the digested backbone. All oligos were synthesized by Integrated DNA Technologies (www.idtdna.com). Site directed mutagenesis was also used in order to generate point mutations within the pXR2 backbone within the HI loop using the Stratagene QuikChange Site-Directed Mutagenesis kit. Primers generated are listed in Table 1.

Virus production

Virus was produced using the triple transfection method developed in our lab as described in Xiao et al. 1998 (159). Cells were transfected with pXR2 containing the capsid mutations, pXX6-80 helper plasmid, and pTR-CMV-Luciferase containing the luciferase reporter transgene flanked by terminal repeats. Cells were harvested 60hrs post transfection and purified using cesium chloride gradient density centrifugation for 5hrs at 65,000 rpm or overnight at 55,000rpm. Gradients were fractionated and virus dialyzed against 1X PBS

supplemented with calcium and magnesium. Viral titers were determined in triplicate by treating 2μl of the virus fractions with DNase, digesting the capsid with proteinase-K and loading the viral genomic DNA on to a Hybond-XL membrane (Amersham). The viral DNA was detected using a ^{32}P-labeled probe complementary to the luciferase transgene. To carry out experiments in the paper we generated over 35 capsid mutants, a subset of which were generated multiple times. For example: AAV2 HI-/- > five times; AAV2 HI4, two times; AAV2 HI5, > five times; and AAV2 F661G two times. Each mutant virus preparation was made in conjunction with control AAV2 for a transfection control and titer comparison. Representative titers and phenotypes were documented in the results.

Western dot blot, heat treatment, and western blot

Production of empty and full capsids was determined post transfection by loading 2ul of the virus fractions onto a nitrocellulose membrane in a dot blot apparatus. Membranes were blocked in 10% milk in PBS for 30mins at RT and incubated with A20 primary antibody (dilution 1:20) (153) in 2% milk for 1 hour at RT. Membranes were washed 5 times with 1X PBS and incubated with goat anti-mouse horseradish peroxidase-conjugated secondary antibody (Pierce dilution 1:5000) for 30mins. The membranes were washed as described above, and capsid production was visualized using the SuperSignal West Femto Maximum Sensitivity Substrate chemiluminescence kit from Pierce. To examine VP1 exposure, capsids were heat treated at a range of temperatures (Results) and blotted onto a nitrocellulose membrane through a dot blot apparatus. The membrane was incubated as described above except A1 (1:20) and B1 (1:20) (153) primary antibodies were used to detect VP1 exposure and capsid viral protein dissociation upon heat treatment, respectively. For

western blotting approximately 1E10 dialyzed vg containing particles were mixed with NuPAGE LDS sample buffer (Invitrogen), run on a NuPAGE gel (Invitrogen), transferred to a nitrocellulose membrane (Invitrogen) and blotted as described above. Other antibodies used to analyze the VP1 unique region during western blotting were anti-aa15-29 (1:1000) and anti-aa60-74 (1:1000) (Pacific Immunology: Grieger, Samulski unpublished). All films were exposed anywhere from 10 seconds to 1 minute.

Viral transduction assay

Viral transduction was analyzed by quantifying the luciferase transgene expression in 293-cell lysate no more than 24hrs post infection. 2E5 293 cells were transduced with 3000 vector genomes (vg) /cell and lysed using 1X Passive Lysis Buffer provided by Promega. Relative light units were analyzed post addition of the D-luciferin substrate (NanoLight) to the cell lysates using a Victor2 Luminometer (PerkinElmer).

Electron microscopy

10μl of purified and dialyzed full and empty virus particles in 1X PBS with Ca^{++} and Mg^{++} were pipetted onto a glow-discharged copper grid. The grid was washed twice with water and then stained with 2% uranyl acetate. EM images were taken with a LEO EM 910 TEM at varying magnifications at the UNC Microscopy Labs.

Heparin binding assay

1E10 vector genome containing particles of virus were incubated with pre-equilibrated heparin type III-S agarose beads (Sigma). The flowthrough was collected and

the beads washed two times with 1X PBS. The washes were collected, and the beads were washed with increasing salt concentrations from 0.2M to 0.6M PBS. A load control, the flowthrough, washes and elutions were blotted onto a nitrocellulose membrane using a dot blot apparatus. The membrane was blocked, incubated with antibody as described earlier in the methods. In this case, A20 was used as the primary antibody in order to detect intact capsids, and determine the affinity of virus mutants to heparin beads.

Confocal microscopy

Coverslips were plated with 50,000 Helas/slip in a 24 well plate. Each well was infected with 30,000vg/cell. 12hrs post infection cells were fixed with 2% paraformaldehyde and washed with 1X PBS. Cells were permeabilized with 0.1% Triton X-100 at room temp for 5mins and washed with 1X PBS and 1X Immunofluorescence wash buffer (IFWB: dH2O, 20mM Tris pH 7.5, 137mM NaCl, 3mM KCl, 1.5mM MgCl2, 5mg/ml BSA, 0.05% Tween). Cells incubated in A20 primary (1:10) in IFWB for 1hr at 37°C. Cells were washed with 1X PBS and incubated with 488nm fluorophore-conjugated secondary antibody (1:1250) in IFWB for 1 hr at 37°C (Abcam). Coverslips were mounted onto slides using Prolong antifade gold with DAPI mounting media. Slides were viewed on a Leica microscope in the Michael Hooker Microscopy Facility at UNC-Chapel Hill.

Molecular modeling studies

Homologous models of HI loop mutants were generated using VIPER (110) and/or Swiss-Model (http://swissmodel.expasy.org) in order to visualize the effects of mutagenesis on the virus capsid. The available structure of AAV2 (PDB accession No. 1LP3) was

supplied as a template for the mutant models generated in the AAV2 background. Once the Swiss-model pdbs were generated, the program O (Jones et al., 1991) was used to generate symmetry related models of the monomer subunits using icosahedral matrix multiplication. Structure visualization of mutant models and the structures of other AAV serotypes whose HI loops were substituted into AAV2 (e.g. AAV4, PDB accession No. 2G8G (38); AAV8, PDB accession No. 2qa0) AAV1 (84) and AAV5 (140) were performed using winCOOT® (http://www.chem.gla.ac.uk/~bernhard/coot/wincoot.html) and images were rendered with MacPyMOL® (http://pymol.sourceforge.net).

Results

With respect to structure and topology, the HI loop is highly conserved between the AAV serotypes and autonomous parvoviruses (Figure 1C); however the amino acid (aa) sequence varies significantly. In order to determine the role of the HI loop as it pertains to the AAV capsid structure and life cycle, the AAV2 HI loop sequence was mutated, swapped between serotypes or substituted, and the resulting viruses assayed for viral assembly, encapsidation of the viral DNA, binding to heparan sulfate, and the ability to successfully infect target cells. Mutagenesis was performed on the ten varying amino acids of the HI loop, starting with serine 658 and ending with alanine 667 in the AAV2 capsid (Figure 1A).

Deletion and glycine substitution mutants

First, mutations were generated in which the AAV2 HI loop amino acids were either deleted (AAV2 HI-/-) or substituted with a poly-glycine peptide (AAV2 poly-glycine). In

the substitution mutant the ten most variable HI loop amino acids were replaced with a chain of glycine residues in order to generate a flexible loop structure devoid of all amino acid side chain contacts between this loop and the EF loop (located between the β-strands βE and βF) in the underlying subunit (Figure 2A). Upon removal of the HI loop, AAV2 HI-/- capsid viral proteins were expressed (data not shown) but unable to assemble into particles as determined by A20 western dot blot analysis (Figure 2B) and DNA dot blot (Table 2). Interestingly, as shown in Figure 2B, the AAV2 poly-glycine mutant formed AAV particles based on western dot blot analysis (see fractions 10 and 11 of the cesium chloride gradient), however, these particles were devoid of DNA (Table 2). The AAV2 poly-glycine empty particles appear to be similar to AAV2 empty particles when analyzed under EM (Figure 2C), with the exception of a ring-like staining pattern more apparent with AAV2 poly-glycine particles. Although no other gross structural changes were evident by EM, potential conformational changes to the capsid were suggested by the ring-like staining therefore, further biochemical analyses were carried out such as heparin binding affinity chromatography. The AAV2 poly-glycine mutant had a comparable affinity for heparin sulfate as wt AAV2 particles as determined through a heparin binding assay, eluting from the heparin column mostly at 0.4M salt (Table 2). From these data, three important conclusions can be drawn; the presence of the HI loop is necessary for capsid assembly, and specific amino acid side-chain interactions within this loop appear to be necessary for packaging the viral genomic DNA. In addition, residues forming the HI loop and adjacent capsid regions do not play a role in heparan sulfate receptor attachment.

HI loop domain swapping

Based on the observations from the glycine residue replacement studies, we carried out HI loop swaps from representative serotypes in hopes of obtaining more information on critical amino acids that have evolved for the HI loops of specific serotypes. The serotypes chosen for this study were AAV1, AAV4, AAV5 and AAV8 which are 83%, 61%, 59% and 83% identical to the overall amino acid sequence of the AAV2 capsid, respectively (Figure 1A) and represent the range of sequence homology between AAV2 and the other serotypes characterized to date (32). The AAV1 and 8 HI loops are similar in conformation (Figure 3B) but vary significantly in amino acid sequence (Figure 3A). AAV2 with the loops from AAV1 (AAV2 HI1) or AAV8 (AAV2 HI8) generated titers only two-fold lower than wt AAV2 at 3E9vg/μl, 3E9vg/μl and 6E9vg/μl, respectively (Figure 3D) and display similar to wt AAV2 heparan sulfate elution profiles (e.g. mostly at 0.4M PBS Figure 3E). As determined through EM analysis, the full particles obtained for the mutant seem to be similar to wt AAV2 full particles in gross conformation (Figure 3C). In addition, as seen in Figure 3D AAV2 HI1, AAV2 HI8 and AAV2 all transduced 293 cells (infected with 3000vg/cell) with similar efficiency as determined through a luciferase assay.

At the other end of the phenotype spectrum, swapping of the HI loops from the less homologous serotypes AAV4 and AAV5 did not produce mutant viruses that were similar to wt AAV2. As shown in Figure 4A, AAV2 HI4 based on dot blot analysis, produced a virus titer one log lower than wt AAV2, 1.05E9vg/μl and 1.13E8vg/μl, respectively. However, when 293 cells were infected with the same number of vector genomes per cell, AAV2 HI4 and wt AAV2 infected cells with similar efficiency (Figure 4A). Interestingly, when wt AAV2 and AAV2 HI4 full particles were heat treated at one-degree increments ranging from 55°C to 65°C, AAV2 capsid dissociation was initiated at temperatures as low as 55°C, with

complete dissociation at 63°C, whereas, AAV2 HI4 did not dissociate and expose VP1 until 63°C (Figure 4B). This observation suggests that the, AAV2 HI4 mutant capsid is more stable than that of wt AAV2, although we are still unsure if there is a correlation between capsid stability and titer.

The AAV5 capsid VP subunit, with 59% homology in amino acid sequence to AAV2, contains an HI loop that is one amino acid shorter than those observed in AAV2 and the other AAV serotypes characterized to date. The AAV5 HI loop is structurally lacking a threonine at the amino acid position equivalent to residue 659 in AAV2. Substitution of this HI loop into AAV2 (AAV2 HI5) resulted in a change in amino acid sequence beginning at position 655 instead of 658 due to the low homology (Figure 5A). Although, AAV2 HI5 can express VP1, 2 and 3 when the cell lysate is subjected to western blot analysis (data not shown) the subunit proteins are unable to assemble into intact capsid particles as determined by A20 western dot blot (Figure 5B). In order to determine if the length of the HI loop is contributing to the inability of AAV2 HI5 to assemble particles, a threonine was inserted into AAV2 HI5 at position 659 (AAV2 HI5 TTSF). The threonine insertion does minimally restore capsid assembly but not packaging based on western dot blot (Figure 5B) and DNA dot blot analyses (Table 2), respectively.

The HI loop swap phenotypes show that specific amino acid side chain interactions of the HI loop can affect particle stability as seen with the AAV2 HI4 mutant, and the length of the HI loop appears to be crucial for maintaining proper capsid assembly as in AAV2 HI5; however DNA packaging ability seems to be more stringently controlled by loop sequence as concluded from the AAV2 poly-glycine mutant. In addition, the data shows that this capsid VP region can tolerate amino acid differences in assembling an AAV capsid seen in AAV2

HI1 and HI8, consistent with the observation of the HI loop in all the parvovirus structures determined to date (Figure 1A) despite the lack of sequence similarity.

Site-directed mutagenesis

To determine which amino acids within the HI loop are critical for viral genome packaging into the assembled capsids, a series of site-directed mutants were generated in this region based on sequence conservation between the AAV serotypes and observed interactions with the underlying amino acids, since replacing the AAV2 HI loop with glycines appears to ablate DNA packaging capabilities. As shown in the serotype sequence alignment in Figure 1A, a phenylalanine at position 661 within the HI loop is conserved in the AAV serotypes aligned. In the crystal structure of AAV2 the side chain of F661 interacts with a conserved proline at position 373 in the EF loop within the underlying subunit possibly through hydrophobic interactions (Figure 7B). Such interactions have been shown to play key roles in protein stability and folding (18). Also seen in the sequence alignment, residue K665 is present in most serotypes (Figure 1A), which based on the crystal structure forms a salt bridge with an aspartic acid at position 368 of the underlying subunit. Another amino acid of interest is F666, which resides in a hydrophobic pocket of the underlying subunit. As seen in the sequence and structure alignment (Figure 1), there is a hydrophobic residue such as valine or isoleucine at this position in all serotypes compared. In order to determine which of these three conserved residues are critical for the AAV2 capsid to fully assemble and package the viral genome, the glycine residues at position 661, 665 and 666 in the AAV2 poly-glycine mutant were individually changed back to the amino acids present in the wt AAV2 HI loop, F661, K665 and F666, respectively. Mutating the residues one at a

time did not restore the ability of the AAV2 poly-glycine mutant to package the viral DNA (Table 2). This suggests that cooperative interactions facilitated by individual residues are critical for maintaining viral genome packaging capabilities, as seen in the AAV2 HI loop swap mutants (Table 2). This conclusion is further substantiated by the experiments mentioned below.

Peptide substitution studies

In order to determine the plasticity of the HI loop, gross mutagenesis of amino acid residues within this region was carried out on the capsid. Since data mentioned previously suggests a cooperative effect between amino acids is necessary for viral genome packaging, semi-conserved residues K665 and F666 were left unchanged. The AAV2 HI loop was substituted with a range of peptide sequences varying in length and beginning at different amino acid positions. First, short RGD peptides were substituted, in an effort to "walk through" the HI loop and characterize the effects of disparate non-AAV sequences on viral assembly and packaging. Amino acid positions 658-660, 660-662, 662-664, and 663-665 were substituted with an RGD peptide (120) (AAV2 RGD 658, AAV2 RGD 660, AAV2 RGD 662 and AAV2 RGD 663, respectively) (Figure 6A). Most mutants were obtained at virus titers within two-fold of wt AAV2 with the exception of mutant AAV2 RGD 660, which was obtained at a six-fold lower titer than wt AAV2 at 1.48E8vg/μl compared to 8.81E8vg/μl (Figure 6B). AAV2 RGD 658 and AAV2 RGD 662, after adjusting for vector genome number, resulted in similar infectivity to wt based on a luciferase assay (Table 2). However, when 293 cells were infected with AAV2 RGD 660, it was five-fold less infectious than wt AAV2 (Figure 6B). RGD 660 was lower in titer and infectivity than wildtype, and

results in the substitution of the conserved F661 (see **Site-directed mutagenesis**) with a glycine residue, suggesting a potential role of F661 in the virus life cycle. In light of this single amino acid and its phenotypic effects, we introduced longer peptides into the AAV2 HI loop for increased amino acid variability, and to gain more insight into structure-function constraints in manipulating this region.

Seven amino acid peptides, successfully used as insertions in previous capsid mutagenesis studies, were chosen in order to determine if the variable region of the HI loop could tolerate these peptides as substitutions. Starting at position 658 in the AAV2 HI loop, we substituted with peptides QPEHSST, VNTANST, SIGYPLP (154) and SGRGDS (70) (Figure 6A). All mutants generated virus. AAV2 QPEHSST was able to make virus in titers similar to that of wt (within 2-fold) followed by AAV2 VNTANST (3.5-fold lower than AAV2), and AAV2 SIGYPLP and AAV2 SGRGDS (4.5-fold lower than AAV2). However, AAV2 VNTANST was 27-fold less infectious than wt AAV2 while, AAV2 SIGYPLP was reduced by approximately 10-fold in infectivity (Table 1). AAV2 SGRGDS and AAV2 QPEHSST were 4.5 and 2-fold less infectious than wt AAV2, respectively (Figure 6B). The aforementioned changes in titer and infectivity upon gross mutagenesis of the AAV2 HI loops suggest that the amino acid interactions between the HI loop and underlying subunit are crucial for maintaining AAV viability. Previous data in the literature suggests that the five-fold axis is necessary for viral genome packaging and VP1 externalization (10, 71, 156). We do see a viral genome packaging defect in some of the mutants mentioned above, correlating with a decrease in infectivity. To further understand the phenotypic changes observed, we carried out a battery of biochemical analyses.

Biochemical analysis

A series of biochemical analyses such as heparin binding, heat treatment and western blotting were performed in order to understand why the titer and infectivity of AAV2 RGD 660, AAV2 VNTANST, AAV2 SIGYPLP and AAV2 SGRGDS were consistently lower than wt AAV2, from such studies, western blot analysis revealed an interesting capsid phenotype as shown in Figure 6C. We used monoclonal antibodies B1 and A1 (153) that recognize the VP3 C-terminus and VP1 unique N-terminus, respectively, to characterize the peptide substitution variants described above. Based on B1 staining, AAV2 VNTANST had decreased VP1 incorporation and an extra protein band between VP2 and VP3. In addition, AAV2 SIGYPLP had decreased VP1 incorporation. Interestingly, when blotted with A1 antibody against the VP1 unique region of AAV2, AAV2 QPEHSST, AAV2 RGD 660, and AAV2 SGRGDS revealed a second band at 77kDa. Notably, AAV2 RGD 660 and the longer peptide substitutions that were detrimental to virus titer and infectivity all changed the amino acid type at the conserved phenylalanine at position 661 (Figure 1C). Therefore the role of this residue in the AAV2 HI loop functionality was further investigated.

Analysis of the conserved F661 residue

F661, which is completely conserved throughout all AAV serotypes (Figure 7A) and interacts with a proline in the underlying VP subunit, was mutated to a glycine residue in AAV2 (AAV2 F661G). AAV2 F661G produced virus five-fold lower in titer than wt AAV2 based on dot blot analysis, 8.2E7vg/μl and 4.1E8 vg/μl respectively (Figure 7C). AAV2 F661G also binds heparin with a similar affinity as wt AAV2 based on heparin column binding and elution with increasing concentrations of salt (Table 2). Interestingly, AAV2

F661G is one log less infectious than AAV2 based on a luciferase assay (Figure 7D). In addition to these data, AAV2 F661G and wt AAV2 capsids were heat treated at 37°C, 50°C, 60°C, 65°C and 75°C. While, AAV2 was able to expose the VP1 N-terminus based on A1 antibody staining at 60°C, AAV2 F661G is unable to do so at this temperature, and can only expose the VP1 N-terminus when heated to 75°C upon capsid dissociation (Figure 8A). To further corroborate the data showing decreased incorporation of VP1 and reduced infectivity of AAV2 F661G, we carried out intracellular trafficking studies using confocal fluorescence microscopy. Briefly, Hela cells were infected with 30,000vg/cell of wt AAV2 and AAV2 F661G particles. The cells were fixed 12hrs post infection and stained with primary A20 antibody for intact capsid detection and then secondary goat-anti mouse 488nm-fluorophore conjugated antibody. In addition, the nuclei were stained with DAPI. Based on this analysis, AAV2 F661G was unable to enter the nucleus efficiently and appeared to remain perinuclear, unlike wt AAV2, which trafficked into the nucleus more efficiently (Figure 8B).

In addition, when 1E9vg dialyzed full particles were run on a western blot and stained with monoclonal B1 and A1 antibodies, AAV2 F661G revealed a fourth molecular weight capsid species between VP1 and VP2 consistently running at 77kDa. Using antibodies that specifically detect amino acids 15-29 and 60-74 in the VP1 unique region (Figure 9A), the capsid band at 77kDa was not detected on the western blot, further confirming an N-terminal truncation of this capsid subunit (Figure 9B). This molecular weight species is identical to the novel protein band seen in the western blot with AAV2 QPEHSST, AAV2 RGD 660 and AAV2 SGRGDS capsid subunit proteins. The novel capsid subunit is approximately 100 amino acid residues shorter than VP1 (Figure 6B), implicating potential proteolytic processing of the exposed VP1 N-terminus in these HI loop variants.

Therefore, the aforementioned data demonstrates that the HI loop can tolerate most amino acid changes, and specific cooperative amino acid interactions are necessary for proper viral genome packaging. Additionally, the F661/P373 hydrophobic interaction appears crucial for proper incorporation of the VP1 subunit into the AAV2 capsid. Without the proper interactions a distinct VP1 subunit lacking its N-terminus containing the phospholipase activity is incorporated into the capsid, directly impacting virus infectivity.

Discussion

With the availability of the AAV2 crystal structure (160), many aspects of the adeno-associated virus life cycle including host cell recognition (3, 20, 64, 105, 142), intracellular trafficking (7, 23) and uncoating (131) are now possible to correlate to structure. The first of such studies have centered around the three-fold loops and the determination that they are key topological features in host cell recognition (5, 64). Similar structure-function studies have extended from the three-fold loops to the five-fold axis and the location of the virion pore and its potential role in viral genome packaging, capsid assembly and VP1 unique N-terminal exposure (10, 71, 156). Interestingly, the HI loop surrounds the five-fold pore, and has an essential structural role in viral assembly by overlapping the neighboring VP3 subunit forming amino acid interactions with the underlying EF loop (see Figure 1). Recently Dr. Mavis Agbandje-McKenna has observed the HI loop flipping up 90° upon AAV2-heparan sulfate proteoglycan binding suggesting a dynamic role of this structure in the viral infectious pathway (75). To better understand the role of this capsid structure, we chose to characterize in detail the HI loop as it may contribute to specific stages in the virus life cycle such as viral

genome packaging, assembly, and subsequent stages during the infectious pathway. The results of this study demonstrate that the AAV2 HI loop is essential for proper capsid assembly, packaging of the viral DNA, and viral infectivity when the conserved phenylalanine at amino acid position 661 is altered.

We carried out a comprehensive amino acid deletion and substitution study to uncover the role of the HI loop in the AAV life cycle. From these efforts we determined that removal of the HI loop (AAV2 HI-/-) leads to capsids that cannot assemble (Figure 2). We assayed viral assembly primarily using the monoclonal A20 antibody (153) that detects tertiary structure of properly assembled AAV capsids. Viruses that were unable to form virions were further studied using gradients and western blot analyses that confirmed the ability to synthesize viral protein subunits (data not shown). Although we relied primarily on A20 recognition to confirm the ability to form proper virion structures, additional studies such as iodixanol gradient purified AAV2 HI-/- cell lysate followed by EM analysis further determined that this mutant only appears to generate monomer subunits (data not shown). In contrast, substitution of the loop with glycines (AAV2 poly-glycine) generated A20 recognizable assembled capsids, however these capsids were deficient in the ability to package the viral DNA. Even though this mutant provided sufficient structure to assemble intact AAV particles, the glycine substitutions specifically ablate amino acid side-chain interactions with the EF loop of the underlying subunit, suggesting that the HI loop structure and the backbone interactions of the HI loop with the underlying subunit are sufficient enough to facilitate capsid formation. However, the specific amino acid interactions are required for efficient packaging of the viral DNA. Although we can not draw from our studies the exact mechanism for the viral genome packaging deficiencies of the glycine

substitution mutant, it is interesting to speculate that this phenotype can possibly be attributed to gross conformational changes in the structure of the five-fold pore since the five-fold pore has been implicated as the site of Rep protein binding, a necessary step for efficient DNA encapsidation (9, 10). As a result, it will be of interest to determine ability of HI loop mutants to bind Rep protein in pull down experiments as previously described (9).

In addition to the deletion and substitution studies above, we decided to swap the AAV2 HI loop with those from representative serotypes. Domain swapping, specifically between virus serotypes allows for determination of the role of that specific region of the capsid in the virus life cycle. For example, in adenovirus, the fiber necessary for host cell recognition (155), was swapped between adenovirus subgroups resulting in alteration of intracellular trafficking of the adenovirus vectors (85). Alternatively, in the case of AAV, domains were swapped between AAV1 and 2 in order to characterize determinants necessary for AAV1 muscle tropism (46). In a similar study regarding AAV, domains from AAV2 were swapped with those from AAV8, demonstrating that Loop IV of AAV8 at the three-fold axis of symmetry is responsibly for dictating liver tropism (118). Interestingly in our studies, swapping the HI loop with that of AAV1 and AAV8 did not affect titer, transduction, heparin binding or gross conformation. However, this can be expected due to the relatively higher sequence homology between AAV2 and these serotypes. More importantly, these results suggest that the HI loop most likely does not contain determinants of tissue tropism or receptor binding. This was further confirmed via mouse intramuscular injections with AAV2 RGD 662. Briefly, bioluminescence imaging revealed similar *in vivo* transduction profiles for AAV2 RGD 662 and wt AAV2 one-week post administration (data not shown).

In the case of AAV4 and AAV5 HI loops, significant phenotypic variations were seen possibly due to lower sequence homology with AAV2. For instance, the AAV4 HI loop is comprised of a higher number of hydrophobic residues than the loop from AAV2 based on the amino acid sequence and crystal structure (38). The 3-dimensional structure of the AAV2 VP3 monomer (Figure 4C) shows that the side chains of residues 659 and 660 point away from the capsid and do not interact with the residues in the underlying subunit. On the other hand, the conserved phenylalanine at position 661 interacts with proline 373 in the EF loop of the underlying subunit as mentioned in the results. The alanine-to-serine change at position 663 of the AAV2 HI4 mutant might contribute a hydrogen bond interaction due to a potentially accessible hydroxyl group that is not present in the AAV2 HI loop. The K665P change in AAV2 HI4 suggests a possible contribution to increased hydrophobic interactions with proline, valine, phenylalanine and methionine residues found in the underlying subunit of AAV2. However, this assessment is based on a structure model of AAV2 HI4 and a more accurate analysis of the AAV4 HI loop amino acid contributions to AAV2 capsid stability is dependent upon knowing the crystal structure of the AAV2 HI4 mutant.

Collectively, the aforementioned amino acid changes in AAV2 HI4 could enhance HI loop-EF loop interactions and thereby could well account for increased capsid stability as demonstrated through increased resistance to heat treatment in comparison to AAV2. In addition, such increases in capsid stability and possible gross conformational changes to the five-fold pore might account for lower packaging efficiency and titers seen with the AAV2 HI4 mutant. It is possible that the AAV capsid "breathes" or expands in volume during viral genome packaging, and if the capsid is too stable or held too tightly together, it may be more difficult for the Rep protein to package the viral genome. The idea of capsid expansion has

been studied in bacteriophage, and it has been shown that during the DNA packaging process a conformational change occurs which causes an increase in capsid volume (56).

Additionally, previous data suggest that the Rep protein is bound in higher quantities to the capsids of packaging deficient mutants (9) possibly due to "jamming" of the genome threading machinery. Such has also been noted in the case of AAV2 HI4, wherein the particle bound increased amounts of Rep protein in comparison with AAV2 (data not shown). For the AAV2 HI4 mutant, it is possible that there is increased stability of the particle based on the presence of another protein or proteins on the capsid surface.

In the case of AAV2 HI5, despite normal expression of capsid subunit proteins, no intact capsid assembly is observed. This was further confirmed via EM analysis on cesium chloride gradient fractions of the AAV2 HI5 transfected cell lysate. It was determined that the AAV2 HI5 mutant may form pentamers, but does not form proper intact particles (data not shown). This phenotype is likely attributable to the fact that the AAV5 HI loop is one amino acid shorter, based on the crystal structure (140) than the wt AAV2 HI loop. In corollary, insertion of the missing threonine at position 659, minimally rescues capsid assembly. Therefore, the length of the HI loop in relation to the underlying subunit appears to be crucial for proper capsid assembly, while the loop amino acid interactions with the underlying subunit dictate genome packaging efficiency. This was further corroborated by the fact the AAV2 HI loop glycine extensions formed intact virus particles, but were unable to package the viral genome based on dot blot and western dot blot analyses (data not shown).

Following the domain swaps we decided to use peptide substitutions in order to mutate multiple residues of the HI loop. Many groups have successfully inserted peptides,

specifically at the three-fold loops, on the capsid surface as a means to retarget the virus for specific tissue types (35, 120, 121, 154). In this study we used peptides, not as insertions, but substitutions in a novel region of the capsid. Peptide substitution within the AAV2 HI loop showed that certain amino acid changes do not affect virus titer and transduction, as seen with the AAV2 RGD 658, AAV2 RGD 662 and AAV2 QPEHSST mutants. However, some peptide substitutions resulted in marked changes in phenotype that were dependent on the amino acid position substituted. For instance, substitution with peptide RGD at position 660 (AAV2 RGD 660), SGRGDS starting at position 658 (AAV2 SGRGDS), VNTANST starting at position 658 (AAV2 VNTANST) and SIGYPLP also starting at position 658 (AAV2 SIGYPLP) resulted in decreased titer and infectivity. All of these mutants replace the conserved F661 residue observed in all serotypes.

Interestingly, a number of these mutants, such as AAV2 VNTANST, SIGYPLP, RGD 660 and SGRGDS, also revealed differential banding patterns seen with B1 antibody staining of a western blot (Figure 6C). Specifically, there appears to be a decreased incorporation of VP1 capsid subunits in these mutant capsids. It is likely that such phenotype, which would reduce the effectiveness of the PLA2 domain (located in the VP1 N-terminal domain) required for endosomal escape and nuclear entry of the viral capsid, could explain the decrease in transduction seen with these mutants (36, 40, 71, 125). The lower titers of the aforementioned mutants can possibly be attributed to improper capsid assembly (9, 132) and defective packaging (9). In the AAV2 VNTANST mutant there is an additional protein band seen between VP2 and VP3 with B1 staining that is yet to be identified. The observed protein product is most likely due to proteolytic processing of VP1, which could also account for the decreased amount of VP1 present in this capsid mutant. The 77kDa

protein band in the case of AAV2 RGD 660 and AAV2 SGRGDS seen with A1 staining further corroborates these speculations (Figure 6C).

As mentioned above one commonality shared by these defective peptide substitution mutants is that they span the conserved phenylalanine at amino acid position 661. F661 interacts with P373 in the EF loop in the underlying subunit of all serotypes through interactions (Figure 7B). This interaction appears critical for stability (18) of assembled capsid subunits since the HI loop is the only region at the five-fold axis of symmetry that extends from one subunit and overlaps the underlying subunit. Mutation of F661 results in a phenotype similar to that seen with peptide substitutions spanning this region. Based on data shown in Figure 9, we hypothesize that the interaction between F661 and P373 is necessary to stabilize the capsid around the five-fold axis of symmetry, being of great importance due the five-fold pores' contribution to viral genome packaging and infectivity (10, 156). Disruption of this interaction appears in particular, to reduce the amount of VP1 incorporated into these mutant capsids (Figure 9B).

Additionally, such mutagenesis could result in improper incorporation of VP1 subunits at the five-fold axis of symmetry, which would expose the critical PLA2 domain to cellular proteases during virus production. If unassembled VP1 monomers or loosely assembled particles exposing the VP1 unique N-terminus are present, it is possible that they may be susceptible to cellular proteases. This may not occur as readily in wildtype or other mutant viruses that are able to assemble the VP monomers efficiently in a stable configuration.

In conjunction with this observation, a similar phenomenon may be occurring in the AAV baculovirus production system (124, 135). There appears to be inefficient

incorporation of VP1 into the AAV2 capsid during production in insect cells, and this may be due to the susceptibility of VP1 to cellular protease in the non mammalian cell environment (69). The notion that VP1 is susceptible to cellular proteases is further substantiated by the fact that when mammalian cells are transfected with VP1 constructs, specifically VP1NLSFKN and VP1FKN, a second molecular weight band is detected between VP1 and VP2 in the cell lysates (40) similar to the result obtained in this study. Upon mutation of F661 this molecular weight species was not only generated but also incorporated into the intact capsid.

In addition, it is not surprising that a single amino acid on the AAV capsid such as F661 could significantly impact the biology of the virus. A recent study from our lab has shown that a single amino acid mutation, specifically K531E in AAV6 and E531K in AAV1, suppress and enhance heparin binding, respectively (157). Taken together, our data supports the role of the HI loop as an important AAV capsid structural element, necessary for proper incorporation of VP1 into an assembled infectious particle and a functional five-fold pore that allows efficient packaging of viral genomes.

Acknowledgments

Nina DiPrimio is the recipient of the Pharmacology Training Grant 2-T32-GM007040 from the National Institutes of Health (NIGMS). Special thanks to Ryan Nelson for assistance with heat treatment experiments and Brittney Gurda at the University of Florida in Dr. Mavis-Agbandje McKenna's laboratory for performing EM analyses on AAV2 HI5 and

AAV2 HI-/- mutants. We would also like to acknowledge NIH (P01HL051818; R.J.S P01 HL59412 and P01 HL51811; MA-M) for research funding.

Table 1: Primers utilized for AAV2 HI loop mutant capsid generation

Primer name	Forward	Reverse
AAV2 HI-/-	5' TCC TTC ATC ACA CAG TAC TCC ACG GGA CAG G 3'	5' AGG ATT CGC AGG TAC CGG GGT GTT CTT GAT GAG 3'
AAV2 poly-glycine	5' GGA GGA GGA GGA GGA GGA GGA GGA GGA GGA TCC TTC ATC ACA CAG TAC TCC ACG GGA CAG G 3'	TCC TCC TCC TCC TCC TCC TCC TCC TCC TCC AGG ATT CGC AGG TAC CGG GGT GTT CTT GAT GAG 3'
AAV2 poly-glycine F661	5' GCG AAT CCT GGA GGA GGA TTC GGA GGA GGA GGA GGA 3'	N/A
AAV2 poly-glycine K665	5' GGA GGA GGA GGA GGA AAG GGA GGA TCC TTC ATC 3'	N/A
AAV2 poly-glycine F666	5' GGA GGA GGA GGA GGA TTT GGA TCC TTC ATC ACA CAG 3'	N/A
pXSA for HI loop serotype swaps	**(Sbf1)** 5' AGA GAT GTG TAC CTG CAG GGG CCC ATC TGG 3' **(Afe1)** 5; AAG GAA AAC AGC AAG CGC TGG AAT CCC GAA 3'	N/A
AAV5 HI loop	5' GAT CCT GCA GGG ACC CAT CTG GGC CAA GAT C 3'	5' GCT TGG AGT TTT CCT TCT TGA GCT CCC AC 3'
AAV4 HI loop	5' GAT CCT GCA GGG TCC CAT TTG GGC CAA GAT T 3'	5' GTT TGG ACC GCT CCT TCT GGA TCT CCC 3'
AAV2 HI5 TTSF	5' CCC GGA AAT ATC ACC ACC AGC TTC TCG GAC GTG 3'	N/A
pAge1 Nhel	**(Age1))** 5' CTC ATC AAG AAC ACA CCG GTA CCT GCG 3' **(Nhe1)** 5' GCG GCA AAG TTT GCT AGC TTC ATC ACA CAG TAC TCC 3'	N/A
AAV2 SIGYPLP	5' AAG AAC ACA CCG GTA CCT GCG AAT CCT AGC ATT GGT TAT CCT CTT CCT AAG TTT GCT AGC TTC ATC 3'	5' GAT GAA GCT AGC AAA CTT AGG AAG AGG ATA ACC AAT GCT AGG ATT CGC AGG TAC CGG TGT GTT CTT 3'
AAV2 VNTANST	5' AAG AAC ACA CCG GTA CCT GCG AAT CCT GTT AAT ACT GCT AAT AGC ACT AAG TTT GCT AGC TTC ATC 3'	5' GAT GAA GCT AGC AAA CTT AGT GCT ATT AGC AGT ATT AAC AGG ATT CGC AGG TAC CGG TGT GTT CTT 3'
AAV2 QPEHSST	5' AAG AAC ACA CCG GTA CCT GCG AAT CCT CAA CCT GAA CAT AGC AGC ACT AAG TTT GCT AGC TTC	5' GAT GAA GCT AGC AAA CTT AGT GCT GCT ATG TTC AGG TTG AGG ATT CGC AGG TAC CGG TGT

	ATC 3’	GTT CTT 3’
AAV2 RGD 658	5’ AAG AAC ACA CCG GTA CCT GCG AAT CCT CGA GGA GAC TTC AGT GCG GCA AAG TTT GCT AGC TTC ATC 3’	5’ GAT GAA GCT AGC AAA CTT TGC CGC ACT GAA GTC TCC TCG AGG ATT CGC AGG TAC CGG TGT GTT CTT 3’
AAV2 RGD 660	5’ AAG AAC ACA CCG GTA CCT GCG AAT CCT TCG ACC CGA GGA GAC GCG GCA AAG TTT GCT AGC TTC ATC 3’	5’ GAT GAA GCT AGC AAA CTT TGC CGC GTC TCC TCG GGT CGA AGG ATT CGC AGG TAC CGG TGT GTT CTT 3’
AAV2 RGD 662	5’ AAG AAC ACA CCG GTA CCT GCG AAT CCT TCG ACC ACC TTC CGA GGA GAC AAG TTT GCT AGC TTC ATC 3’	5’ GAT GAA GCT AGC AAA CTT GTC TCC TCG GAA GGT GGT CGA AGG ATT CGC AGG TAC CGG TGT GTT CTT 3’
AAV2 RGD 663	5’ AAG AAC ACA CCG GTA CCT GCG AAT CCT TCG ACC ACC TTC AGT CGA GGA GAC TTT GCT AGC TTC ATC 3’	5’ GAT GAA GCT AGC AAA GTC TCC TCG ACT GAA GGT GGT CGA AGG ATT CGC AGG TAC CGG TGT GTT CTT 3’
AAV2 SGRGDS	5’ AAG AAC ACA CCG GTA CCT GCG AAT CCT TCG GGA CGA GGA GAC TCG GCG AAG TTT GCT AGC TTC ATC 3’	5’ GAT GAA GCT AGC AAA CTT CGC CGA GTC TCC TCG TCC CGA AGG ATT CGC AGG TAC CGG TGT GTT CTT 3’
AAV2 F661G	5’ GCG AAT CCT TCG ACC ACC GGC AGT GCG GCA AAG TTT GCT TCC 3’	N/A

Table 2. Phenotype comparison between AAV2 HI loop capsid mutants

Mutant	Sequence	Assembly (western dot blot)	Packaging (DNA dot blot)	Heparin Binding	[a]Infectivity (luciferase assay)	Alternative VP1 (western blot)
AAV2 HI -/-	(655) ANP----------SFI	-	-	N/A	N/A	N/A
AAV2 poly-glycine	(655) ANP GGGGGGGGGG SFI	+	-	+	N/A	-
AAV2 G661F	(655) ANP GGGFGGGGGG SFI	+	-	N/D	N/A	N/D
AAV2 G665K	(655) ANP GGGGGGGKGG SFI	+	-	N/D	N/A	N/D
AAV2 G666F	(655) ANP GGGGGGGGFG SFI	+	-	N/D	N/A	N/D
AAV2 HI1	(655) ANP PAEFSATKFA SFI	+	+	+	No change	-
AAV2 HI8	(655) ANP PTTFNSQKLN SFI	+	+	+	No change	-
AAV2 HI4	(655) ANP ATTFSSTPVN SFI	+	-	+	No change	-
AAV2 HI5	(655) GNI T- SFSDVPVS SFI	-	-	N/A	N/A	N/A
AAV2 RGD 658	(655) ANP RGDFSAAKFA SFI	+	+	N/D	No change	-
AAV2 RGD 660	(655) ANP STRGDAAKFA SFI	+	+/-	N/D	4.7	+
AAV2 RGD 662	(655) ANP STTFRGDKFA SFI	+	+	N/D	No change	-
AAV2 RGD 663	(655) ANP STTFSRGDFA SFI	+	+/-	N/D	[b]No change	-
AAV2 VNTANST	(655) ANP VNTANSTKFA SFI	+	+/-	+	27	+
AAV2 QPEHSST	(655) ANP QPEHSSTKFA SFI	+	+	+	2	+
AAV2 SIGYPLP	(655) ANP SIGYPLPKFA SFI	+	+/-	N/D	10.4	+
AAV2 SGRGDS	(655) ANP SGRGDSAKFA SFI	+	+/-	N/D	4.5	+
AAV2 F661G	(655) ANP STTGSAAKFA SFI	+	+/-	+	13.55	+

[a] = Fold decrease in infectivity

[b] = In SK-OV3 cells

\+ = Similar to wt

+/- = Packaging: Approximately 5-fold lower in titer than wt

\- = Packaging: One log lower in titer than wt or unable to package the viral genome

N/A = Not applicable

N/D = Not determined

Figure 1. HI loop comparison between various AAV serotypes and autonomous parvoviruses

A.

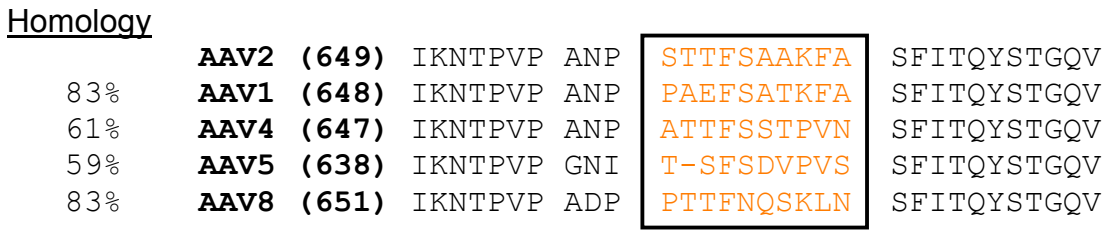

B.

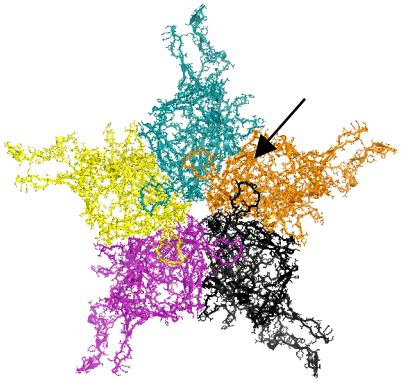

C.

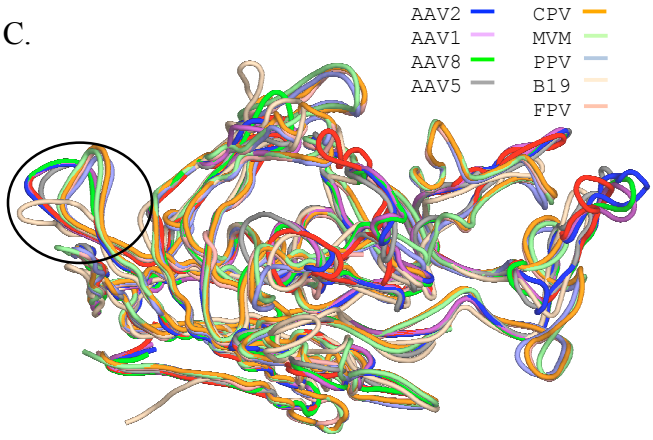

Figure 1. HI loop comparison between various AAV serotypes and autonomous parvoviruses. (A) Comparison of amino acid sequence homologies between representative AAV serotypes. The HI loop amino acid sequence alignment is shown on the right. Boxed are the ten most variable amino acids. (B) An arrow indicates the HI loop on an AAV2 pentamer, which extends from one VP subunit and overlaps the neighboring VP. (C) Circled in black are the HI loops on a structural superimposition of the VP monomer subunits of multiple AAV serotypes, AAV2 (blue), AAV4 (red), AAV5 (gray), AAV1 (purple) and AAV8 (green) and autonomous parvoviruses CPV (orange), FPV (salmon), B19 (wheat), MVM (lime) and PPV (slate).

Figure 2. AAV2 HI loop deletion and glycine substitution characterizations

A.

```
AAV2                (648)   IKNTPVPANP STTFSAAKFA SFITQYSTGQV
AAV2 HI-/-          (648)   IKNTPVPANP ---------- SFITQYSTGQV
AAV2 poly-glycine   (648)   IKNTPVPANP GGGGGGGGGG SFITQYSTGQV
```

B.

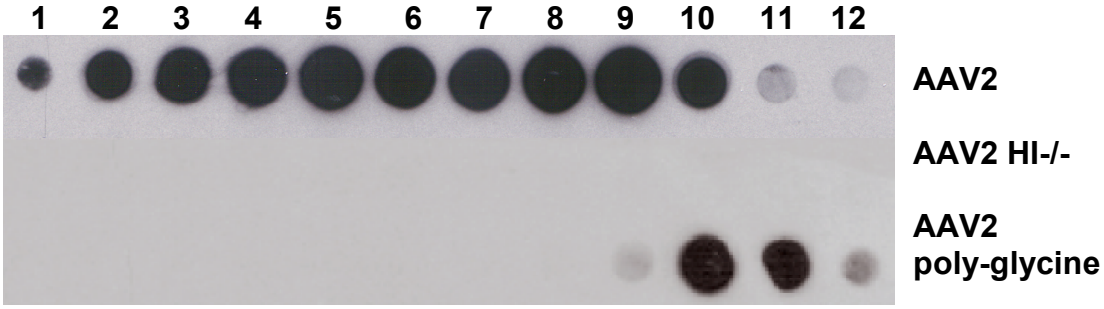

C.

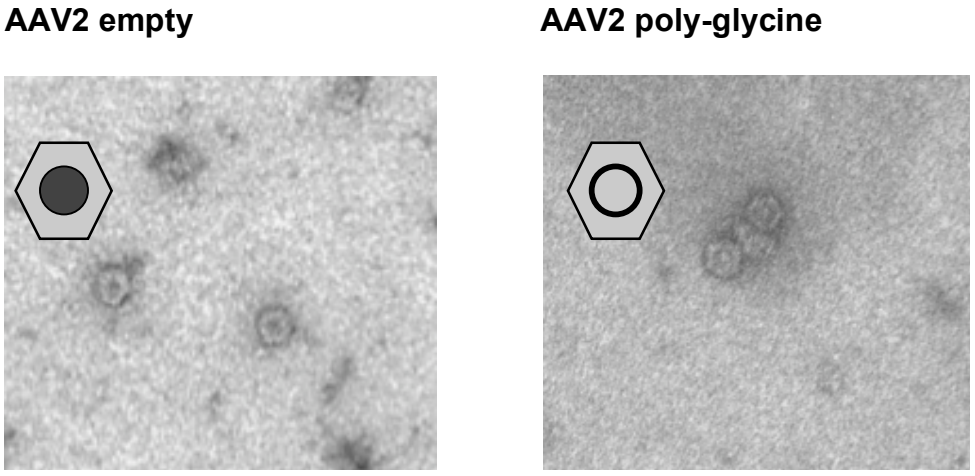

Figure 2. AAV2 HI loop deletion and glycine substitution characterizations. (A) AAV2 HI loop sequence alignment showing amino acids 658-667 that were removed (AAV2 HI-/-) or substituted with glycine residues (AAV2 poly-glycine). (B) Western dot blot analysis of CsCl gradient fractions from AAV2, AAV2 HI-/- and AAV2 poly-glycine preparations with A20 antibody. Gradient fractions were collected, and blotted onto a nitrocellulose membrane. The membrane was incubated with primary antibody A20 (1:20) and incubated with

horseradish peroxidase conjugated secondary goat anti-mouse (1:5000). (C) Electron micrograph images of empty AAV2 and AAV2 poly-glycine particles. Gradient purified, 1X PBS Ca^{++}/Mg^{++} dialyzed AAV2 (left panel) and AAV2 poly-glycine (right panel) empties were incubated on glow discharged copper grids negatively stained with 2% uranyl acetate.

Figure 3. AAV2 HI1 and AAV2 HI8 substitution mutant characterization

A.

AAV2	**(648)**	IKNTPVPANP	STTFSAAKFA	SFITQYSTGQV
AAV2 HI1	**(648)**	IKNTPVPANP	PAEFSATKFA	SFITQYSTGQV
AAV2 HI8	**(648)**	IKNTPVPADP	PTTFNQSKLN	SFITQYSTGQV

B.

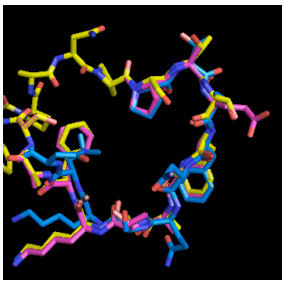

C.

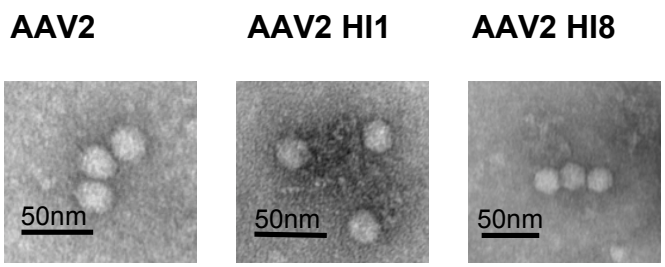

D.

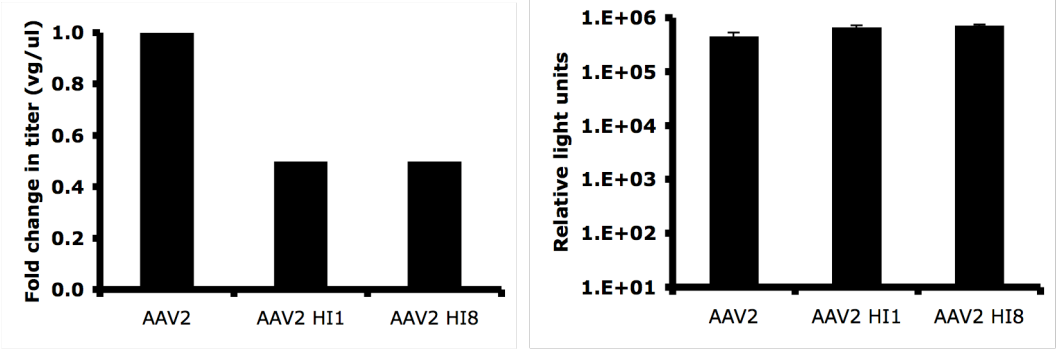

E.

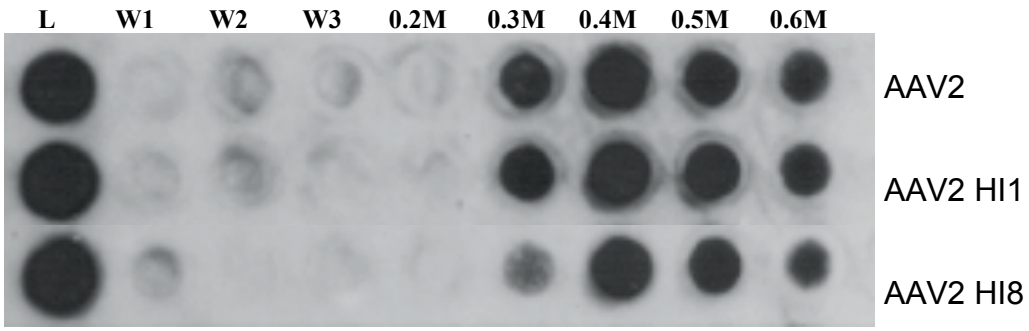

Figure 3. AAV2 HI1 and AAV2 HI8 substitution mutant characterization. (A) Sequence alignment of AAV2, AAV1 and AAV8 HI loop amino acids. (B) Structural alignment of AAV2, AAV1 and AAV8 HI loops (yellow, pink and blue). (C) Electron micrograph images of AAV2, AAV2 HI1 and AAV2 HI8 1XPBS Ca^{++}/Mg^{++} dialyzed CsCl purified (previously mentioned) DNA containing particles. (D) Radioactive DNA dot blot shown as fold change in titer (left panel) and luciferase assay on infected 293 cells with 3000 vg/cell (right panel n=3 SD=black bars). (E) Heparin binding profiles of AAV2, AAV2 HI1 and AAV2 HI8. 500ul of heparin type IIIS conjugated agarose beads (Sigma) were incubated with 1E10 vector genome containing particles (L = load) for 10mins at room temperature. The washes (1X PBS) and elutions (0.2M-0.6M PBS) were collected and capsids were detected via western dot blot analysis with A20 monoclonal antibody (1:20).

Figure 4. AAV2 HI4 subsitution mutant characterization

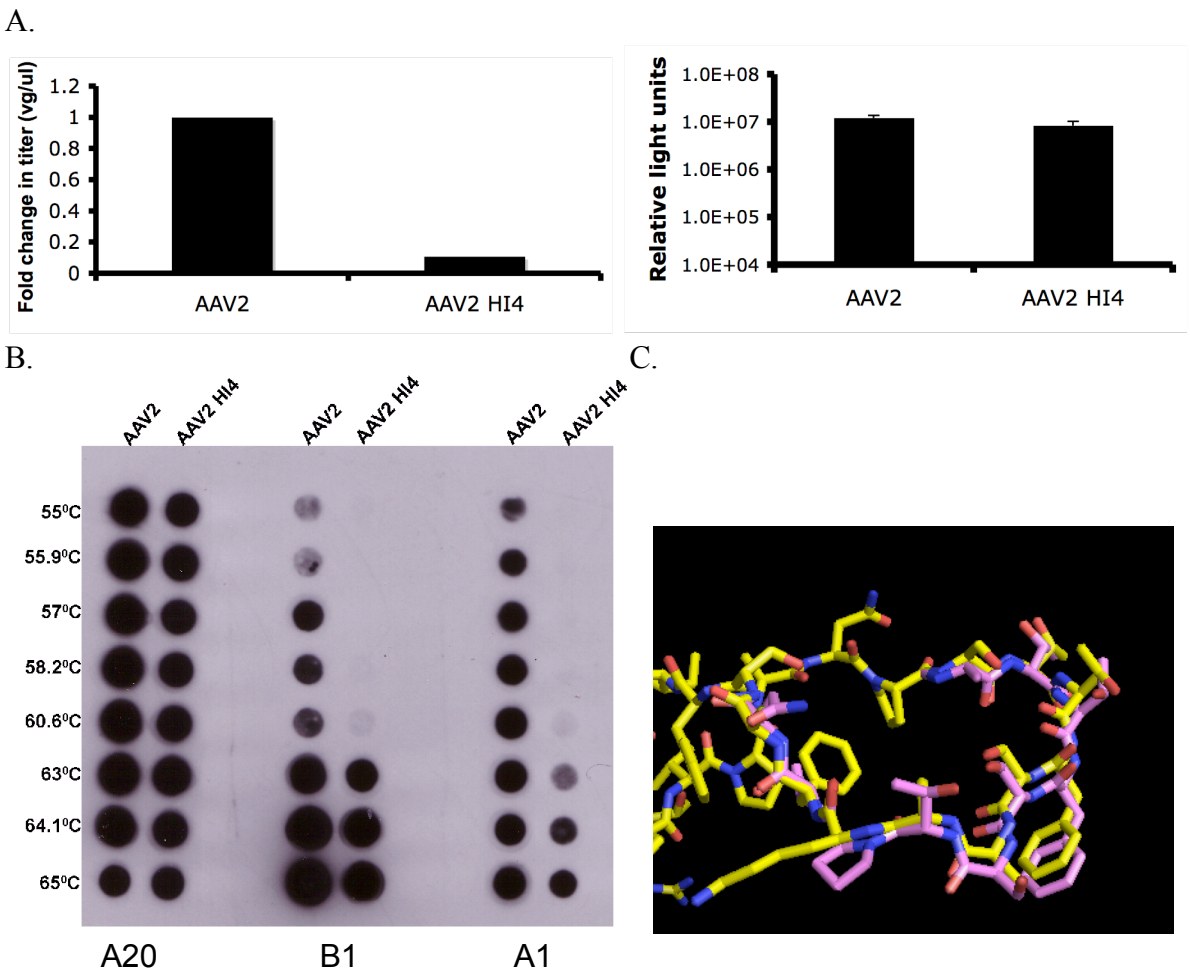

Figure 4. AAV2 HI4 substitution mutant characterization. (A) AAV2 HI4 titer and transduction. AAV2 and AAV2 HI4 titers were quantified via radioactive DNA dot blot against the luciferase transgene, shown as fold change in titer (left panel). AAV2 HI4 transduction was quantified via luciferase assay of 293 cells infected with 3000 vg/cell (right panel n=3 SD=black bars). (B) Heat treatment of 6E8 AAV2 and AAV2 HI4 viral DNA containing particles, with temperatures tested on the left hand side were transferred to a nitrocellulose membrane and blotted with the antibodies listed across the bottom at a ratio of 1:20. (C) Structural alignment of the AAV2 (yellow) and AAV4 (pink) HI loops from VP subunits.

Figure 5. AAV2 HI5 substitution mutant characterization

A.

AAV2 (655) ANPSTTFSAAKFA
AAV2 HI5 (655) GNIT-SFSDVPVS

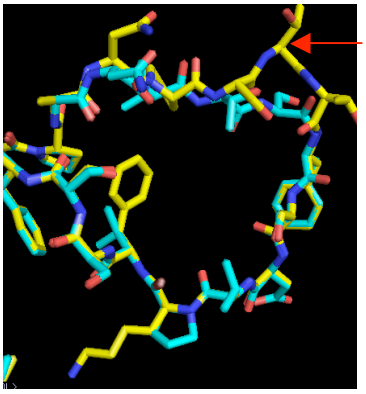

B.

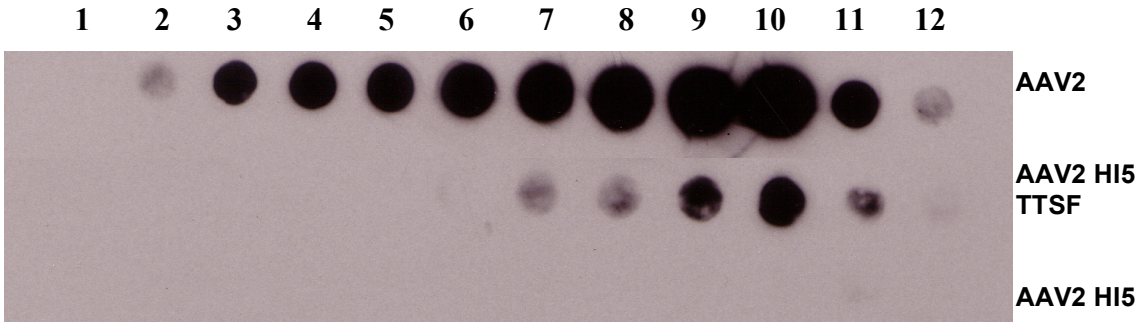

Figure 5. AAV2 HI5 substitution mutant characterization. (A) A sequence alignment of AAV2 and AAV5 HI loop residues (left hand side) and a structural alignment of AAV2 (yellow) and AAV5 (cyan) HI loops (right hand side). The amino acid position deleted in AAV5 relative to AAV2 in this region is depicted as a dash in the alignment and the threonine residue "inserted" at this position in AAV2 is indicated with a red arrow on the structural superimposition. (B) Western dot blot analysis of AAV2, AAV2 HI5, and AAV2 HI5 TTSF (threonine inserted at amino acid position 659) CsCl gradient fractions blotted with A20 antibody (1:20).

Figure 6. AAV2 HI loop peptide substitution mutant characterizations

A.

AAV2 (658)	STTFSAAKFA	**AAV2 RGD 658**	RGDFSAAKFA
AAV2 VNTANST	VNTANSTKFA	**AAV2 RGD 660**	STRGDAAKFA
AAV2 QPEHSST	QPEHSSTKFA	**AAV2 RGD 662**	STTFRGDKFA
AAV2 SIGYPLP	SIGYPLPKFA	**AAV2 SGRGDS**	SGRGDSAKFA

B.

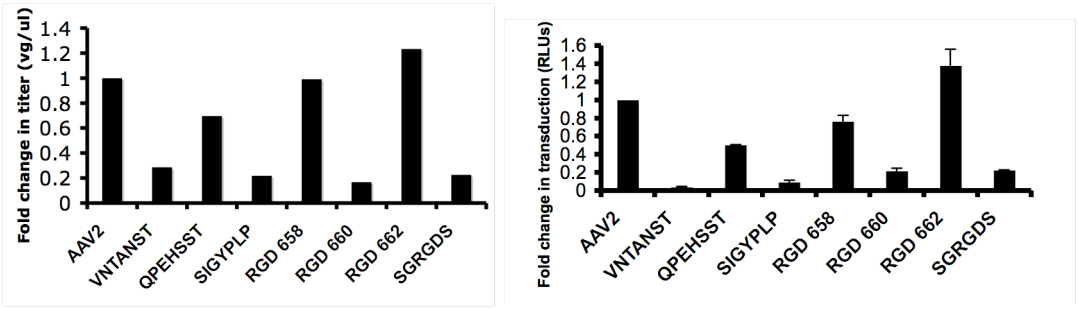

C.

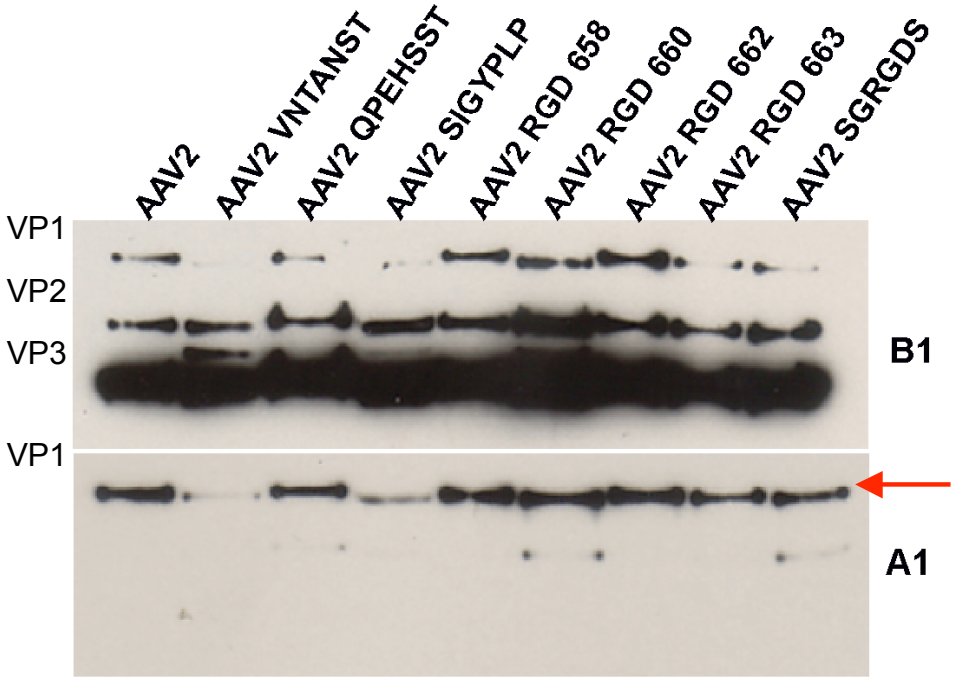

Figure 6. AAV2 HI loop peptide substitution mutant characterizations. (A) A sequence alignment shows residues in the AAV2 HI loop that were substituted with specific peptides indicated in orange. (B) HI loop peptide substitution titer and transduction. Fold change in titer as compared to AAV2 determined by radioactive DNA dot blot analysis (left panel). Fold change in transduction of infected 293 cells (3000 vg/cell) determined by luciferase assay (right panel n=3 SD=black bars). (C) Western blot analysis of peptide substitution mutants incubated overnight at 4°C with A1 (1:20) and B1 (1:20) monoclonal antibodies. A red arrow indicates an additional protein band detected with A1 antibody (bottom panel).

Figure 7. Residue F661 structure model and sequence alignment and AAV2 F661G substitution mutant characterization

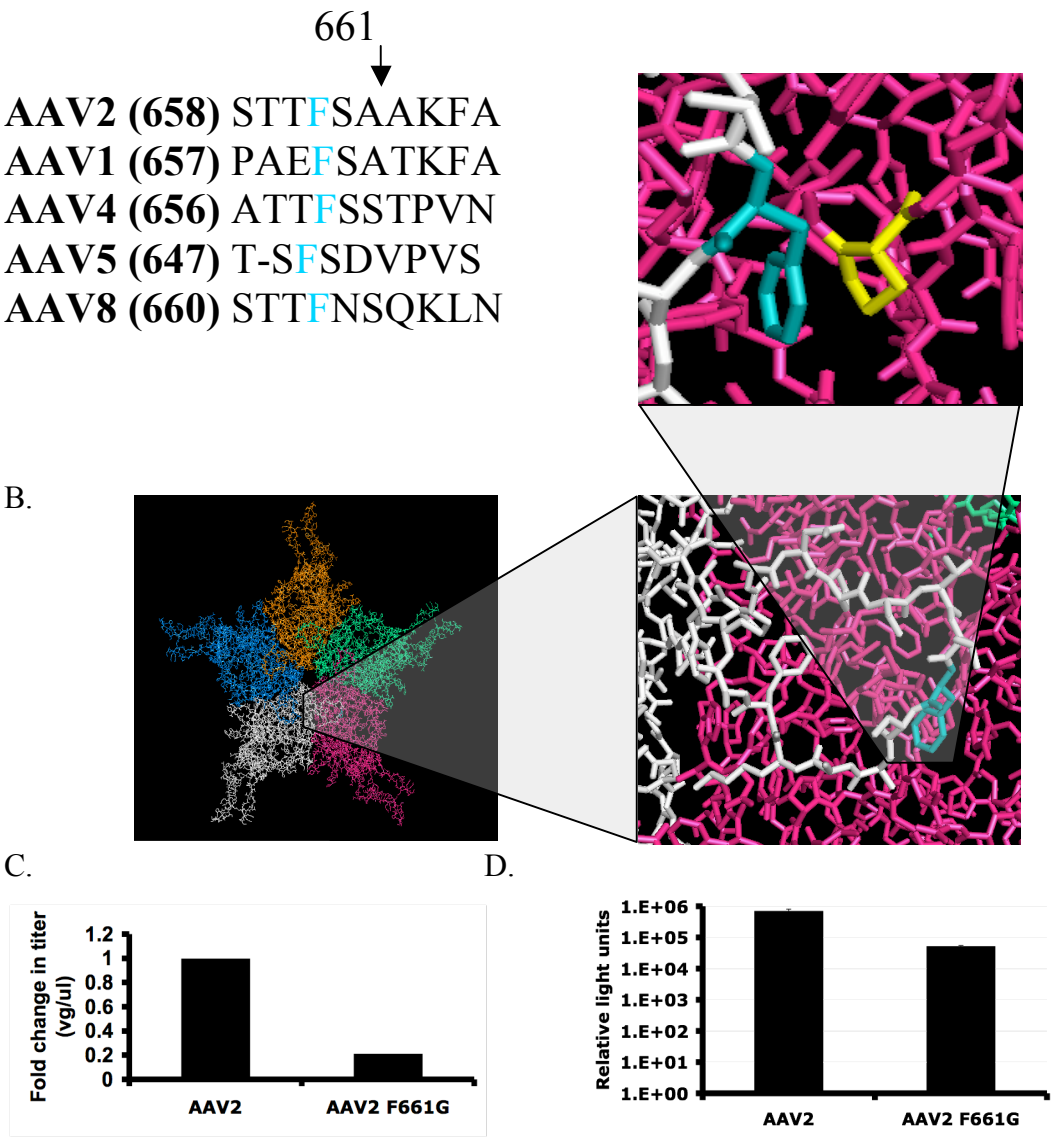

Figure 7. Residue F661 structure model and sequence alignment and AAV2 F661G substitution mutant characterization. (A) Sequence alignment of representative serotypes shows that F661 is conserved (cyan). (B) The HI loop located on a pentamer at the five-fold face (bottom left) is magnified (bottom right) showing the HI loop from one VP (white)

extends over the underlying VP (pink). F661 side chain (cyan) near the center of the HI loop forms a hydrophobic interaction with a conserved proline residue (yellow) of the underlying adjacent VP (top right). (C) Fold change in AAV2 F661G viral titer determined by radioactive DNA dot blot against the luciferase transgene. (D) Transduction quantified post 293 cell infection with AAV2 and AAV2 F661G (3000 vg/cell) and evaluated via luciferase assay (n=3 SD=black bars).

Figure 8. AAV2 F661G VP1 externalization and virus infectivity

A.

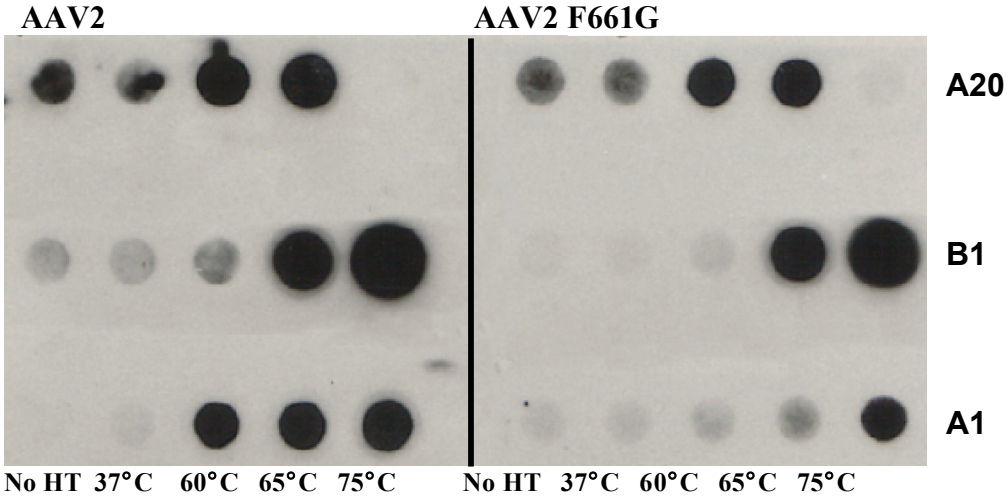

B.

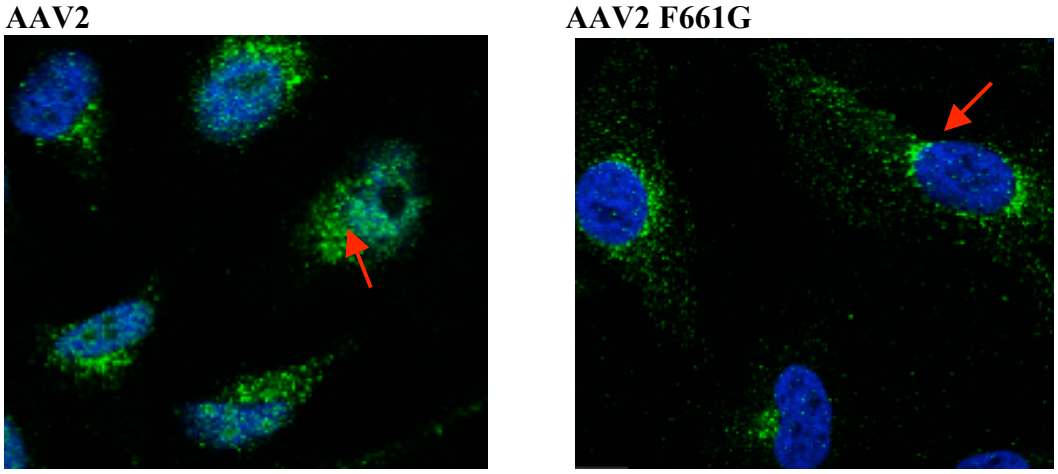

Figure 8. AAV2 F661G VP1 externalization and virus infectivity. (A) Heat treatment of 6E8 AAV2 and AAV2 F661G viral DNA containing particles (temperatures across the bottom). Treated capsids were blotted on a nitrocellulose membrane and intact capsids, dissociated VPs and externalized VP1 unique N-termini were detected with A20, B1 and A1 antibodies (1:20) as indicated on the right hand side. (B) Hela cells were infected with 50000 vg containing particles of AAV2 or AAV2 F661G. Cells were fixed and permeabilized, and intact capsids were detected with primary A20 antibody (1:10) and 488nm fluorophore-

conjugated secondary antibody (1:1250). The nucleus was stained blue with DAPI. Red arrows indicate AAV2 (left panel) and AAV2 F661G (right panel) intact capsids.

Figure 9. AAV2 F661G viral protein incorporation

A.

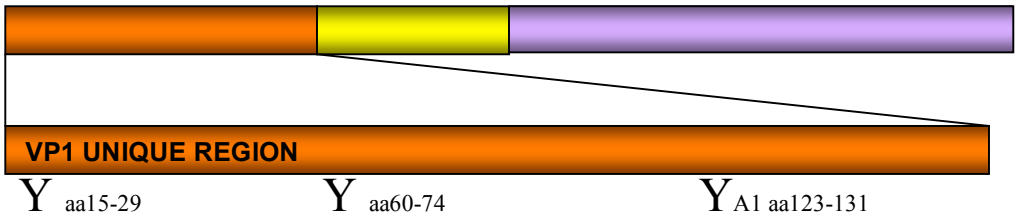

B.

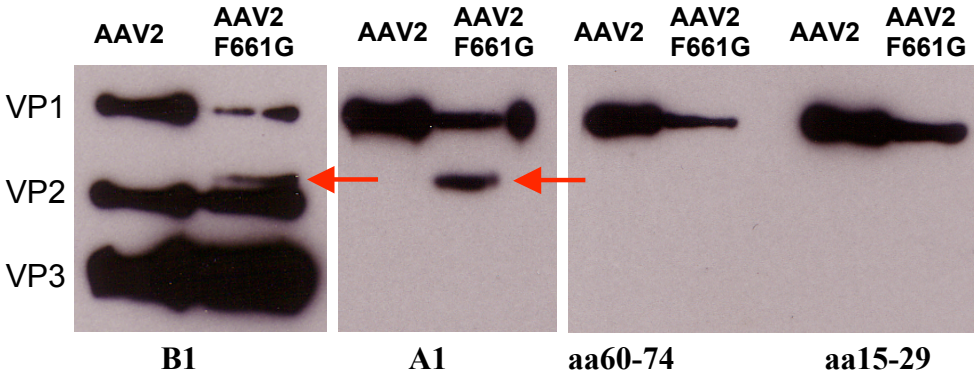

Figure 9. AAV2 F661G viral protein incorporation. (A) The schematic represents AAV2 VP3 with an enlargement of the VP1 unique region (orange). The yellow and purple regions represent VP1/VP2 and the VP1/VP2/VP3 common regions, respectively. Antibodies generated (Pacific Immunology) recognize specific amino acid stretches in the VP1 unique region as indicated at the bottom of the schematic (1:1000). (B) Western blot analysis of AAV2 and AAV2 F661G capsids with B1 and A1 antibodies (1:20), listed below the blot, detected an additional protein band at ~77kDa (red arrows).

CHAPTER III

Multi-functional capsids: Site-specific incorporation of a hexa-histidine motif

Abstract

The ability to manipulate the adeno-associated virus capsid allows researchers to understand capsid domains and develop efficient vectors for gene delivery. In this report we have focused on the HI loop, a previously characterized capsid domain. We substituted specific amino acids, AAV2 aa662-667, located within this region of AAV2 and AAV9 capsids with a hexa-histidine tag without disrupting key amino acid contacts shown to be important for viral assembly. The resulting AAV2 HI6xHis and AAV9 HI6xHis could be purified via nickel affinity chromatography as a potential universal purification scheme for AAV vectors. Further we were able to conjugate Ni-NTA gold nanoparticles to these capsids, thereby demonstrating their potential as novel reagents for EM applications, such as the determination of VP location in the intact capsid and histological analysis of patient samples. While the presence of hexa-histidine tags on the surface did not affect capsid infectivity *in vitro*, significantly reduced transduction was observed following intramuscular administration in mice. Interestingly, his-tagged AAV capsids were detargeted from the liver following intravenous administration. However upon generation of chimeras with fewer hexa-histidines tags on the surface, transduction is rescued *in vivo*. In summary, we have introduced a multifunctional domain into a novel site on the capsid surface that can be utilized for universal AAV vector purification, capsid labeling with gold nanoparticles and generating vectors detargeted from the liver.

Introduction

As gene therapists we are constantly manipulating the AAV capsid in order to generate vectors for gene delivery. Understanding the domains and individual amino acids on the surface of each AAV serotype allows for the creation of tailored vectors with specific tissue tropisms and subsequently disease targets. Not only do we need to understand the capsid function of specific serotypes as they relate to vector design but also need to produce and purify the vectors for such usage. Currently there is no universal method for purification of all AAV serotypes, however, there are many techniques that are being utilized for multiple serotypes and are necessary for progress in the field and the development of clinical vectors.

For AAV2 the preferred purification method is separating empty particles from genome containing particles via iodixanol gradient and then purification on a heparin column to remove cellular protein post gradient centrifugation. AAV2 can be purified on a heparin column since it binds heparan sulfate as a primary receptor however, other AAV serotypes do not bind heparan sulfate as a primary receptor, or their primary receptors are not yet known.

Recently Smith et al. 2007 described a technique involving polyethylene-glycol purification, anion-exchange chromatography and gel filtration. This method has been shown to be a technique with the capabilities of separating empty from genome containing capsids. First the authors report using a POROS 50HS for cation-exchange followed by anion exchange resin Q-sepharose XL (106). All techniques have their advantages and disadvantages but have yet to be expanded and applied to all serotypes and their variants. These advances in purification are vital for production of clinical grade vectors.

There have been many other advances in AAV purification post-production in recent years. A few researchers have inserted tags on the virus surface, specifically a hexa-histidine tag at the VP3 N-terminus (165) and also at the 3-fold loops at amino acid position 585 (68). These techniques may become useful with further development and *in vivo* tissue tropism characterization.

Previous studies focused on the five-fold axis of symmetry (10, 24, 40, 96) have allowed for further understanding of capsid structure and function. The five-fold axis of symmetry has been implicated in multiple roles such as vector genome packaging, viral capsid assembly, and VP1 externalization. Recent data has described this region of the capsid as being crucial for proper VP1 incorporation into the intact particle (24) and additionally, during primary receptor attachment has been shown to change conformation upon heparan binding using cryo-EM and image reconstruction (75).

In the current study based on the need for a universal purification scheme, we have expanded on our previous work with the HI loop as a novel site on the AAV capsid for peptide substitution without disrupting primary receptor recognition (24). We substituted amino acids at the five-fold of AAV2 and AAV9 that were not crucial for capsid integrity with a hexa-histidine domain, utilized for affinity column purification. Additionally, we demonstrated the ability to use the hexa-histidine vector as a tool for nanogold labeling for EM application. Another interesting feature observed was the detargeting ability of the histidine tagged AAV capsids from the liver as a function of the ratio of hexa-histidines on the capsid surface. In this manuscript, we have illustrated the use of a novel site on the AAV capsid for a single peptide substitution, generating a multifunctional tool for applications in basic virology and vectorology.

Materials and Methods

Generation of mutants

AAV2 HI6xHis mutants were generated using PCR with the Expand Long Template PCR kit (Roche) or site directed mutagenesis (Stratagene QuikChange). Primers complementary to the pXR2 backbone were generated by Integrated DNA Technologies (www.idtdna.com) with nucleotide extensions coding for the histidine tag. The primers used for AAV2 HI6xHis were 5'-CACCATCACCATCACCATTCCTTCATCACACAGTACTCCACGGGACAG-3' and 5'-ATGGTGATGGTGATGGTGGAAGGTGGTCGAAGGATTCGCAGGTAC-3' (PCR Expand Long Template) Amino acids 662-667 in VP3 were replaced with the histidine residues. For the mutants containing fewer histidine residues within the HI loop primers were designed as follows for use in site-directed mutagenesis: AAV2 HI1His: 5'- GAATCCTTCGACCACCTTCAGTCACGCAAAGTTTGCTTCCTTC-3', AAV2 HI2His: 5'-CCTGCGAATCCTTCGACCACCTTCAGTCACCACAAGTTTGCTTCC-3', AAV2 HI3His:
5'-CCTTCGACCACCTTCCACCACCACAAGTTTGCTTCCTTCATCACACAG-3',
AAV2 HI4His:
5'-CCTGCGAATCCTTCGACCACCTTCCATCACCACCACTTTGCTTCCTTC-3', AAV2 HI5His:
5'-GCGAATCCTTCGACCACCTTCCATCACCACCACCACGCTTCCTTCATCAC-3'.AAV9 HI6xHis was generated by GeneArt.

Virus production

Virus was produced using the triple transfection method described in Xiao *et. al.* 1998 (159). Cells were transfected with pXR (pXR2 or pXR9) containing the capsid mutations, pXX6-80 helper plasmid, and pTR-CMV- or CBA-Luciferase. In the case of chimeric mutants, pXR2 and pXR2 HI6xHis was transfected at a ratio of 1:1 or 5:1, respectively, totaling 10ug plasmid DNA (107). Cells were harvested 60hrs post transfection and purified using cesium chloride gradient density centrifugation for 5hrs at 65,000 rpm or overnight at 55,000rpm for iodixanol gradient centrifugation. CsCl gradients were fractionated and virus dialyzed against 1X PBS with calcium and magnesium, or the layer between 40 and 60% iodixanol was pulled from the gradient and further purified on the FPLC 1ml His-Trap HP nickel column (Amersham). Viral titers were determined by dot blot analysis or q-PCR using primers specific to the TR-Luciferase transgene.

Fast protein liquid chromatography

Various volume and vector genome quantities of iodixanol gradient purified virus was further purified through a nickel column (HisTrap HP 1ml column, Amersham) at a flow rate of 0.2ml/min. Load volumes were mixed with binding buffer (5mM imidazole, 20mM sodium phosphate and 0.5M NaCl pH 7.4)) prior to loading. The column was washed with 5 column volumes water, equilibrated with 5 column volumes binding buffer, 5ml of sample mixed with binding buffer was injected into the column, washed with 5 column volumes binding buffer, and eluted with 5 volumes elution buffer (500mM imidazole, 20mM sodium phosphate and 0.5M NaCl pH7.4). Peak fractions were detected based on UV absorbance at

280nm and verified by vector genome quantification using q-PCR with primers specific to the luciferase transgene. Peak fractions were dialyzed against 1X PBS Ca++ Mg++.

In vitro transduction assays

293 cells were infected with 1000 to 3000 vector genome containing particles of AAV2 HI6xHis per cell pre and post FPLC column elution. Cells were lysed with 100ul 1X passive lysis buffer (Promega) and the lysates were mixed with 100ul luciferin (Promega). Relative light units were detected with a Victor2 Luminometer.

Gold particle conjugation

Approximately 1E9 virus particles (AAV2 or AAV2HI6xHis eluted from the nickel column) were blocked with 0.05%Tween, 20mM NaCl and 50mM Tris pH7.5 for 30mins at room temperature. The gold particles (www.nanoprobes.com) were added to the blocked virus particles and incubated anywhere from 5 to 30mins at room temperature at a concentration 60 times the nanomolar amount of His tags present in the sample.

Electron microscopy

Glow discharged carbon coated copper grids were incubated with 15ul virus or virus pre-incubated with gold particles for 2minutes. For virus not conjugated to gold particles, the grids were washed twice with ddH2O and then negatively stained with 2% uranyl acetate stain for 30 seconds. For virus conjugated to gold particles, grids were washed 2x with wash buffer containing 200mM NaCl and 20mM imidazole to remove nonspecific binding. They were then washed with ddH2O and stained with Nanovan (Nanoprobes-

www.nanoprobes.com). Grids were visualized using the Leo 910 TEM in the Microscopy Laboratory Services at the University of North Carolina at Chapel Hill.

In vivo experiments

Balb/C female mice were injected via tail vein with 1E10 or 1E11 or intramuscular injection into the gastrocnemus with 1E10 vector genome containing particles (AAV2, AAV2 HI—His mutants, AAV9, AAV9 HI6xHis). Mice were imaged at weekly intervals post injection following intraperitoneal injection with D-Luciferin (NanoLight) using the IVIS Xenogen imaging system. Mice were imaged for 1 minute or 5 minutes at 5 minutes post administration of D-luciferin substrate.

Tissue harvesting and genome quantification

Animals were sacrificed two weeks post IV injection. The liver was harvested and a section of the liver was homogenized and incubated with 180ul ATL buffer and 20ul proteinase K solution (Qiagen DNeasy Blood and Tissue Isolation Kit). The tissue was incubated at 50 degrees overnight and genomes in the tissue were quantified via q-PCR (Roche) with primers specific to the luciferase transgene. The primers used were 5'-AAV AGC ACT CTG ATT GAC AAA TAC-3' and 5'-CCT TCG CTT CAA AAA ATG GAA C-3'. The mouse lamin B2 gene was also quantified and vector genome copies were normalized to the number of diploid genomes present in the sample. Additionally, total vector genomes were quantified in the blood stream at various timepoints post injection as indicated in the figures. Blood was collected in EDTA coated capillaries and total viral genome DNA was isolated via DNeasy Blood and Tissue Kit (Qiagen).

Blood incubation studies

1E10 vector genome containing particles were incubated with blood for determination of particle stability and hepatocyte binding. For particle stability in mouse blood AAV2 and AAV2 HI6xHis were incubated with 10ul of blood from an uninfected mouse at room temperature for 30minutes and then treated with DNase at 37°C (plus calcium and magnesium) for 1hour or not incubated with blood and solely incubated with DNase. DNase was inactivated upon addition of 4ul of 0.5M EDTA. Total vector genomes were isolated via DNeasy Blood and Tissue Kit (Qiagen) and quantified via q-PCR with primers specific to the luciferase transgene. For hepatocyte binding studies, hepatocytes were isolated from an uninfected mouse liver post liver perfusion with 20ml collagenase at a concentration of 2.5mg/ml in 1XPBS. The liver was spun in 40ml 1X PBS for 2hours at 4°C until cells were in suspension. Cells were pelleted at 2500rpm for 5min and 20ml of supernatant was disposed. Cells were resuspended in remaining 20ml and aliquots were pipetted into 1.5ml eppendorf tubes. Samples were spun at 50g for 4min to pellet the PCs (parenchymal cells). The PCs were resuspended in 1X PBS and spun at 50g for 4min. This was repeated 3 times with 1X PBS. Finally the PCs were spun at 250g for 4min and the PC supernatant was removed and pelleted. 1E10 vector genome containing particles alone or preincubated with mouse blood were incubated with PCs at 4°C for 1hour in rotating suspension. Post incubation cells were maintained on ice and unbound virus was removed via multiple wash steps with 1X PBS post centrifugation at 50g for 4mins. The pelleted cells were lysed and total DNA was isolated (viral and mouse genomic) with the DNeasy Blood and Tissue Kit

(Qiagen). The genomes were quantified via q-PCR against the luciferase transgene and the mouse lamin gene as a control.

Results

As a gene therapy vector, AAV is under constant characterization and modification in hopes of developing a more efficient vector for gene therapy. To generate enhanced vectors, we focus on capsid structure-function relationships. Over the years research has shown that specific regions of the virus capsid are crucial for specific virus functions. For instance, the VP1 N-terminus for phospholipase activity necessary for virus trafficking (125), basic regions for capsid assembly and nuclear localization (42), and the five-fold pore for viral genome packaging and potentially Rep protein interactions and VP1 unique N-terminal externalization (10). Recently, it has been shown that the HI loop on the capsid surface is necessary for proper VP incorporation into the intact particle. Additionally, it was determined that the HI loop is highly plastic, meaning that certain residues can be substituted while retaining wildtype properties as long as specific amino acid interactions are maintained between the HI loop and the underlying subunit. Based on these structure-function studies, we demonstrated the plasticity of this novel capsid region, and its ability to tolerate amino acid substitutions.

Specifically, we substituted amino acids 662-667 with six histidines for tagged universal metal affinity purification of all AAV serotypes. There are multiple proposed purification techniques such as antibody purification and column chromatography (68), both of which are waiting expansion to other serotypes. Additionally there are reports of tagged

purification methods involving insertion peptides at the VP2 N terminus or the heparin binding sited within VP3, both of which provide potential reagents for various applications. This study aids in the development of a universal purification method for all AAV serotypes, demonstrates the utilization of this domain as a site for gold particle conjugation, and displays a novel method for vector tropism alteration.

AAV hexa-histidine production and *in vitro* characterization

The HI loop, surrounding the five-fold pore, was chosen as the site of peptide substitution due to the previously established plasticity of this region of the capsid. Without affecting the conserved capsid stabilizing phenylalanine-proline interaction at amino acid position 661, residues 662-667 (VP1 numbering) of the AAV2 capsid were substituted with six histidine residues via PCR. The histidine residues were chosen due to the necessity for the development of a universal purification method of all AAV serotypes. Virus particles generated contained 60 copies of the tag due to its presence in each VP3 monomer. Incorporation of the hexa-histidine motif into the virus capsid did not affect virus titer and transduction based on luciferase assay post infection of 3000 vector genome containing particles per 293 cell (Figure 1). The hexa-histidine tag was also incorporated into the AAV9 capsid at the same location (GeneArt) for further purification characterization.

Affinity column purification of AAV hexa-histidine vectors

The hexa-histidine tag was tolerated by the AAV2 and AAV9 capsid, therefore, it was necessary to determine if these particles could bind a nickel column and be eluted from that column in a pure peak fraction. We first validated virus particle nickel-binding affinities

with Micro Bio-Spin Chromatography Columns (BioRad) packed with nickel-agarose beads (Ni-NTA Qiagen). Beads were incubated with 1E10 vector genome containing particles (cesium chloride gradient purified). Flow through, wash and elution fractions (buffers from Qiagen Ni-NTA kit) were collected and blotted on a nitrocellulose membrane. AAV2 HI6xHis bound the nickel beads and were eluted from the packed column, whereas AAV2 wildtype particles were unable to bind the column based A20 primary antibody staining detecting intact capsids on a nitrocellulose membrane (data not shown).

In order to further assess the nickel binding capabilities of the tagged virus, iodixanol gradient purified virus was loaded onto an FPLC nickel His-Trap HP column (Amersham). Following equilibration, approximately, 1E13 vector genome containing particles of AAV2 HI6xHis were injected onto the column. AAV2 HI6xHis bound to the column and eluted primarily in a peak elution fraction based on FPLC protein detection at 280nm (Figure 2A). In order to confirm the elution of vector genome containing particles q-PCR of the luciferase transgene was performed on each FPLC fraction (Figure 2B). The protein detection in the peak elution fraction directly corresponded with the vector genomes recovered from that fraction. Therefore, viral particles remained intact during the elution from the nickel column. On the other hand, AAV2 wildtype particles did not bind to the column efficiently and primarily eluted in the column wash fractions based on the protein chromatogram and vector genome quantification (Figure 2A and B). To further substantiate the capability of the AAV particle containing the hexa-histidine tag to bind nickel, AAV9 HI6xHis was passed through the nickel column. In corroboration with previous data, AAV9 HI6xHis bound the nickel column and eluted off with 500mM imidazole with a similar chromatographic and vector genome quantification profile as to AAV2 HI6xHis (Figure 2A and B). Collectively,

aforementioned results suggest potential development of a universal purification scheme for AAV vectors.

AAV hexa-histidine particles purity

Additional biochemical analyses were performed in order to further characterize the purity and infectivity of the virus particles eluted from the FPLC nickel column. AAV2 HI6xHis and AAV9 HI6xHis FPLC column fractions (30ul), including the load, were run on a 10% Bis-Tris acrylamide gel (NuPage, Invitrogen). Gels were silver stained with Invitrogen Silver Express and fraction 14, the peak elution fraction from the FPLC column runs involving AAV2 HI6xHis and AAV9 HI6xHis showed pure, concentrated viral protein bands of VP1, VP2 and VP3 as compared to the load control (Figure 3A).

Using a Leo 910 TEM, electron micrographs were taken of the load and peak fractions of AAV2 HI6xHis and AAV9 HI6xHis FPLC column runs. EM images revealed the purity of peak column fractions, potentially slightly increased from the load, and the maintenance of particle gross conformation post column elution (Figure 3B). Not only did virus sample purity increase post nickel column purification (Figure 3A), but also virus infectivity was maintained (data not shown). This data demonstrates that replacing amino acids 662-667 with a hexa-histidine tag is a valid method for AAV universal purification. The hexa-histidine peptide allows for recovery of a pure virus fraction post metal affinity purification (Figure 3A and B). Based on these data, we chose to characterize the virus *in vivo*.

Hexa-histidine nanogold labeling

In addition to the aforementioned studies, we evaluated the potential for exploiting the hexa-histidine tag on the AAV capsid for nanogold labeling in EM application. From Nanoprobes, Ni-NTA-nanogold of 1.8nm in diameter was obtained and incubated in excess with AAV2 and AAV2 HI6xHis virus particles. Post incubation the virus particles were incubated and stained on a copper grid. As expected the Ni-NTA-nanogold particles bound to AAV2 HI6xHis containing the hexa-histidine tag but did not bind the wildtype AAV2 particles that are lacking the tag as detected by electron microscopy (Figure 3C). Therefore, this domain is a novel site to use for gold particle conjugation, and in this case potentially for the purpose of labeling a viral particle as a means to characterize its properties *in vitro*, such as subunit detection, viral particle tracking, or detection in tissue samples for histological analysis.

AAV hexa-histidine vectors are detargeted from the liver

The utilization of the vector as a tool for universal purification is extremely promising but would be further validated by its ability to maintain wildtype properties *in vivo*. Therefore we injected our histidine tag intramuscularly (IM) and intravenously (IV) in order to monitor tropism and transduction levels as compared to wildtype AAV2 particles carrying the luciferase transgene. First, we injected AAV2 and AAV2 HI6xHis IM. Contrary to the *in vitro* data where AAV2 HI6xHis and AAV2 were similar in heparin binding (data not shown) and 293 cell transduction (Figure 1), AAV2 HI6xHis was ten fold lower in muscle transduction than AAV2 as determined by photon quantification (Figure 4A) post animal imaging. Strikingly, AAV2 HI6xHis was unable to transduce the liver post IV injection based on luciferase imaging (Figure 4B).

To further substantiate this data AAV9 and AAV9 HI6xHis was injected via tail vein to analyze transduction capabilities. AAV9 was able to transduce tissue systemically, as defined in the literature (54). However, like AAV2 HI6xHis, AAV9 HI6xHis displayed reduced muscle transduction and was unable to transduce the liver based on photon quantification post live animal imaging (Figure 4C). Based on these data, it is believed that the hexa-histidine tag, is disrupting the ability of the virus to transduce cells *in vivo*. In order to determine if the hexa-histidine tag was altering vector tropism, we generated chimeric vectors containing fewer hexa-histidine peptides on the capsid surface.

With regards to AAV2 H6xHis, we wanted to determine if this mutant was retargeted to another organ or circulating in the blood for a longer period of time than AAV2 due to it being detargeted from the liver. However, what we found was that AAV2 HI6xHis virus has similar vector genome distribution to AAV2 in the lung, heart, spleen and kidney, but not in the liver. AAV2 on average presented five-fold more vector genome copies in the liver than AAV2 HI6xHis (Figure 4D). In addition, AAV2 HI6xHis based on vector genome distribution in the blood at 1, 3, 6, 24, and 48 hours post IV injection, displayed a similar circulation pattern as AAV2. Therefore this mutant is not retargeted to another organ, nor is it circulating in the bloodstream for an extended period of time.

Hexa-histidine chimeras rescue vector tropism

AAV2 HI6xHis contains 60 copies of the hexa-histidine tag, therefore we generated chimeras containing fewer copies. We transfected cells with multiple ratios of pXR2 wildtype to pXR2 HI6xHis, with 1:1 or 4:1, respectively. The ratios are indicators of the amount of VP incorporated containing the tag based on work previously done by Joe

Rabinowitz (107). Therefore capsids will contain approximately 30 wildtype AAV2 VPs and 30 AAV2 HI6xHis VPs or 48 wildtype AAV2 VPs and 12 AAV2 HI6xHis VPs. These chimeras were generated to determine if fewer copies of the hexa-histidine tag on the capsid surface would allow for rescued transduction in the muscle and liver.

Prior to *in vivo* characterization of the chimeras AAV2 1: AAV2 HI6xHis 1 and AAV2 4: AAV2 HI6xHis were passed through the FPLC nickel column to eliminate wildtype particles that may have been generated during virus production. Interestingly, AAV2 1: AAV2 HI6xHis 1 bound and eluted from the column with a similar profile to AAV2 HI6xHis and AAV2 4: AAV2 HI6xHis 1 bound and eluted from the column with an elution profile similar to AAV2 and AAV2 HI6xHis (Figure 5A and 2B). Based on q-PCR of eluted vector genomes, AAV2 4: AAV2 HI6xHis 1 eluted from the column similar to AAV2 HI6xHis in the flowthrough, and then progressively eluted in the wash fractions similar to AAV2, where increased vector genomes were detected (Figure 5A). AAV2 4: AAV2 HI6xHis 1 particles and AAV2 1: AAV2 HI6xHis 1 particles eluted primarily in elution 2 (Figure 5A) as seen with AAV2 HI6xHis and AAV9 HI6xHis (Figure 2B).

Post purification, we injected our chimeric mutants containing fewer copies of the hexa-histidine tags on the capsid surface IM and IV along with AAV2 for comparison. AAV2 1: AAV2 HI6xHis 1, which based on plasmid ratios during transfection of virus production should have 30 monomer copies of AAV2 and AAV2 HI6xHis, behaved similarly to AAV2 HI6xHis intramuscularly (Figure 4B and 5B), demonstrating a ten fold lower transduction as compared to wildtype AAV2 particles post photon quantification (Figure 5D). However, AAV2 4: AAV2 HI6xHis 1 shows similar transduction to AAV2 wildtype particles, with a complete rescue of virus infectivity in skeletal muscle (Figure 5B and D).

Therefore, the reduced number of hexa-histidine peptides on the surface of the capsid allowed for complete rescue of vector transduction in the muscle.

Interestingly, a different phenotype was observed post IV injection via the tail vein. When comparing the 1:1 ratio of AAV2: AAV2 HI6xHis viral particles to the 4:1 ratio there is an increase in liver transduction (Figure 5C), however not to wildtype levels seen with AAV2. Muscle transduction with the 4:1 particles averaged five-fold higher than the 1:1 ratio when 1E10 vector genome containing particles were injected (Figure 5D). Interestingly, AAV2 1: AAV2 HI6xHis 1 liver transduction resembled that of AAV2 HI6xHis (Figure 4B), and there is a slight rescue of liver transduction with the 4:1 chimeric as seen in Figure 5C. The transduction observed with the 4:1 chimeric is not a full rescue as determined by luminescence and vector genome quantification in the liver (Figure 5B and C).

Liver detargeting due to hexa-histidine motif

In addition to the molecular manipulation via the generation of chimeric particles containing fewer hexa-histidine motifs, genetic manipulation was also performed in order to determine if mutation of the HI loop or the number of histidines on the surface was responsible for the observed liver detargeting phenotype. The HI loop was mutated in order to contain fewer histidine residues; 1, 3, and 4, generating AAV2 HI1xHis, AAV2 HI3xHis, and AAV2 HI4xHis, respectively.

These vectors containing the luciferase transgene were injected intramuscularly and intravenously to examine muscle and liver transduction. Post IM injection of 1E10 vector genome containing particles of AAV HI1, HI3, HI4, and HI6xHis in comparison to AAV2 control, it was determined that all vectors containing fewer than six histidines in the HI loop

were able to transduce muscle similarly to AAV2 control (Figure 6A), whereas AAV2 HI6xHis transduced five- to tenfold less efficiently than AAV2 based on photon quantification from animal imaging (data not shown).

Post systemic injection of 1E11 vector genome containing particles of the histidine HI loop mutants, a more remarkable phenotype was observed. AAV2 HI1, HI3 and HI4xHis were able to transduce the liver to the same efficiency as that of AAV2 control, and did not display an ablation of transduction as observed with the AAV2 HI6xHis vector (Figure 6B). These data strongly suggest that the detargeting phenotype is solely due to the presence of the hexa-histidine domain and not mutation of the HI loop or the number of histidines on the capsid surface.

Discussion

Most proteins purified via a hexa-histidine peptide are tagged at the N or C terminus (116, 136) for efficient nickel binding. However, the AAV VP monomer assembles leaving the N and C – termini of the viral protein monomers hidden. The N termini of the VPs are internal to the capsid until triggered by a stage in the virus life cycle to extrude (71) and the C termini are folded within the two-fold axis of symmetry, but are surface accessible. Despite this fact the C-terminus of VP3 was utilized as a site for a poly-histidine insertion in the AAV capsids for universal purification (165). This was an advancement in the field towards the development of a purification method, requiring the need for multiple construct transfection in order to produce VP1 and VP2 without the presence of the tag. It would be

beneficial to carry the research further and determine if insertion into this location affects natural virus tropism and structure.

In efforts to characterize specific regions on the AAV capsid, many researchers have identified locations on the capsid surface that could tolerate peptide insertions in order to redirect vector tissue tropism. For instance, in 2000 one of the first studies executed, determined key spots on the capsid surface, including loop regions and the N-terminus of VP1 and VP2 as sites that can accept insertions, specifically the HA epitope (156). Since this finding was prior to the determination of the AAV2 crystal structure (163), it was believed that if regions could tolerate these peptides, by retaining AAV wildtype phenotype and gaining HA binding capabilities, they were most likely surface loops, giving the AAV community insight as to what regions of the capsid were surface exposed. Also, in doing so, the potential sites for heparin binding were determined, due to the generation of insertion mutants with decreased infectivity and heparin binding capabilities. Therefore, this study alone, was a gateway for determining sites that could tolerate insertions and key functions of various locations on the capsid surface.

After these studies, there was a surge in studies involving AAV2 retargeting. An early study involved tumor-targeting peptides and their incorporation into two putative loops on the AAV surface at amino acid positions 449 and 588. Loop replacements or substitutions were also generated, but the loop insertions outperformed the replacements based on biochemical assays. However, it was determined that altering these two sites on the capsid surface ablated heparin binding and allowed for virus retargeting (43). In a similar study (119), altered AAV2 vectors with insertion peptides on the capsid surface, again eluding to regions on the capsid that might be responsible for heparin binding. Not only were capsid

insertions used to determine sites of receptor interaction but also sites of capsid immunogenicity, which based on studies converges with the heparin binding site (53, 137). After the resolution of the AAV2 crystal structure (160) it was confirmed that the three-fold is on the surface and combined with data from above can tolerate peptide insertions (88, 101, 148, 149, 154).

The three-fold was an obvious choice for peptide insertion for virus retargeting based on the toleration of insertions and ablation of heparin binding. However, in our study it was important to maintain heparin binding properties due to the necessity of AAV2 phenotypic retention. Therefore, based on work performed at the five-fold axis (24) it grew apparent that this site, specifically the HI loop, could tolerate change. The positions in which to place the tag were chosen based on previous work performed in our laboratory. The six variable residues after the conserved F661 were substituted with six histidines prior to the start of the conserved portion of the loop as it enters the beta sheet within VPs. Therefore, all subunits contained the hexa histidine peptide, being present 60 times on the capsid surface.

Instead of inserting a peptide, this is the first published account of the capsid tolerating a peptide substitution at a prominent surface loop and its utilization for multiple applications. The HI loop was an obvious choice based on its apparent inability to affect virus tropism and the potential to tolerate amino acid changes (24). The substitution of this region with histidines did not affect AAV2 wildtype properties such as titer, infectivity (Figure 1), and overall gross conformation based on EM analysis. Therefore, we decided to characterize this mutant with regards to vector purification.

The viral vectors were purified on a nickel column via FPLC. AAV2 was unable to bind the column efficiently as expected, and mostly eluted in the sample

injection/flowthrough fractions, whereas AAV2 HI6xHis and AAV9 HI6xHis eluted primary in peak elution fraction 2. Interestingly, capsids containing the histidine tags eluted from the column in elution fraction 2, being the optimal location for peak virus elution based on vector genome quantification and protein detection (Figure 2). When calculated, AAV2 HI6xHis vector recovery in the peak elution fraction was approximately 39% of the total preparation loaded, but further optimization might be required in order to determine the optimal flow rate and column size for vector recovery.

It is clear that AAV2 and AAV9 vectors containing the hexa-histidine tag can be purified via nickel column. To check vector purity we analyzed the FPLC fractions via silver stain. AAV2 and AAV9 HI6xHis both displayed vector purity in the peak elution fraction (elution 2), corresponding to the peak fraction vector genome containing fraction (Figure 2A and 3B). To further characterize vector purity, electron microscopy was performed on the load and peak elution fractions. Based on EM it is apparent that iodixanol purification is clean, as seen in Figure 2, but FPLC nickel column purification post iodixanol gradient slightly improves vector purity due to the presence of fewer cellular contaminants (Figure 3B). In addition to this data, AAV2 HI6xHis peak elution fraction is similar in infectivity to its load fraction (data not shown). Additionally, the hexa-histidine tag on the virus particle allows for conjugation of a Ni-NTA nanogold particle for capsid labeling. This reagent may prove useful for the ability to follow the viral particle through the cell and understand capsid trafficking via electron microscopy.

Post *in vitro* characterization and validation we injected these vectors *in vivo* for further assessment. Earlier Koerber et al. (68) demonstrated the ability of the AAV2 capsid to tolerate a hexa-histidine insertion at the three-fold heparin binding site. This insertion

decreased heparin binding capabilities due to its location, but when tested in the brain, proved to be functional (68). Indeed, it has been shown that vectors that do not bind heparin, display increased vector spread in the CNS (19). However, it is unclear how the vector would behave in other organs and/or the bloodstream, and if placement of the histidine tag in another location on the capsid would alter the *in vivo* tropism profile.

In the current study, we first injected AAV2 and AAV2 HI6xHis IM. Based on luciferase imaging AAV2 HI6xHis transduced the muscle ten-fold lower than AAV2 (Figure 4A). Knowing that AAV2 transduces the liver, we wanted to examine the behavior of AAV2 HI6xHis post systemic injection (31). Along with the reduced transduction of the muscle tissue seen with AAV2 HI6xHis there appeared to be no liver transduction of AAV2 HI6xHis. From this data it was apparent that the presence of sixty hexa-histidine tags on the capsid surface was altering the ability to enter tissues. In congruence, AAV9 HI6xHis produced similar results. AAV9 HI6xHis was unable to transduce the liver and displayed decreased muscle transduction as compared to AAV9, which transduces systemically post IV injection (Figure 4C).

In order to determine if the hexa-histidines were altering vector transduction and tropism, chimeric vectors were generated (40, 107) containing fewer tags than 60 on the surface, approximately 30 and 12 based on transfection ratios. As expected AAV2 1: AAV HI6xHis 1 displayed a similar elution profile to AAV2 HI6xHis from the nickel column, presumably due to the number of hexa-histidine peptides on the capsid surface. Whereas, AAV2 4: AAV2 HI6xHis 1 displayed a similar elution profile to AAV2 in the wash fractions, due to the prevalence of more wildtype VPs and less hexa-histidine tags on the capsid surface based on transfection ratios during virus production.

Post purification we injected mice IM and IV with the chimeras. Strikingly, post IM injection of the AAV2 4: AAV2 HI6xHis 1 chimera, there was a complete rescue of virus infectivity, based on animal imaging. However, in the liver there was only a partial rescue of transduction with the AAV2 4: AAV2 HI6xHis 1 chimera based on imaging and vector genome quantification (Figure 5B and C).

There may be multiple reasons for this disparity. It was considered possible that the presence of the histidine residues in the HI loop could be altering receptor interactions that may be occurring with this region of the capsid. Based on the ability of AAV2 HI6xHis to bind heparin with a similar affinity as AAV2 (data not shown) and earlier studies (24) we did not believe this to be the case. However, to further prove that the HI loop is not involved in receptor binding, we substituted the HI loop with a decreasing number of histidine residues, 4, 3, and 1, and all mutants were able to transduce the muscle similarly to AAV2. Additionally all mutants were able to transduce the liver as well as AAV2, unlike AAV2 HI6xHis (Figure 6A and B). Therefore, the HI loop does not seem to be playing a role in receptor binding in the context of AAV2 in the muscle and liver. In addition, from these experiments, it was determined that it is not the number of histidines on the capsid surface that is causing the liver detargeting phenotype, but solely the hexa-histidine motif. This was concluded from the *in vivo* data involving AAV2 HI4xHis and AAV2 4: AAV2 HI6xHis 1 vectors. AAV2 HI4xHis contains a total of 240 histidines on the capsid surface and is able to transduce the muscle and liver similarly to AAV2 (Figure 6), whereas AAV2 4: AAV2 HI6xHis 1 contains approximately 72 histidines on the capsid surface and is unable to transduce the liver to the same efficiency as wildtype (Figure 5C).

In order to further assess the observed phenotypes we performed capsid stability assessments in mouse blood and also hepatocyte binding studies *ex vivo* (Figure 7A and B). Interestingly, we were unable to demonstrate the inability to bind hepatocytes as potentially seen *in vivo* with genome quantification post liver harvestation (Figure 5D). When capsids were incubated with blood, and then parenchymal cells for cell surface binding, there was no difference between control AAV2 and AAV2 HI6xHis and AAV2+blood and AAV2 HI6xHis+blood (Figure 7B). Therefore, mouse blood, in an *ex vivo* setting was not affecting viral particle binding, however, this may be due to the fact that the ratio of virus particles to blood *ex vivo* was much greater than it would be *in vivo*. Knowing that binding to hepatocytes in this system was unaffected, particle stability in blood was assessed. AAV2 and AAV2 HI6xHis vector genome containing particles were incubated with blood for 30mins at room temperature and then treated with DNase. Compared to control particles incubated with DNase, there appeared to be a slight drop in quantified vector genomes post DNase treatment of AAV2 and a more remarkable decrease in vector genome copies of AAV2 HI6xHis (Figure 7B). Therefore it stands to reason that the AAV2 HI6xHis virus particles may have an altered conformation in the blood leading to a less stable particle, ablating its ability to efficiently infect certain tissues *in vivo*.

It is known that histidine residues chelate ions such as copper, cobalt, nickel, cadmium, and calcium (15464) in the context of histidine rich calcium binding protein (HRC) (65, 113) in mice. Interestingly, bis-histidine stimulates the uptake of cobalt, cadmium and zinc into erythrocytes (50), all ions being present in the blood plasma. Therefore, it is quite possible that post intravenous administration, the capsids, which are covered in histidine residues are chelating ions in the bloodstream, preventing the capsids

from successfully entering the liver. The capsid binding to ions may induce a conformational change at the three-fold, inhibiting primary receptor recognition for cellular entry. For example, ions induce a conformational change in the HIV virion infectivity factor affecting protein aggregation (100) and hepatitis B virus capsid protein affecting capsid assembly (127).

In addition to HRC, HRG (histidine rich glycoprotein), whose exact function is unknown, binds heme, divalent metal ions (86), heparan sulfate (11), plasminogen (12), thrombospondin (74), insoluble IgGs (37) and may be involved in blood coagulation (134). Therefore, it is possible that when the his tagged AAV capsids are in contact with blood, they may be participating in interactions with any of the aforementioned molecules. These interactions may be affecting particle stability in the bloodstream and/or generating large complexes unable to enter the hepatocytes, and are rather being degraded following uptake by Kupffer cells. This may explain why AAV2 HI6xHis and the AAV2/AAV2 HI6xHis chimeras are able to transduce the muscle and not the liver as efficiently.

This unique phenotype may allow for vector development, specifically for diseases where the liver is not a target organ. Therefore the AAV9 HI6xHis virus might be a potential candidate for further development as a vector since it retains the ability to transduce multiple organs with the exception of the liver.

We have located a novel site on the virus capsid that can be utilized for substitution with a hexa-histidine motif. This motif can be used for viral protein purification. Additionally, the hexa-histidine motif present on the capsid surface can be used for gold particle conjugation for EM applications. Finally, by altering the ratio of hexa-histidines on the capsid surface, it is possible to modulate tissue tropism, where we can control liver

targeting. In summary, HI loop substitution with a hexa-histidine motif generates multifunctional AAV capsids important for the advancement of tools in gene therapy applications

Acknowledgments

I would like to thank Xinghua Zeng at the UNC-CH Vector Core for assistance with the FPLC and Victoria Madden at the UNC-CH Microscopy Labs for assistance with nanogold staining optimization.

Figure 1. Substitution of the AAV2 HI loop with a hexa-histidine motif

A.

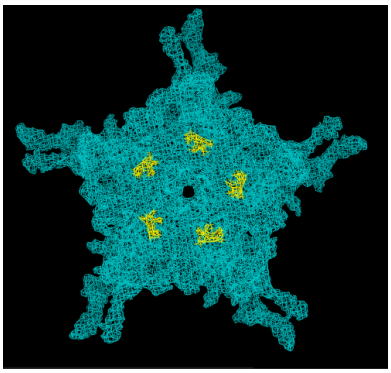

AAV2 (658) STTFSAAKFA
AAV2 HI6xHis (658) STTFHHHHHH

B.

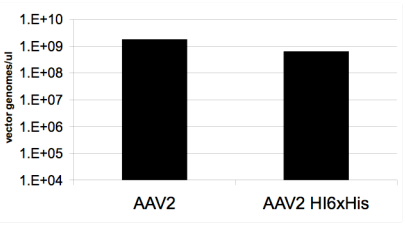

C.

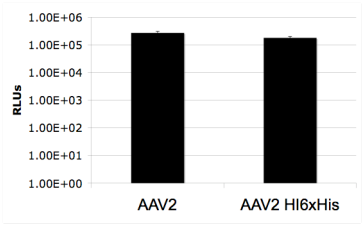

Figure 1. Substitution of the AAV2 HI loop with a hexa-histidine motif. (A) Model of the AAV2 capsid pentamer using MacPymol (http://pymol.sourceforge.net/). The HI loop, amino acids 662-667, is substituted with six histidine residues as depicted by the model of the five-fold axis (left) and the sequence alignment (right). (B) AAV2 HI6xHis titer was determined via q-PCR of the luciferase transgene and compared to AAV2 wildtype titer. (C) AAV2 and AAV2 HI6xHis transduction was quantified via luciferase assay of 293 cells infected with 3000 vector genomes per cell (N=3 SD=black bars).

Figure 2. Affinity chromatography purification of AAV capsids

A.

AAV2 HI6xHis AAV9 HI6xHis

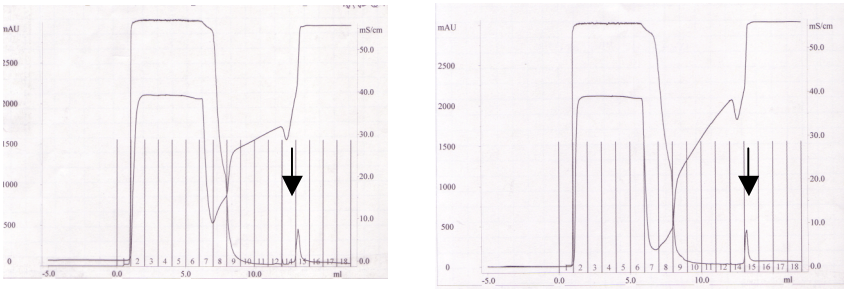

B.

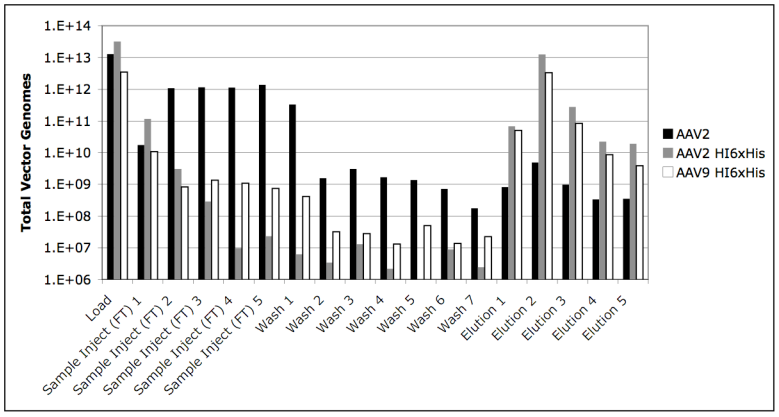

Figure 2. Affinity chromatography purification of AAV capsids containing the hexa-histidine motif. (A) AAV2 HI6xHis (left) and AAV9 HI6xHis (right) was purified via metal affinity chromatography through a 1ml His-Trap HP nickel column (Amersham). At a wavelength of 280nm the FPLC detector determined the peak protein elution fraction. An arrow indicates the peak elution fraction of virus protein from the column. (B) Vector genome quantification of AAV2 HI6xHis and AAV9 HI6xHis nickel column fractions as compared to AAV2. Approximately 1E13 vector genome containing particles were loaded in the injection loop and injected across the nickel column. Total vector genomes in each column fractions were quantified via q-PCR against the luciferase transgene.

Figure 3. Vector purity and gold particle labeling

A.

AAV2 HI6xHis

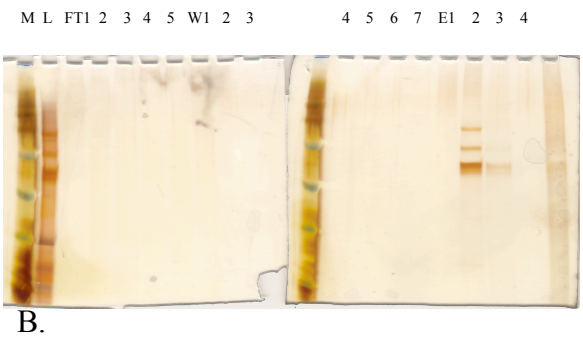

AAV9 HI6xHis

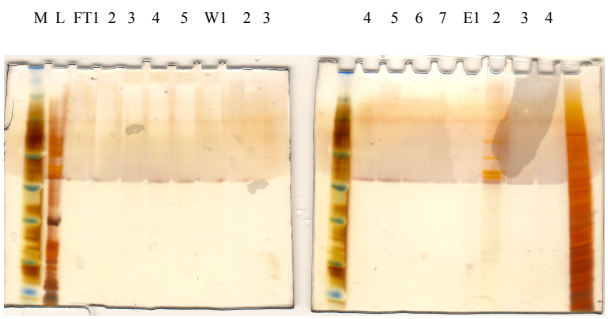

B.

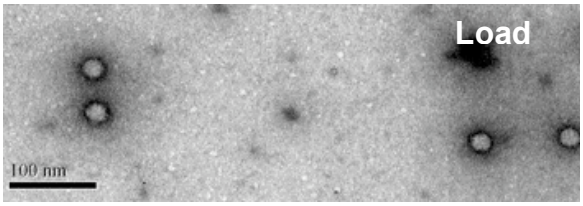

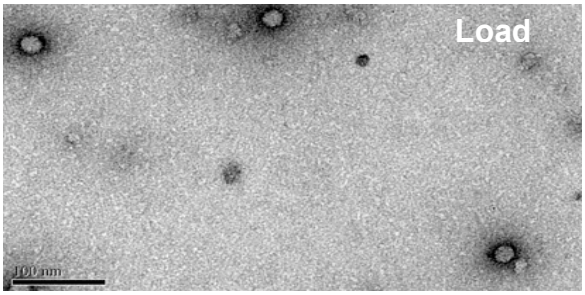

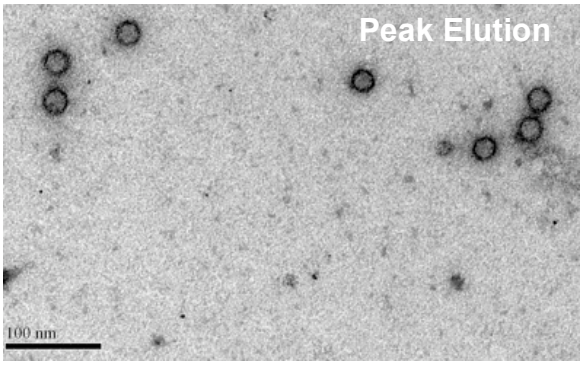

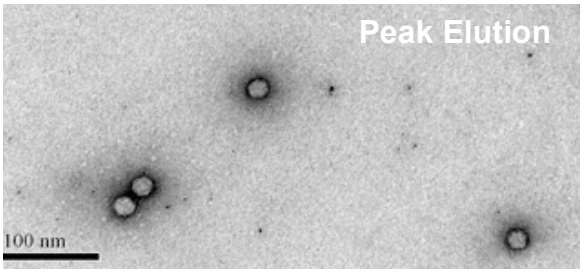

C.

AAV2

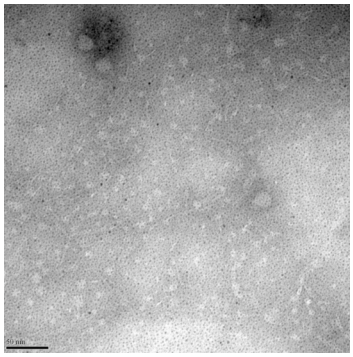

AAV2 HI6xHis

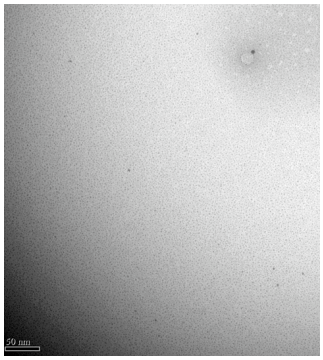

AAV2 HI6xHis

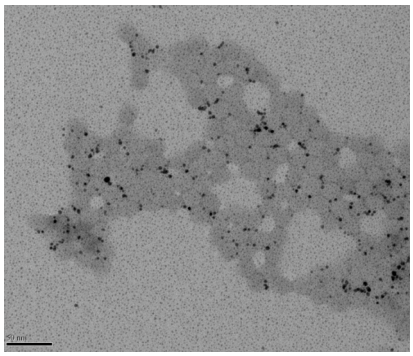

Figure 3. Vector purity and nanogold particle labeling. (A) Silver stain analysis of AAV2 HI6xHis and AAV9 HI6xHis nickel column fractions. 30ul of the load (L), flowthrough (FT), wash (W) and elution (E) fractions were loaded onto a NuPage gel (Invitrogen). Protein was detected via Silver Express (Invitrogen). (B). EM analysis of viral particle purity post nickel column purification. 15ul of AAV2 HI6xHis (left) and AAV9 HI6xHis (right) load and peak elution fractions were incubated on glow discharged carbon coated copper grids. (C) EM analysis of Ni-NTA gold particle labeled AAV2 HI6xHis capsids. AAV2 (left) and AAV2 HI6xHis (right) were incubated with Ni-NTA nanogold particles (Nanoprobes).

Figure 4. Hexa-histidine vectors detarget the liver

A.

AAV2 AAV2 HI6xHis

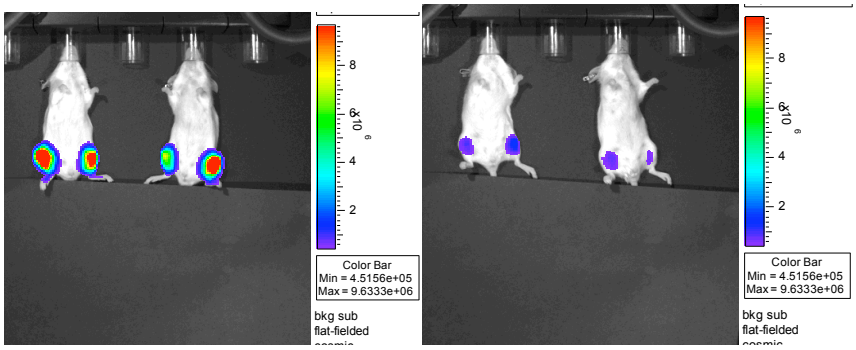

B.

AAV2 AAV2 HI6xHis

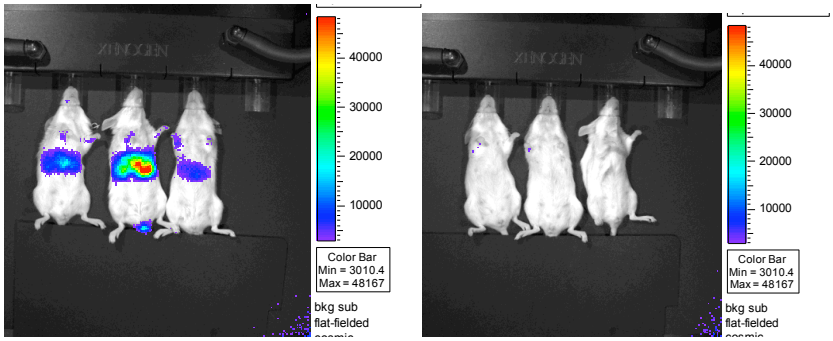

C.

AAV9 AAV9 HI6xHis

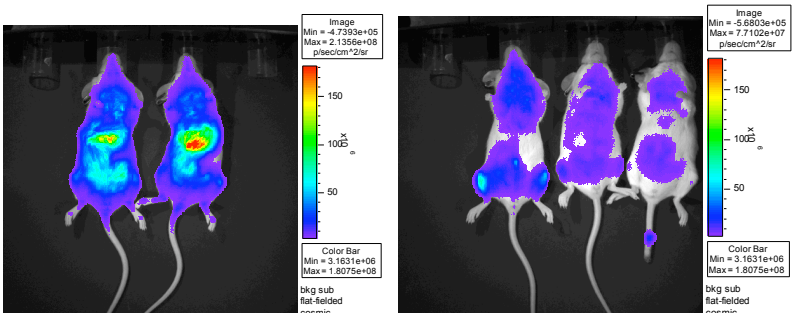

D.

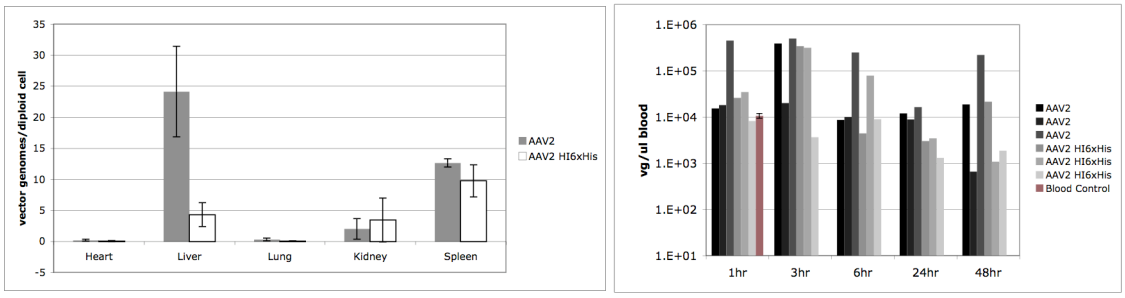

Figure 4. Hexa-histidine vectors detarget the liver. (A) 1E10 vector genome containing AAV2 and AAV2 HI6xHis were injected intramuscularly and (B) intravenously. Two weeks post vector administration mice were injected IP with D-luciferin firefly luciferase substrate (Nanolight) and imaged for 1minute or 5minutes, respectively via an IVIS Xenogen imaging system 5minutes post substrate administration. (C) 1E11 vector genome containing particles of AAV9 and AAV9 HI6xHis were injected intravenously and imaged as mentioned above. (D) AAV2 and AAV2 HI6xHis vector genomes were quantified in multiple organs via q-PCR of the luciferase transgene 48hrs post systemic injection (left panel) and in the blood post systemic injection at 1, 3, 6, 24 and 48hrs post systemic injection (right panel). SD=black bars N=3.

Figure 5. Chimeric hexa-histidine vectors rescue tissue transduction *in vivo*

A.

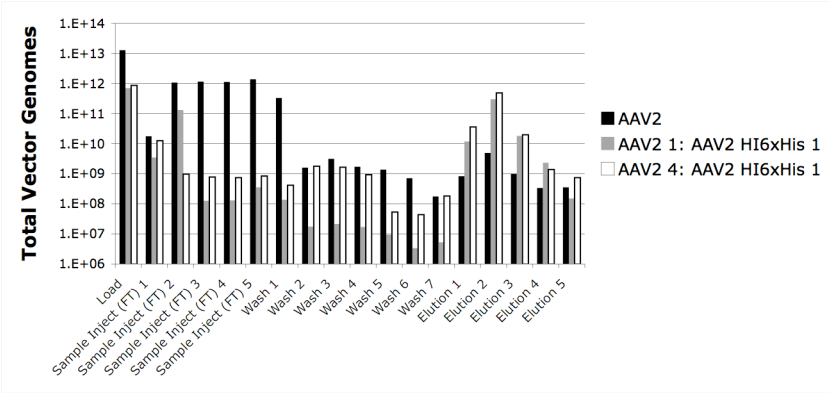

B.

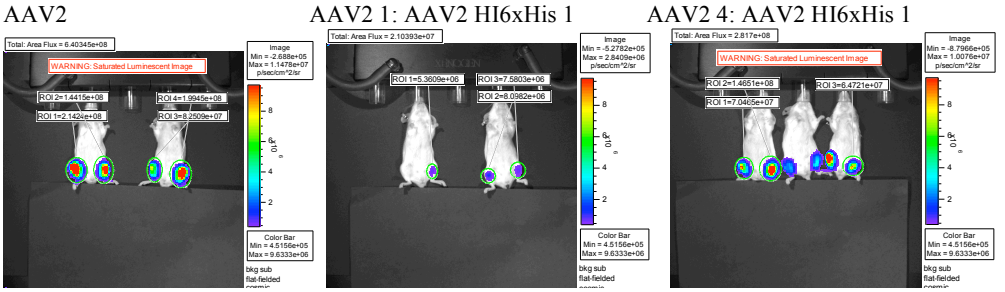

C.

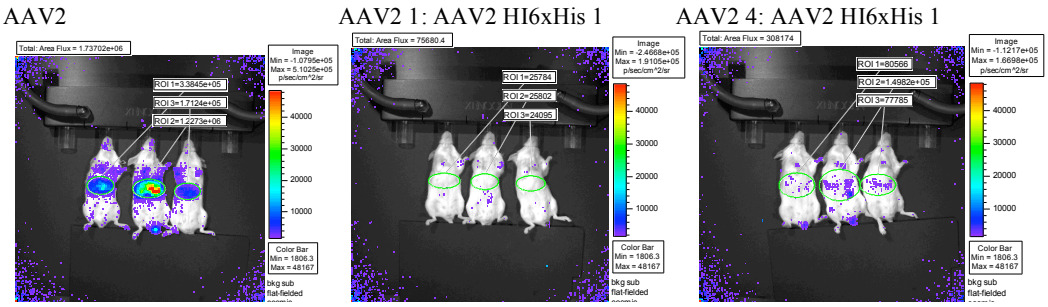

D.

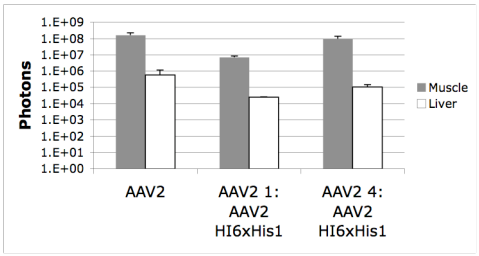

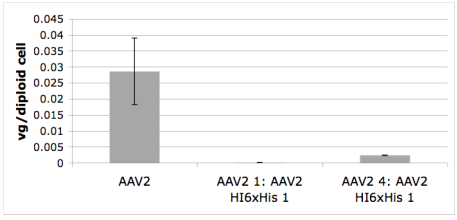

Figure 5. Chimeric hexa-histidine vectors rescue tissue transduction *in vivo*. (A) 1E12 vector genome containing AAV2 1: AAV2 HI6xHis 1 and AAV2 4: AAV2 HI6xHis 1 chimeras were passed through the FPLC nickel column. Flowthrough (FT), wash (W), and elution (E) column fractions were collected and vector genomes in each fraction were quantified via q-PCR of the luciferase transgene. (B) 1E10 vector genome containing AAV2 1: AAV2 HI6xHis 1 (middle) and AAV2 4: AAV2 HI6xHis 1 (right) were injected intramuscularly into the right and left gastrocnemus. Animals were imaged as described previously and photons were quantified via Living Imaging 2.5 Software. (C) 1E10 AAV2, AAV2 1: AAV2 HI6xHis 1, and AAV2 4: AAV2 HI6xHis 1 vector genome containing particles were injected intravenously. Two weeks post IV injection the mice were imaged as described above. (D) Photons emitted post IM and IV injection were quantified and graphed (left panel). Liver tissue was harvested 2 weeks post IV injection and vector genomes present in the liver post IV injection were quantified via q-PCR with primers against the luciferase transgene (right panel). The m-lam gene present in the sample was quantified as a control. N=3 or 4 and SD=black bars.

Figure 6. HI loop replacement with fewer histidines does not alter virus transduction

A.

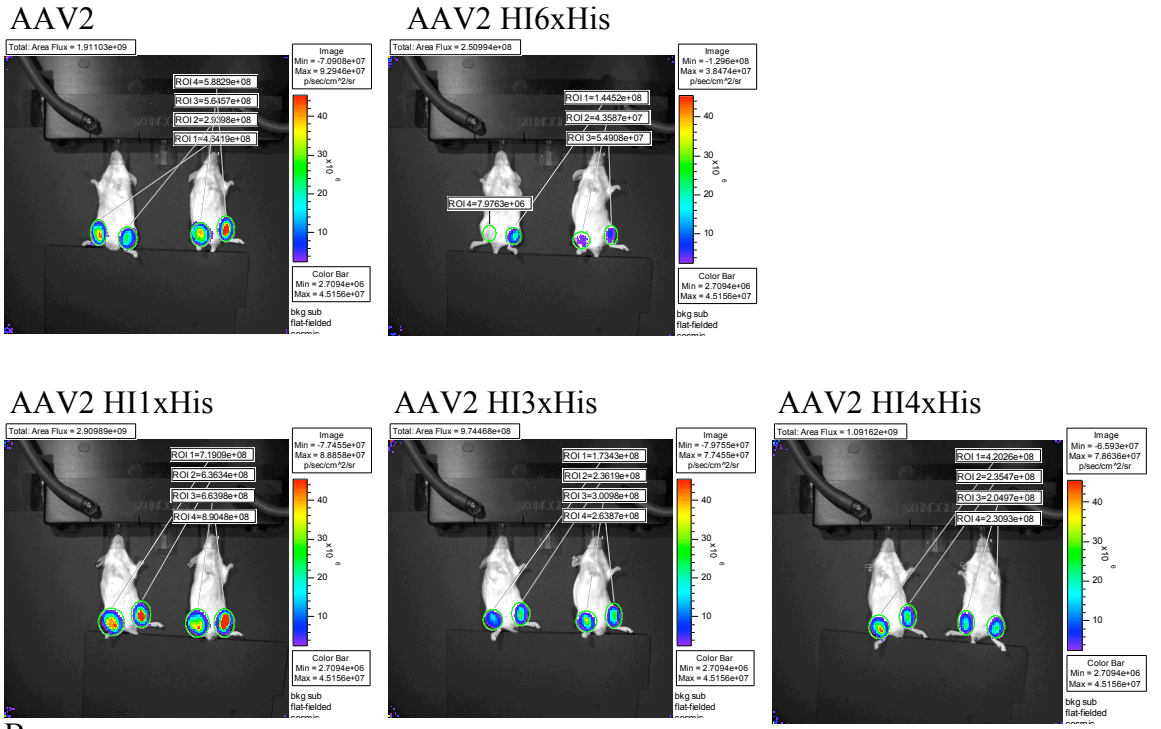

B.

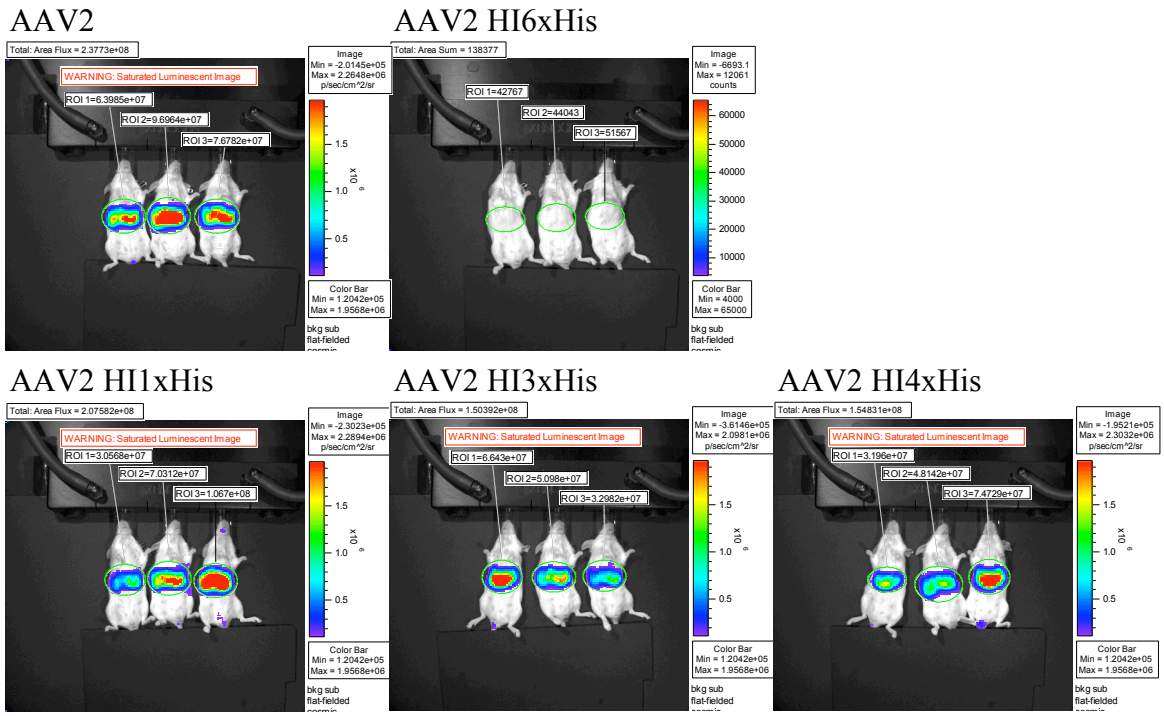

Figure 6. HI loop replacement with fewer histidines does not alter virus transduction. (A) 1E10 vector genome containing particles of AAV2, AAV2 HI6xHis, AAV2 HI1xHis, AAV2 HI3xHis and AAV2 HI4xHis were injected intramuscularly and mice were imaged three weeks post injection as described previously. (B) 1E11 vector genome containing particles of AAV2, AAV2 HI6xHis, AAV2 HI1xHis, AAV2 HI3xHis and AAV2 HI4xHis were injected systemically and also imaged three weeks post injection as previously mentioned.

Figure 7. AAV2 HI6xHis displays an altered phenotype in the presence of blood

A. B.

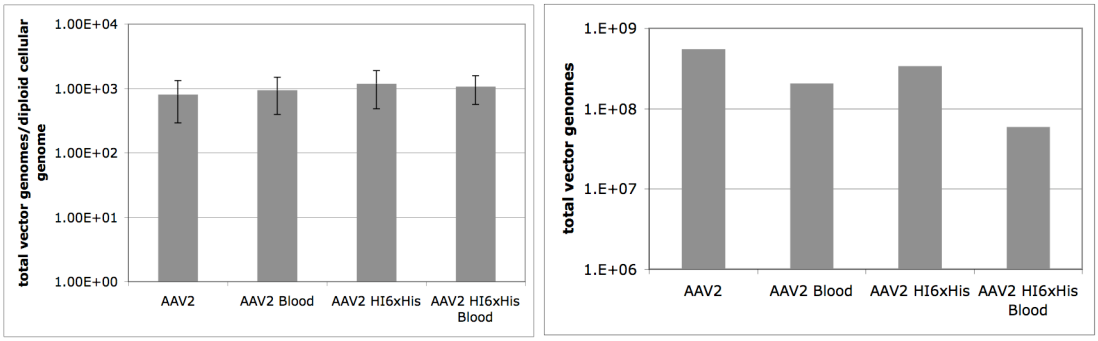

Figure 7. AAV2 HI6xHis displays an altered phenotype in the presence of blood. (A) 1E10 vector genome containing particles of AAV2 and AAV2 HI6xHis were incubated with serum for 30minutes at room temperature and were then incubated with isolated mouse hepatocytes for 1hour at 4°C. Hepatocytes were pelleted and washed with 1X PBS and vector genomes bound to the cells were quantified via q-PCR with primers specific to the luciferase transgene. (B) 1E10 vector genome containing particles of AAV2 and AAV2 HI6xHis were incubated with mouse blood for thirty minutes at room temperature and then with DNase for 1hour at 37°C. Total vector genomes were quantified via q-PCR as mentioned previously post DNase treatment and DNA isolation.

CHAPTER IV

Redefining the dead zone

Abstract

By characterizing surface domains on the AAV capsid, we are able to gain insight on capsid regions required for specific stages in the life cycle. In order to utilize AAV to its full potential as a viral vector, more has to be learnt about the vector as a virus. In previous research, I uncovered a domain on the capsid crucial for maintaining primary contacts at the five-fold axis necessary for proper viral assembly (24). Determining this not only shed light on AAV biology but also regions of the capsid that are or are not amenable to manipulation for uses in gene therapy. Therefore, it was necessary to further characterize other surface loops in order to uncover more about the AAV life cycle and advance developments in vectorology. Based on the literature and previous research in the lab (Bowles unpublished), the surface loop I between the five-fold and two-fold axis a region in the dead zone became an obvious choice due to its potential roll in virus infectivity (79, 156). A series of AAV2 insertion and AAV1 substitution and deletion mutants in surface loop I amino acid 265 were generated. It was determined that alteration of this position lead to a series of mutants with enhanced tissue transduction in muscle and liver tissues. This observation was further substantiated by the insertion of an amino acid into position 265 of a vector unable to transduce the liver (AAV2i8), which completely rescued its detargeted phenotype. Via further analyses, it was determined that the mutations led to a gain of function at the cellular entry level, aiding in the development of vectors with enhanced transduction capabilities for efficient gene delivery.

Introduction

As determined by the AAV2 crystal structure (163) the two-fold axis of symmetry is the weakest region of the AAV capsid based on amino acid contact energies. Additionally, it is not a region of topological variance between serotypes, unlike the three-fold axis, which is necessary for host cell receptor recognitions due to the variability of the three-fold peaks. Furthermore, the region between the two-fold and five-fold axes has been deemed the dead zone, for it has been involved in multiple mutagenesis studies determining that mutation to this region is detrimental to virus transduction even though the capsid does not utilize this region to interact with heparan sulfate primary receptor (79, 156). Recent cryo-EM analysis has further substantiated this fact via capsid-heparin footprint analysis (94), however, this observation does not rule out the possibility of this region interacting with co-receptors on the cell surface or being involved in other stages in the AAV life cycle.

During the realization that this region was not involved in receptor recognition, it was uncovered that this area was playing a role in a specific stage of the virus life cycle, infectivity. One mutagenesis study by Lochrie et. al. (79), demonstrated that mutation of the dead zone loop led to increased viral transduction. Specifically, mutation of S267 to A or T increased transduction four-fold to nine-fold respectively. Other mutations to the dead zone decreased virus transduction without affecting heparan binding. Additionally, in another mutagenesis study (156), involving this surface loop generated non-infectious particles, or particles that were partially defective in infectivity and lacking A20 antibody recognition.

Recently, a study also confirmed this general region as a hot spot on the capsid surface (168). The authors mutated all surface tyrosine residues to phenylalanines, due to the possibility of capsid tyrosine phosphorylation, and the necessity to determine the role of

capsid phosphorylation in the virus life cycle. Specifically tyrosine 730 at the two-fold axis of symmetry, in close proximity to the 265 surface loop, participates in virus transduction upon mutagenesis. Alteration of this single tyrosine increased virus transduction in specific tissue types and further research is being performed to determine the mechanism.

Additionally, research from our lab by Dawn Bowles (unpublished) determined that 5 residues in the AAV1 capsid were necessary for the increased muscle transduction as compared to AAV2. Amino acids in AAV2 were mutated to those present in the two-fold and between the two and five-fold of the AAV1 capsid, increasing AAV2 muscle transduction *in vivo* and decreasing AAV2 neutralizing antibody recognition. This mutant was deemed AAV2.5 and is currently in clinical trial for muscular dystrophy. However, the mechanisms leading to the observed phenotypes from the aforementioned mutations remain unknown. Therefore, in this study we characterized the loop between the two- and five-fold (surface loop I) in hopes to further understand the mechanism of increased transduction. Specifically, we characterized position 265 on the AAV2 capsid, obtaining striking results with regards to transduction in specific tissues. Due to the studies mentioned above and the research that will be presented in Chapter 4 of this dissertation, this region of the capsid is no longer the "dead zone," but a hot zone that upon mutagenesis results in remarkable levels of increased virus transduction in multiple AAV backgrounds.

Materials and methods

Generation of mutants

All constructs were generated in the pXR2, pXR2 2i8 or pXR1 backbone. Site directed mutagenesis (Stratagene QuikChange Site-Directed Mutagenesis kit) was used in order to insert or substitute point mutations or delete existing nucleotides.

Virus production

Virus was produced using the triple transfection method developed in our lab as described in Xiao *et. al.* 1998 (159). Cells were transfected with pXR2, pXR2i8 or pXR1 containing the capsid mutations, pXX6-80 helper plasmid, and pTR-CBA-Luciferase containing the luciferase reporter transgene flanked by terminal repeats. Cells were harvested 60hrs post transfection and purified using cesium chloride gradient density centrifugation for 5hrs at 65,000 rpm or overnight at 55,000rpm. Gradients were fractionated and virus dialyzed against 1X PBS supplemented with calcium and magnesium. Viral titers were determined by q-PCR with primers specific to the luciferase transgene.

Western dot blot, heat treatment, and western blot

Production of empty and full capsids was determined post transfection by loading 2ul of the virus fractions onto a nitrocellulose membrane in a dot blot apparatus. Membranes were blocked in 10% milk in PBS for 30mins at RT and incubated with A20 primary antibody (dilution 1:20) (153) in 2% milk for 1 hour at RT. Membranes were washed 5 times with 1X PBS and incubated with goat anti-mouse horseradish peroxidase-conjugated secondary antibody (Pierce dilution 1:5000) for 30mins. The membranes were washed as described above, and capsid production was visualized using the SuperSignal West Femto

Maximum Sensitivity Substrate chemiluminescence kit from Pierce. To examine VP1 exposure, capsids were heat treated at a range of temperatures (Results) and blotted onto a nitrocellulose membrane through a dot blot apparatus. The membrane was incubated as described above except A1 (1:20) and B1 (1:20) (153) primary antibodies were used to detect VP1 exposure and capsid viral protein dissociation upon heat treatment, respectively. For western blotting approximately 1E10 dialyzed vg containing particles were mixed with NuPAGE LDS sample buffer (Invitrogen), run on a NuPAGE gel (Invitrogen), transferred to a nitrocellulose membrane (Invitrogen) and blotted as described above.

Cell culture

C2C12 muscle cells were cultured with DMEM 10%FBS. Cells were plated in 12 well plates and differentiated with DMEM 10%Horse serum. HUVEC (human umbilical vein endothelial cells), C166 yolk sac/vascular endothelial cells, and MEC (mouse myocardial endothelial cells) were obtained from Cam Patterson's laboratory at the University of North Carolina at Chapel Hill. The C166 and MEC lines were cultured with High Glucose DMEM and 10%FBS (Gibco). The HUVEC line was cultured in EBM-2 (Lonza).

***In vitro* transduction assays**

Viral transduction was characterized in multiple cell lines. Cells were infected with dialyzed virus. 293 and C2C12 cells plated at a density of 4E5cells/well were infected with 3000 vector genome containing particles. HUVEC, C166 and MEC cells lines were infected with 1000 vector genome containing particles per cell. 24hours post infection media was

removed from the wells and cells were lysed with 1X passive lysis buffer (Promega). Luciferin substrate was added to the cells (Promega Luciferase Assay Kit) and relative light units were collected using a Victor 2 luminometer.

In vivo infectivity

AAV2 and AAV1 variants carrying the CBA-luciferase transgene were injected into mice at varying viral genome amounts. Female Balb/C mice were injected with AAV2, AAV1 265 and AAV2i8 265 mutants. AAV2 and AAV1 265 mutants were injected intramuscularly at 1E10vector genome particles unless indicated otherwise. AAV2 2i8 was injected tail vein for systemic transduction at a titer of 1E11 vector genome containing particles. Mice were injected with D-luciferin substrate (Nanolight) and 5mins post injection were imaged in the Xenogen IVIS system. Images were quantified using the Igor Pro 3.0 software. Animals were imaged for multiple exposure time durations and timepoints post viral injection as indicated in the Results.

In vitro uncoating Assay

Female Balb/C mice were injected with 1E10 vector genome containing particles of AAV2 and AAV2 265D carrying the GFP transgene in the gastrocnemus muscle. Mice were perfused with 4% paraformaldehyde and muscle tissue was harvested at 24hrs, 48hrs, 72hrs and 1week post injection. Muscle tissue was fixed in 4% paraformaldehyde for 48hrs and then maintained in 30% sucrose. Muscle tissue was homogenized via three freeze/thaws and mortar and pestle grinding. Half of the tissue was sonicated and treated with DNase at 37C for 1hour. All preparations were incubated with Proteinase K and ATL lysis buffer from the

Qiagen DNeasy Blood and Tissue Kit. Total vector genomes per mg tissue was determined via q-PCR with primers specific to the GFP transgene.

PC and NPC separation

Mice were injected with 1E10 vector genomes of AAV 265 insertion mutants. Two weeks post IV injection, hepatocytes were isolated from mouse liver post liver perfusion with 20ml collagenase at a concentration of 2.5mg/ml in 1XPBS. The liver was spun in 1X PBS for 2hours at 4°C until cells were in suspension. Cells were pelleted at 2500rpm for 5min and 20ml of supernatant was disposed. Cells were resuspended in remaining 20ml and aliquots were pipetted into 1.5ml eppendorf tubes. They were spun at 50g for 4min to pellet the PCs (parenchymal cells) and the supernatant was transferred to a new tube for NPC harvesting. The PCs were resuspended in 1X PBS and both PC and NPC tubes were spun at 50g for 4min. The PC supernatant was removed and cells were again resuspended in 1X PBS and the NPC supernatant was transferred to a new collection tube. Both PCs and NPCs were spun at 250g for 4min and the PC supernatant was removed and pellet frozen and the NPC supernatant was further spun intensely on a desktop microfuge in order to pellet the NPCs. The genomes were quantified via q-PCR against the luciferase transgene and the mouse lamin gene as a control.

Results

In this study we characterized the dead zone loop (surface loop I) on the capsid surface (Figure 1), as it pertains to virus transduction *in vitro* and *in vivo*. As mentioned

previously, this region of the capsid in the past, did not warrant much attention due to its lack of participation in receptor recognition like the three-fold loops, and viral genome packaging, viral assembly, and potential Rep binding like the five-fold axis. Mutagenesis studies in the distant and recent past have described this surface loop as being important in viral transduction, altering virus infectivity upon mutation. Strikingly, multiple studies describe specific positions within this region, that upon mutation to alternate amino acids increase transduction significantly. In this study we further characterize this region of the capsid for a greater understanding of the contribution of this region of the capsid to AAV biology and vectorology.

In vitro characterization of AAV2 265 mutants

All amino acids were inserted into amino acid position 265 of the AAV2 capsid in order to determine the phenotype described by AAV2 265T transduction. It was unclear as to if the increase in transduction was due to the specific threonine amino acid inserted into the position or if it was a phenotypic product of mutating the 265 position within the surface loop. Therefore, all twenty amino acids were inserted into this position and mutants were characterized biochemically via titer, western dot blot, western blot and cell infectivity analyses. Titer was quantified via q-PCR of the produced mutants. Viral titers between mutant capsids were equivalent to each other. However, all titers were slightly lower than AAV2 wildtype. Post titer evaluation, the mutant capsids were western blotted in comparison to AAV2 in order to determine if the viral proteins were incorporated into the capsid at the expected 1:1:10 ratio. All AAV2 265 insertion mutants contained the appropriate ratios of

viral proteins when compared to AAV2 on a western blot, as detected by primary B1 antibody against dissociated capsid proteins.

Post titer and western blot characterization, AAV2 265 insertion mutants were blotted on a nitrocellulose membrane to determine the ratio of empty to full capsids with primary A20 antibody detection against the intact particle. A20 was unable to detect the AAV2 265 mutants, except for AAV2 265G, eluding to the importance of this site on the antibody-capsid recognition footprint (Table 2). Post biochemical analysis we determined cell infectivity of these mutants in two different cell lines, 293, in which AAV2 transduces well and C2C12. C2C12 cells may mimic observed phenotypes *in vivo* since we are injecting mouse muscle tissue with our AAV2 variants. AAV2 265 insertion mutants were able to transduce 293 and differentiated C2C12 cells similarly based on luciferase assay. Interestingly, the mutant with the most variant cell infectivity in 293 cells was AAV2 265C with reasons to be touched on in the Discussion. Post analysis *in vitro* we injected our mutants *in vivo* to determine *in vivo* transduction levels based on animal imaging (Figure 2).

AAV2 265 insertion mutants display increased transduction in muscle and liver

All AAV2 265 mutants at a vector genome copy number of 1E10 were injected intramusculary into the right and left gastrocnemus. Animals were imaged at 1wk, 2wks, 4wks and 8wks. From this first round of animal injections, we decided to further characterize a subset of these mutants that displayed an increased transduction pattern *in vivo* (data not shown). AAV2, AAV2 265 D, E, F, K, L, P, T, and V were examined further *in vivo* (Figure 2).

These viruses were reinjected at 1E10 vector genome containing particles. Mice were imaged at one-week intervals to track the gene expression pattern between variants. Interestingly, most variants displayed increased transduction as compared to AAV2 over a five week period, however, there were a few 265 insertion mutants that displayed increased transduction, anywhere from five to ten fold over AAV2 wildtype particles. These mutants were AAV2 265D, E, and F. Amino acids D (aspartic acid) and E (glutamic acid) are negatively charged while, F is a bulky hydrophobic residue. Strikingly, AAV2 265T, the original mutation derived from AAV1, did not display as large of an increase in muscle transduction as AAV2 265D and F. Therefore, other mutations to this region of the capsid can increase infectivity more so than the parent amino acid sequences (Figure 2).

Similar to the observed phenotype in muscle, displayed was an increase in transduction post intravenous injection. 1E10 vector genome containing particles of AAV2, AAV2 265D, AAV2 265T and AAV2 265P were injected via tail vein and mice were imaged two weeks post injection. Post photon quantification, all AAV2 265 insertion mutants transduced the liver tissue anywhere from 10 to 100 fold greater than AAV2. Therefore, the insertion mutation can increase AAV2 transduction in multiple tissue types (Figure 3A and B).

AAV1 265 substitution biochemical analysis

AAV1 was chosen as the next candidate to receive the transduction increasing mutations. As mentioned previously, the AAV2 265 mutants were generated based on a sequence alignment between AAV2 and AAV1 (Figure 4A), describing this site as a potential site for the increased transduction observed post AAV1 intramuscular transduction

as compared to AAV2. In the amino acid alignment, AAV1 is one amino acid longer, the threonine at position 265 is an insertion as compared to the AAV2 capsid surface loop I. Therefore, we chose to mutate the AAV1 threonine amino acid to D, E, or F or delete the threonine to make the loop similar to AAV2 in amino acid length. The hypotheses being that mutation of the threonine will either cause AAV1 to behave more like AAV2, or it will cause an increase in transduction if the disruption of the 265 loop is a universal gain of function effect.

AAV1 T265D, E, F and del were generated and characterized first *in vitro*. These mutants were able to generate titers similar to wildtype AAV1. Additionally, when western blotted, these mutants contained the appropriate ratio of VP1, VP2 and VP3 as expected. When assayed for infectivity in tissue culture, similar to AAV2 and the 265 insertion mutants, all AAV1 mutants infected 293 cells anywhere from five to tenfold less than AAV1 when infected with 3000 vector genome containing particles per cell. Virus infectivity in C2C12 cells was similar to 293 cells, with an infectivity of five to tenfold lower than the parent AAV1 with the exception of AAV1 T265F, being about five-fold higher in infectivity when compared to AAV1 (Figure 4A). However, due to the inconsistency in infectivity between *in vitro* and *in vivo* results as seen with the AAV2 265 insertion mutants, the AAV1 mutants were further characterized *in vivo*.

AAV1 265 substitution mutants *in vivo*

The AAV1 T265 substitution mutants were injected intramuscularly in two different vector genome doses, 1E9 and 1E10. Interestingly, at a dose of 1E9 vector genome containing particles, there was a significant increase in vector transduction between the T265

mutants and AAV1 wildtype particles. AAV1 265 mutants ranged from ten to one hundred fold higher in infectivity as compared to AAV1 based on photon quantification post animal imaging (Figure 4B). These mutants were higher transducers at a dose of 1E9 vector genome containing particles than the AAV2 265 substitution mutants at a 1E10 dose. Once the dose of the AAV1 T265 mutants was increased to 1E10 vector genome containing particles a different phenotype is observed. At a higher dose, the AAV1 T265 substitution and deletion mutants do not display a striking increase in vector transduction as compared to wildtype AAV1 particles (Figure 4C).

Of all mutants, the one with the largest increase in transduction was AAV1 T265 deletion (Figure 4B), with an increase of five-fold greater than AAV1 at 1week post and sustained at 6 weeks post IM injection. Therefore, the observed increase in transduction upon mutation of this region of the capsid was not serotype or capsid background specific, as seen with the increases in both AAV1 and AAV2 muscle and liver transduction, respectively.

AAV2 2i8 insertion mutants *in vivo*

Due to the dramatic increases in transduction observed with the AAV1 and AAV2 265 mutants, it was decided to generate the in another backbone. AAV2i8, a vector generated by Asokan et al. 2009 (unpublished), detargets the liver, but transduces systemically similar to AAV8 based on photon quantification post animal imaging and vector genome distribution analysis. The observed phenotype is due to the presence of the AAV8 three-fold loop on the AAV2 capsid, ablating the ability of AAV2 to bind heparin sulfate. AAV2i8 was of interest for this study due to its liver detargeting capabilities, and the potential of the 265 insertion mutant to increase or rescue transduction in the liver.

Therefore, 265D, E, and F were inserted into AAV2i8, along with Q as an arbitrary mutation to this region of the capsid. Interestingly, when 293 cells were infected with AAV2i8, there was decreased transduction as compared to AAV2 as expected due to the lack of heparin binding capabilities, however AAV2i8 265D, E, F and Q increased AAV2i8 transduction ten fold (Figure 5B). Based on these data, it was apparent, that these vectors should be injected *in vivo* for complete transduction characterization. 1E10 vector genome containing particles of AAV2i8 265E were injected via tail vein into mice in order to monitor systemic transduction. As mentioned previously AAV2i8 cannot efficiently transduce the liver, however, AAV2i8 265E (Figure 5C), D, F and Q (data not shown) were able to rescue liver transduction based on photon quantification post animal imaging and vector genome quantification (Figure 5).

Therefore, it is apparent that the 265 position on the AAV capsid plays an important role in virus infectivity, shown with an increase in tissue transduction when insertions are generated in AAV2, AAV1 is mutated, and an insertion is generated in a mutant unable to transduce a certain tissue type efficiently in the case of AAV2i8. Due to this observed effect it was imperative to determine the mechanism behind observed phenotype, whether it be due to pre or post entry mechanisms.

AAV2 265 insertion mutant mechanism

Uncoating

Due to the observed increase in transduction upon mutation of the 265 region of the capsid, multiple possibilities were explored. Our first hypothesis was that mutation of this region affected vector uncoating. First, vector stability was examined via heat treatment

analysis. 1E10 viral particles of AAV2 and AAV2 265D were incubated at a range of temperatures as indicated in the results and blotted onto a nitrocellulose membrane. Capsid viral proteins at the various temperatures were detected via B1 antibody against dissociated viral proteins and A1 antibody against the VP1 unique N-terminus. A20 antibody to detect intact particles could not be used since the 265 mutants were undetectable by this antibody. In doing so it was determined that based on heat treatment of the capsid particles, there was no difference in stability of AAV2 and AAV2 265D at varying temperatures (Figure 6A).

Not only did we look at particle stability, but also the ability of the viral capsid to protect genomes *in vivo*. AAV2 and AAV2 265D were injected at a vector genome containing number of 1E10 into the left and right gastrocnemus. The muscle was harvested at 24hrs, 48hrs, 72hrs and 1week post infection. The muscle tissue was homogenized and left untreated or treated with DNase to degrade genomes that were unprotected by capsid particles. Following treatment the muscle was treated with proteinase K and lysis buffer (Qiagen) in order to break down the tissue and open any capsid particles that remained intact. Therefore, we could compare protected viral genomes to unprotected. Based on q-PCR quantification of vector genomes, on average, there appears to be a trend in the reduction of AAV2 265D genomes protected over time as compared to AAV2 on average. However, due to large error bars, the trend is not statistically significant, and based on data mentioned in this chapter, uncoating does not appear to be the mechanism behind the increase in 265 mutant transduction (Figure 6B).

Endothelial cell infectivity

An alternate mechanism for the ability of increased viral transduction observed *in vivo*, is the ability of the 265 mutants to enter a cell type that they were unable to transduce prior to mutation of this region. Based on aforementioned data it is apparent that the AAV2 265 insertion mutants transduced 293 cells similar to each other and less efficiently than AAV2, not being a reflection of what occurred *in vivo*. Additionally, when infectivity of these mutants was assayed on differentiated C2C12 cells a similar result was observed. The AAV2 265 mutants transduced similarly to each other, some of which similar to AAV2 and some slightly less than (Figure 7A).

Since we observed the increased transduction *in vivo*, knowing that the mutants were able to infect muscle and liver well *in vivo* based on animal imaging post 265 mutant infection, it was hypothesized that the 265 insertion mutants might be infecting a common cell type found in multiple tissues, such as endothelial cells. Therefore, we obtained multiple endothelial cell lines for *in vitro* transduction assays. Three cell lines were utilized, HUVEC (human embryonic stem cells), C166 (yolk sac/vascular endothelial cells), and MEC (mouse myocardial endothelial cells. With regard to the HUVECS, the AAV2 265 mutants transduced less efficiently than AAV2, however, the AAV2 265 mutants were able to transduce the C166 and MECs more efficiently than AAV2. Of the AAV2 265 mutants tested, all were able to transduce C166 cells approximately 50 fold higher than AAV2. Additionally, AAV2 265D and E were able to transduce MECs approximately 3 and 2 fold better than AAV2, respectively whereas AAV2 265T and P were able to transduce 34 and 15 fold better than AAV2, respectively (Figure 7B). Based on the aforementioned *in vitro* data the possibility remains that the AAV2 265 insertion mutants gain the ability to transduce endothelial cells *in vivo*.

Liver PC and NPC infectivity

Based on the increase in endothelial cell transduction *in vitro*, relating this to *in vivo* infectivity was warranted. Post vector uncoating analyses it was determined that the increase in transduction was most likely not associated with this aspect of the virus life cycle but potentially had to do with pre-entry mechanisms. The AAV2 265 insertion mutants and AAV2i8 and AAV2i8 265E vectors were an optimal choice due to the observed increase in transduction and ability of 265E to rescue the lack of liver infectivity seen with the parent AAV2i8 vector, respectively.

In order to determine the mechanism behind the increase in liver transduction with the AAV2 265 and AAV2i8 265E vectors, the liver was harvested two weeks post intravenous injection and separated into its individual cellular components being parenchymal cells (hepatocytes) and nonparenchymal cells (endothelial, Kupffer and stromal cells). PCs and NPCs were separated via centrifugation and vector genomes and mouse lamin genes in each cell population were quantified via q-PCR. Based on the quantification AAV2 265 insertion mutants displayed an appreciable increase in vector genome copies in both PC and NPC fractions as compared to wildtype AAV2 injected animals (Figure 8A) with no cell type preference. Not only did the AAV2 265 insertion mutants display an increase in liver tropism, but also AAV2i8 265E. When AAV2i8 livers were harvested and separated, AAV2i8 265E displayed an increase in vector genome copies on average in both PC and NPC fractions but more a remarkable increase in the NPC fraction over parent AAV2i8 (Figure 8B). From the liver data, it is apparent that it does not take nearly as many genome copies of AAV2i8 265E to display a drastic increase in transduction in the liver

based on luminescence (Figure 6B) as it does the AAV2 control and AAV2 265 insertion mutants (Figure 4).

Discussion

Studies on this region in our laboratory initiated with Dawn Bowles, with the desire to determine the amino acids responsible for AAV1 muscle tropism. Post intramuscular injection, it became clear that AAV1 transduces muscle tissue more efficiently than AAV2 and the mechanism behind that was unknown. Post sequence alignment with the AAV1 and AAV2 capsids, multiple amino acid differences between the two became potential candidates for AAV1's enhanced transduction capabilities. After narrowing down the pool of varying amino acids between AAV1 and AAV2, five were chosen for further analysis. Identified were AAV2 Q263, 265, N709, V712 and T720, and they were mutated to A, T insertion, A, A, and N to the corresponding amino acid in AAV1. From this it was determined that the 265 positional insertion may play an important role in viral infectivity, and warranted further analyses. This was also based on previous work in the literature, since mutations of amino acids in this general region greatly affected virus infectivity, eluding to the fact that the dead zone may be playing an important role yet to be identified.

Triaging amino acid sequences in order to identify those that are important for viral phenotypic properties is commonly performed. In our lab alone, regions identified have been shown to play a role in receptor binding, such as the heparin binding and integrin binding motifs (5, 46, 157). Additionally, recent data has suggested that removal of the heparin binding motif and replacement it with the corresponding amino acids from the other

serotypes, generates viruses with unique tropisms (Asokan unpublished). Therefore, previous research warranted further characterization of disparate regions between serotypes, including the 265 surface loop region within the dead zone.

It is apparent that this region plays a very important role in virus infectivity and potentially antibody recognition. Post biochemical characterization it became clear that mutation of this region did affect A20 primary antibody binding as seen in the literature, but did not affect 293 and C2C12 cell infectivity or other biochemical properties as shown in Figure 2. However, AAV2 265C displayed a decrease in infectivity but this may be due to the abundance of particle aggregates including empty particles visualized via EM analysis (data not shown). The cysteines present on the capsid surface may be creating inter-virion disulfide bonding, leading to the generation of aggregates during viral production and purification. The aggregation, a combination of empty and full particles could be the source of the AAV2 265C inefficient *in vitro* transduction. However, of the insertion mutants tested *in vivo*, AAV2 265 insertion mutants displayed an increase in transduction of muscle and liver tissue based on imaging and vector genome analysis, and infected endothelial cells in tissue culture where AAV2 could not. Due to these results, it was apparent that the mutants gain an ability to infect cells, whether it is specific to a certain type, or a more universal effect. An interesting observation was made during the *in vivo* analyses, was that AAV2i8 265E displayed a drastic increase in liver transduction based on photons, however, not a large increase in vector genomes in the liver, as compared to the AAV2 and AAV2 265 disparity (Figures 6 and 8). This may have to do with the presence of the AAV8 capsid on AAV2i8 265E, as previous research shows that the AAV8 capsid can uncoat more efficiently, leading to an increase in transduction (131). The disparity between the *in vitro* and *in vivo*

transduction results may be due to the variance in receptors expressed on the cell types *in vitro* versus *in vivo*.

However, the overall increase observed with the vectors *in vivo*, may have to do with the 265 mutants' ability to bind a cell surface receptor that it was unable to prior to mutagenesis. Based on modeling, it became apparent that mutagenesis of these region potentially led to an increase in negative charge around the 265 positions specifically at amino acids D470, D473, and E500 (circled in black in Figure 9). Due to the fact that one can make multiple amino acid changes to this region such as 265D, E or F to AAV2, 265Q, D, E or F to AAV2i8, and delete or substitute 265 in AAV1, the observed phenotypes are most likely a result of a local or gross conformational change to the capsid. Therefore the amino acid insertions may cause local conformational changes making the virus amenable for cellular entry via a specific mechanism.

Additionally, it is possible that mutation of surface loop I is greatly affecting the gross conformation of the capsid. For instance, regardless of what mutation is generated in AAV1, whether it is a substitution or deletion of T265, there is an observed increase in vector transduction in the mouse gastrocnemus muscle. Furthermore, substitution of AAV2 265 and AAV2i8 265 with various amino acids generated a pool of vectors with enhanced muscle and liver transduction and rescued liver transduction, respectively. Therefore, mutation of surface loop I in this position may cause a gross conformational change ablating coreceptor or primary receptor interactions at this region or nearby regions of the capsid.

In the case of AAV2 it is well substantiated that these virus particles utilize the three-fold peaks as regions for receptor recognition (5, 79, 96, 157), utilization of other regions of the capsid for coreceptor interactions is not out of the question. Many viruses use the valleys

on the surface as regions for receptor binding, and in this instance, the 265 loop being studied is exposed on the surface between the two-fold and five-fold axes, but does not protrude as much as the three-fold peaks. Rhinovirus, a picornavirus, utilizes a deep crevice, known as the canyon, on the capsid surface for ICAM-1 receptor attachment on host cells (17). Similarly to rhinovirus, poliovirus, another picornavirus binds the primary CD155 (47, 166) in its capsid canyon, and upon entry, the interaction movies deeper into the canyon. This is not unique to these two viruses, coxsackievirus displays the same canyon-receptor recognition (102) further substantiating the idea that AAV could be binding a coreceptor via interactions with the canyons of the capsid.

However, as previously mentioned in this thesis (Chapter II) it is apparent that single amino acid mutations can greatly affect AAV life cycle properties such as receptor recognition. Studies involving gross mutagenesis of the AAV2 capsid have generated an abundance of capsid mutants with multiple phenotypes such as loss of titer, infectivity and heparin binding (9, 10, 79, 96, 156). Due to their abundance, most of these many are yet to be characterized with regards to the mechanism behind their observed phenotypes. However, a few studies have extensively investigated the mechanisms behind the phenotypic changes. Previous research demonstrated that a single mutation E531K in the AAV1 capsid can generate heparan sulfate binding particles, and the converse mutation in AAV6 can remove them (157). Additionally, mutation of surface tyrosines, specifically amino acid 730 (168) can generate particles with enhanced transduction capabilities, due to the apparent ablation of ubiquitinated capsids targeted for degradation. Therefore it is not unlikely that a single amino acid change within some other region of the capsid may lead to alteration of capsid properties.

Additionally, the AAV2 265 mutants may allow for the development of vectors that maintain the ability to escape antibody recognition in the serum post injection (53, 76, 164). Since the AAV2 265 mutants lose the ability to be recognized by primary antibody A20 *in vitro* as described in this chapter and in the literature (79), these mutants may be further investigated for their potential as vectors with the ability to escape the immune response. For preliminary evidence, these mutants were injected intramuscularly along with AAV2 in separate mice, serum was collected, and serum was incubated with the corresponding AAV2 265 mutant or AAV2 for infectivity studies. From this, it was determined that a subset of mutants, display a decrease in antibody titer production or affinity for a neutralizing antibody which will allow for further investigation as a means to develop vectors for multiple injections (data not shown).

Acknowledgments

I would like to thank Janetta Phillips for assistance with animal studies and Julia Conway, Jayme Warischalk, and Becky Sinnott for aiding in the development of mutants for this project. A special thanks to Lauren M. Drouin and Mavis Agbandje-McKenna for generating roadmaps via RIVEM.

Table 1. Primers used for generation of 265 Mutants

AAV2 265 substitutions	5'- CCAGCCAATCANNKGGAGCCTCGAACG -3'
AAV1 T265deletion	5'- CTCCAGTGCTTCAGGGGCCAGCAACG-3'
AAV1 T265D	5'-GCAAATCTCCAGTGCTTCAGACGGGGCCAGCAACGAC-3'
AAV1 T265E	5'-GCAATCTCCAGTGCTTCAGAGGGGGCCAGCAACG-3'
AAV1 T265F	5'-GCAATCTCCAGTGCTTCATTCGGGGCCAGCAACGAC-3'
AAV2i8 265D	5'-ATTTCCAGCCAATCAGACGGAGCCTCGAACGAC-3'
AAV2i8 265E	5'-ATTTCCAGCCAATCAGAGGGAGCCTCGAACGAC-3'
AAV2i8 265F	5'-ATTTCCAGCCAATCATTCGGAGCCTCGAACGAC-3'
AAV2i8 265Q	5'-ATTTCCAGCCAATCACAGGGAGCCTCGAACGAC-3'

Figure 1. Sequence alignment of AAV 265 position

A.

AAV1 (258)KQISSTST-GASND
AAV2 KQISSGS--GASND
AAV3 KQISSQS--GASND
AAV4 KRLGESL-----QS
AAV5 REIKSGS-VDGSNA
AAV6 KQISSAST-GASND
AAV7 KQISSETAG-STND
AAV8 KQISNGTSGGATND
AAV9 KQISNSTSGGSSND
AAV10 KQISNGTSGGSTND
AAV11 LRLGTTS-----SS

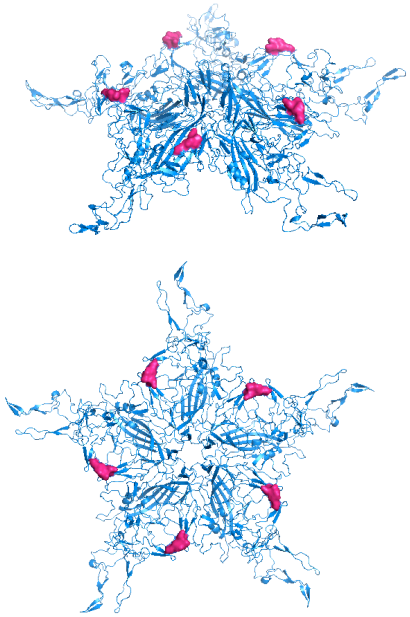

Figure 1. Sequence alignment of AAV 265 position. Aligned is the surface loop I within the dead zone of a variety of AAV serotypes displaying the variability within this region (left panel). To the right is a model of the five-fold axis of symmetry of AAV2 (blue) with the AAV2 265 loop present between the five-fold and two-fold axes highlighted in pink.

Table 2. Phenotypic comparison between AAV2 265 insertion mutants

Insertion mut	Western blot	A20 recognition	Titer	293 infectivity	C2C12 Infectivity
AAV2	++++	++++	++++	++++	++++
AAV2 A	++++	-	++++	+	ND
AAV2 C	++++	-	++++	+	ND
AAV2 D	++++	-	++++	+++	++++
AAV2 E	++++	-	++++	++	++++
AAV2 F	++++	-	++++	++	ND
AAV2 G	++++	++	++++	+++	ND
AAV2 H	++++	-	++++	++	ND
AAV2 K	++++	-	++++	++	+++
AAV2 L	++++	-	++++	++	++++
AAV2 M	++++	-	++++	+	ND
AAV2 N	++++	-	++++	++	ND
AAV2 P	++++	-	++++	++	++++
AAV2 Q	++++	-	++++	++	ND
AAV2 R	++++	-	++++	++	ND
AAV2 S	++++	-	++++	+++	ND
AAV2 T	++++	-	++++	+++	++++
AAV2 V	++++	-	++++	+	++++
AAV2 W	++++	-	++++	++	ND
AAV2 Y	++++	-	++++	++	ND

Table 2. Phenotypic comparison between AAV2 265 insertion mutants. Listed are all AAV2 265 insertion mutants generated and their phenotypes post biochemical analyses. Specifically, all mutants were western blotted and stained with B1 primary antibody (1:20), western dot blotted with A20 primary antibody (1:20), and titered via q-PCR with primers

specific to the luciferase transgene, Viral infectivity was analyzed in 293 (HEK) and differentiated C2C12 cells via luciferase assay as mentioned previously. In the A20 recognition column (-) refers to the lack of A20 recognition. In all columns (++++) denotes similar to wildtype AAV2 capsids, (+++) within 10fold similarity, (++) = 10fold less similar than, (+) more than 10fold lower in similarity. ND= not determined.

Figure 2. AAV2 265 insertions display increase in muscle transduction over time

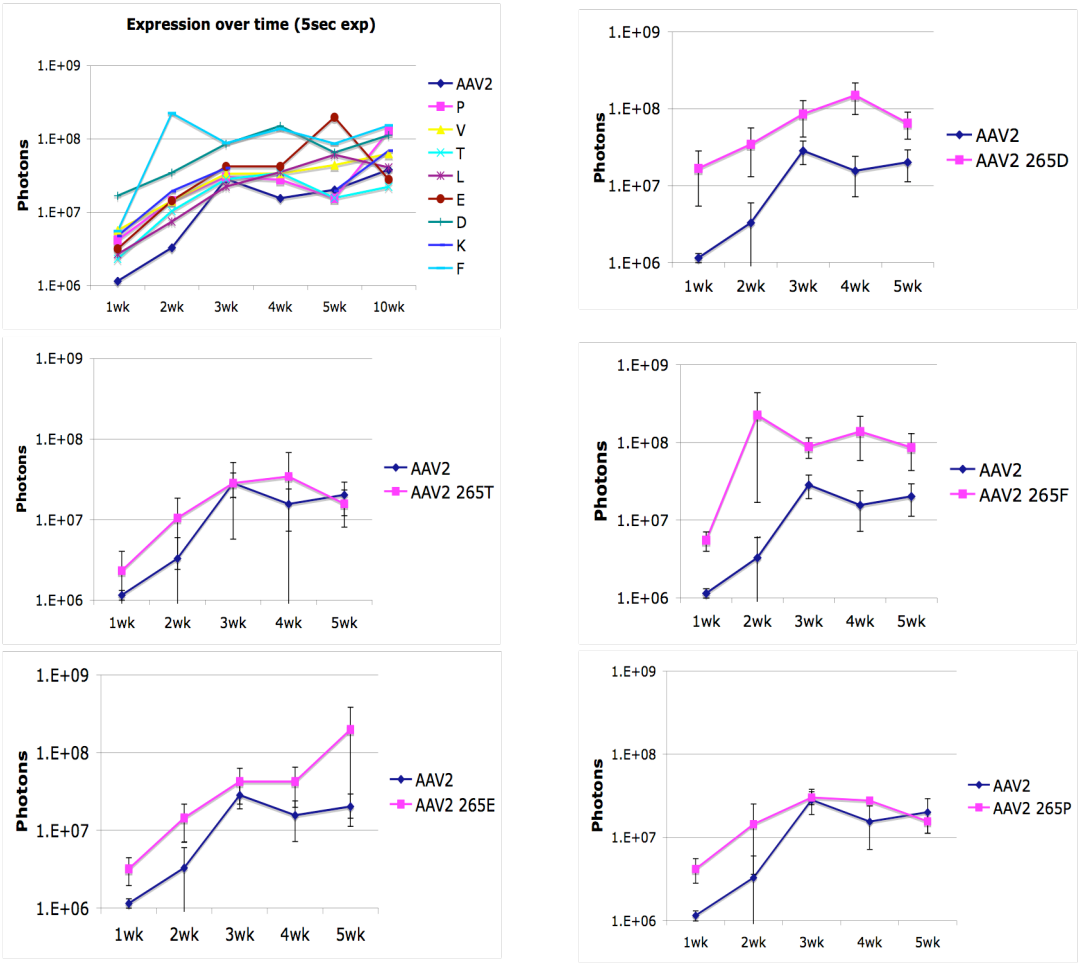

Figure 2. AAV2 265 insertions display increase in muscle transduction over time. Mice were injected intramuscularly (right and left gastrocnemus) with 1E10 vector genome containing particles. Mice were imaged at 1week increments until 5 weeks and then imaged again on week ten via the IVIS Xenogen imaging system. Shown in six panels are multiple AAV2 265 insertion mutant expression compared to AAV2 over time (upper left chart) and select mutants from that chart as compared to AAV2 (AAV2 265D, E, F, T and P). SD=Black bars N=4.

Figure 3. AAV2 265 mutants display an increase in liver transduction

A.

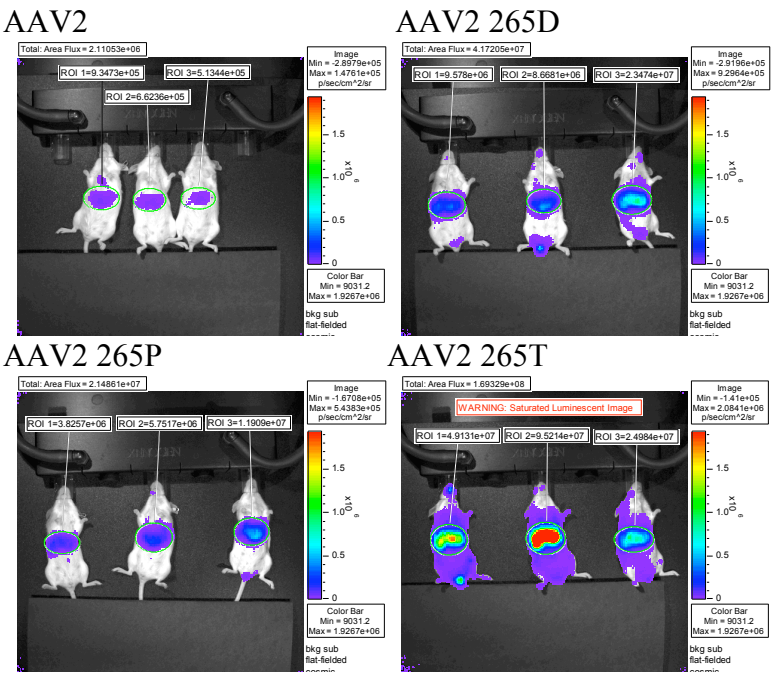

B.

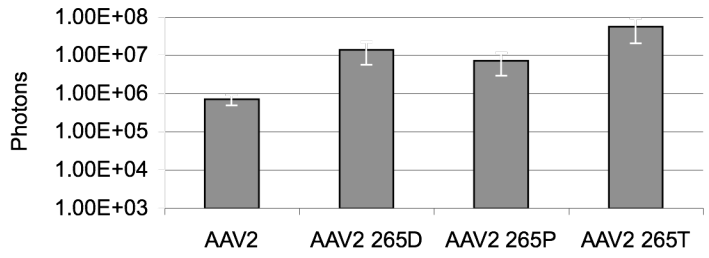

Figure 3. AAV2 265 mutants display an increase in liver transduction. (A) 1E11 vector genome containing particles were injected into mice via tail vein for liver transduction analysis. AAV2 265D, P and T were compared to AAV2 wildtype capsid transduction levels via animal imaging two weeks post intravenous injection. (B) Using the Living Image software 2.5, luciferase gene expression was quantified.

Figure 4. Mutation of aa265 within the AAV1 capsid generates mutants with increased muscular transduction capabilities

A.

```
AAV1 (258)    KQISSTSTGASND
AAV2          KQISSGS—GASND
```

B.

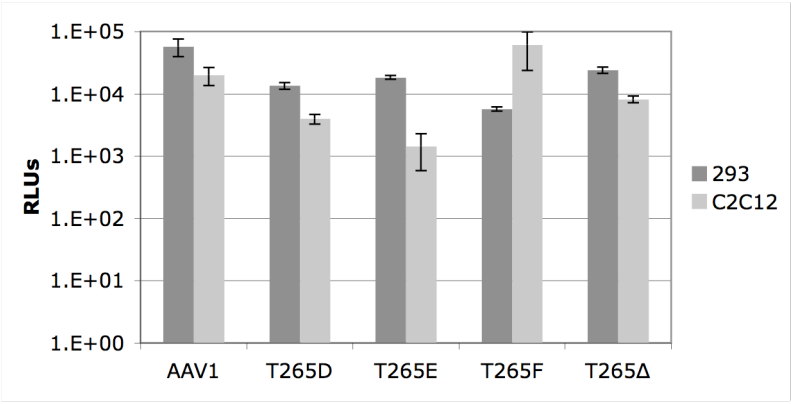

C.

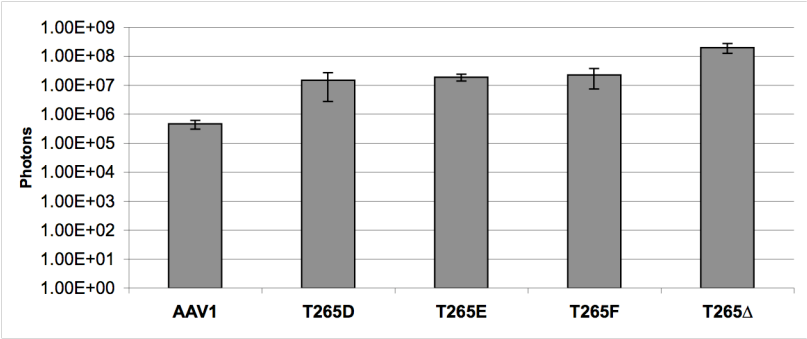

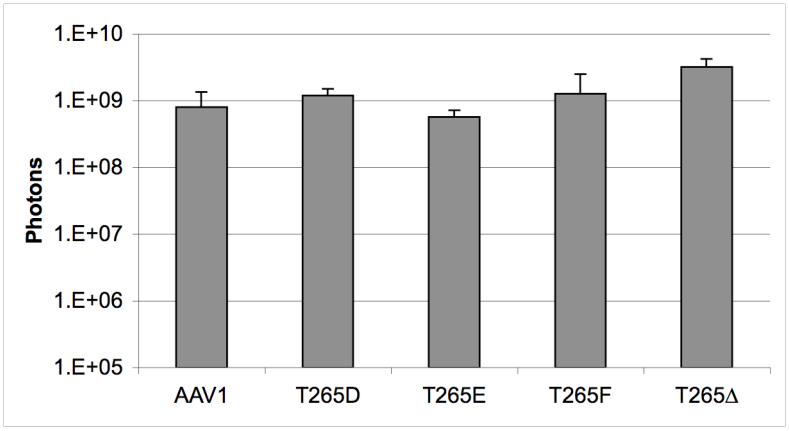

Figure 4. Mutation of aa265 within the AAV1 capsid generates mutants with increased muscular transduction capabilities. (A) AAV1 and AAV2 amino acid sequences of the

region of interest within the surface loop I were aligned via sequence analysis, with AAV1 being one amino acid longer than AAV2 within this region. 293 and C2C12 cells were infected with AAV1 T265D, E, F and deletion (Δ) at 3000 vector genome containing particles per cell. (B) AAV1 T265D, E, F and deletion (Δ) and 1E9 or (C) 1E10 vector genome containing particles were injected intramuscularly. Animals were imaged one week post injection via IVIS Xenogen imaging system and photons emitted quantified via Living Image software 2.5. (SD=black bars, N= 3 or 4)

Figure 5. Double mutant AAV2i8 265E generates vectors with enhanced transduction capabilities

A.

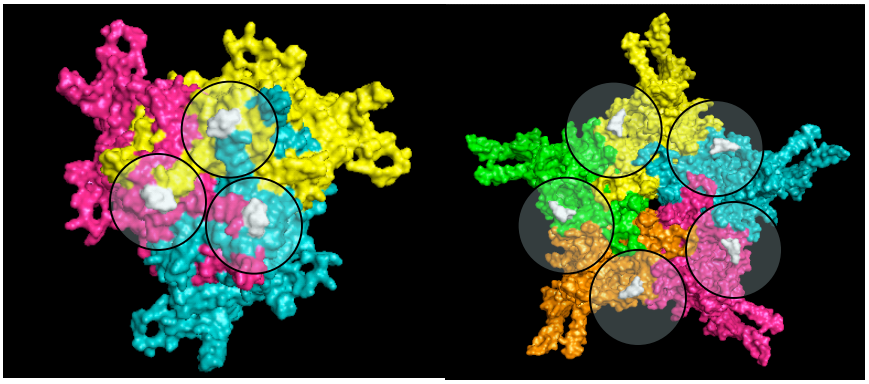

B.

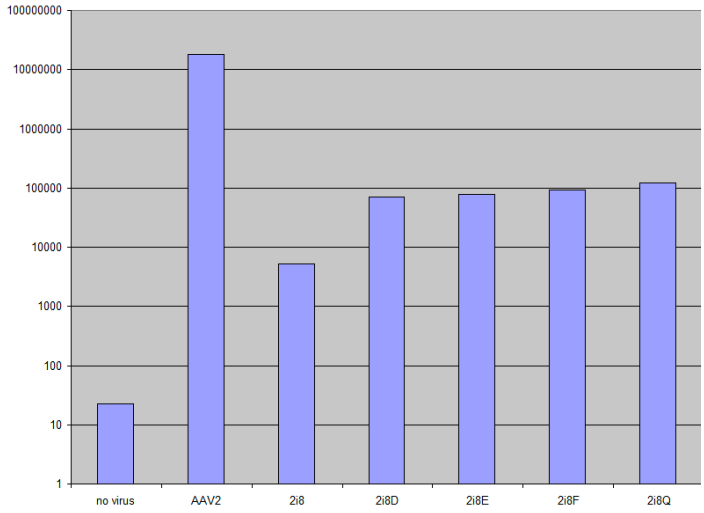

C.

AAV2i8 AAV2i8 265E

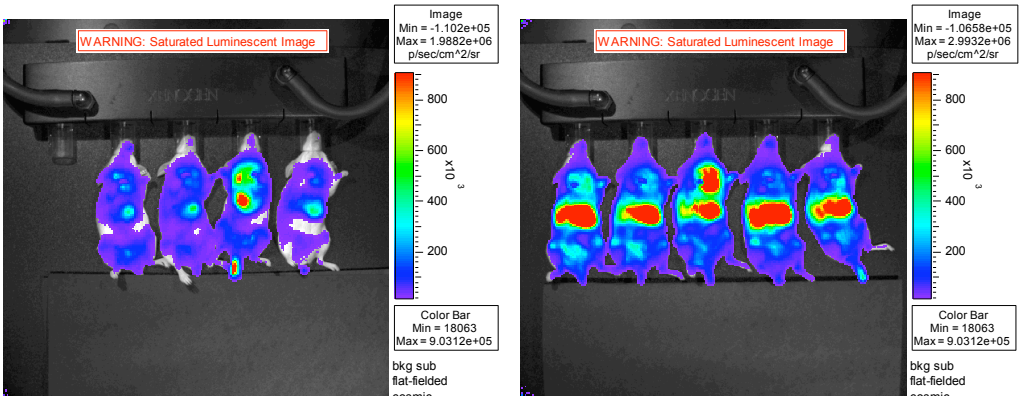

Figure 5. Double mutant AAV2i8 265E generates vectors with enhanced transduction capabilities. (A) Displayed is a model of the three-fold (left) and five-fold (right) of AAV2. Circled in yellow on each model are the locations of mutagenesis, the AAV8 substitution on AAV2 (AAV2i8 left) and the AAV2 265 insertion (right). The resulting virus contained both the 2i8 substitution mutation and the 265E insertion. (B) 293 cells were infected with 3000 vector genome containing particle per cell of AAV2i8 265 mutants and infectivity was quantified via luciferase assay as mentioned previously. (C) 1E10 vector genome containing particles of AAV2i8 and AAV2i8 265E were injected into mice via tail vein for systemic distribution. Mice were imaged 2 weeks post injection via the IVIS Xenogen imaging system as previously mentioned.

Figure 6. Uncoating of AAV2 265 mutant

A.

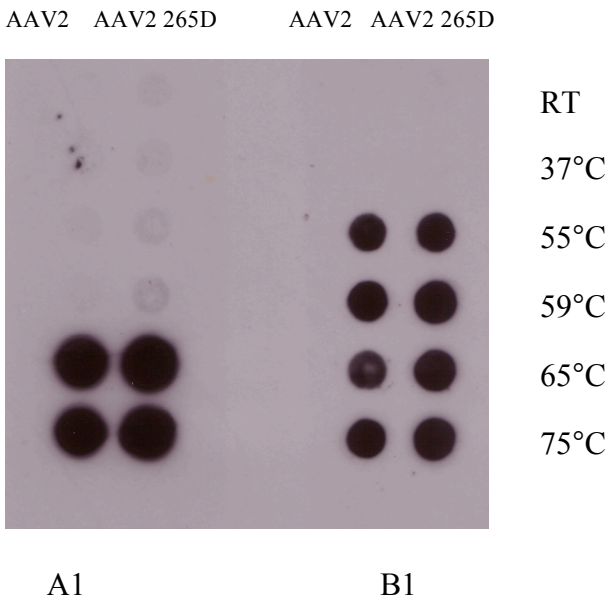

B.

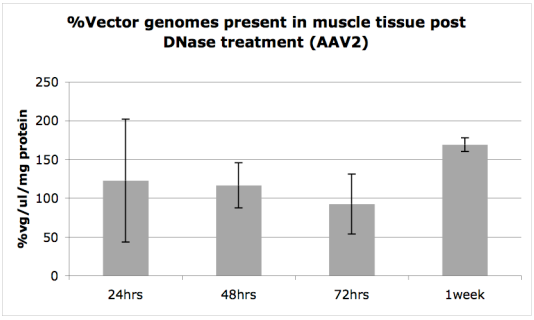

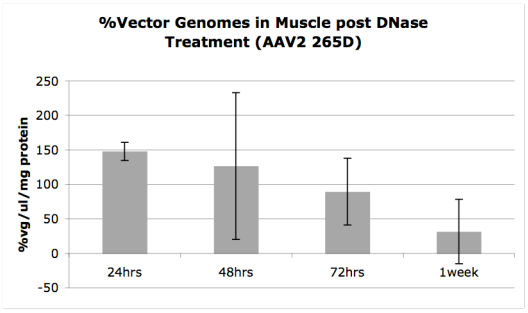

Figure 6. Uncoating of AAV2 265 mutant. (A) 1E10 vector genome containing particles of AAV2 and AAV2 265D were heat treated at increasing temperatures and blotted on a nitrocellulose membrane. Dissociated capsids were detected with A1 (1:20 against the VP1 unique N-terminus) and B1 (1:20 against the VP C-termini). (B) Female Balb/C mice were injected with 1E10 vector genome containing particles of AAV2 or AAV2 265D in the gastrocnemus. Muscle was harvested at 24hrs, 48hrs, 72hrs, and 1week post injection. Half of the homogenized muscle tissue was sonicated and incubated with DNase. Vector genomes

were quantified via q-PCR using primers specific to the luciferase transgene and normalized per milligram weight of the tissue sample.

Figure 7. AAV2 265 mutants gain endothelial cell transduction capabilities *in vitro*

A.

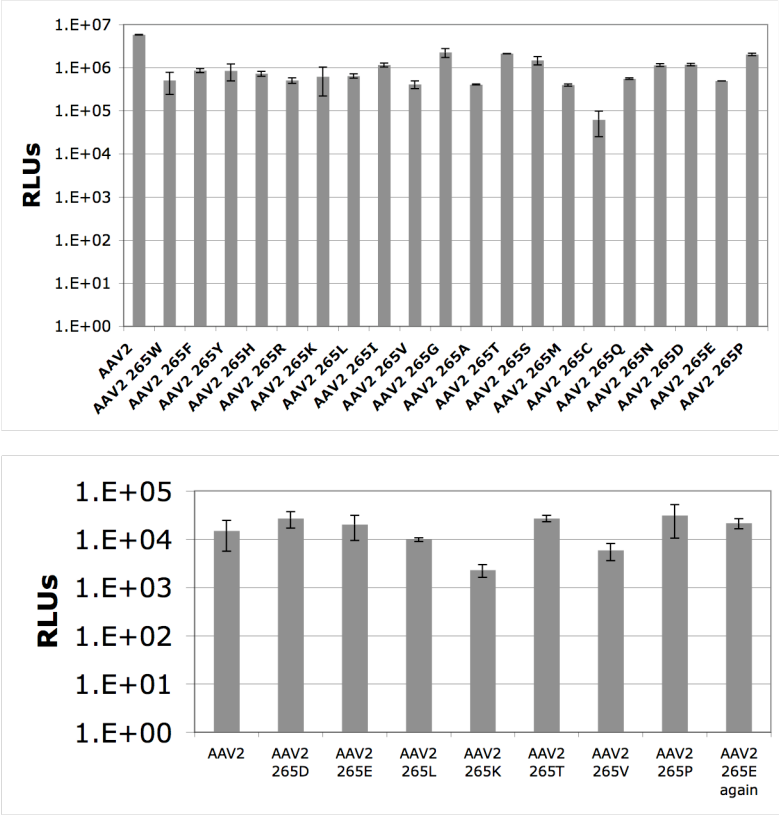

B.

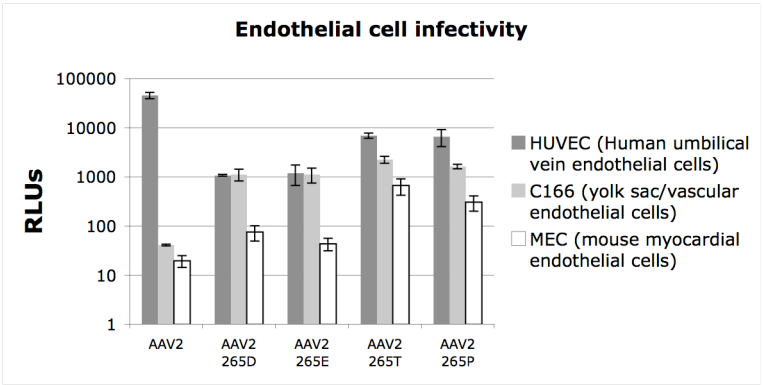

Figure 7. AAV2 265 mutants gain endothelial cell transduction capabilities *in vitro*. (A) 293 cells (top) and differentiated C2C12 cells (bottom) were infected with 3000 vector

genomes per cell of all AAV2 265 insertion mutants carrying the luciferase transgene. Infectivity was quantified via luciferase assay as mentioned previously (Promega). (B) Endothelial cells (HUVEC, C166 and MEC) were infected with 1000 vector genomes per cell with a collection of AAV2 265 insertion mutants, AAV2 265D, E, T and P and infectivity was quantified via luciferase assay 24hrs post infection.

Figure 8. AAV 265 insertion mutants infect PC and NPCs efficiently.

A.

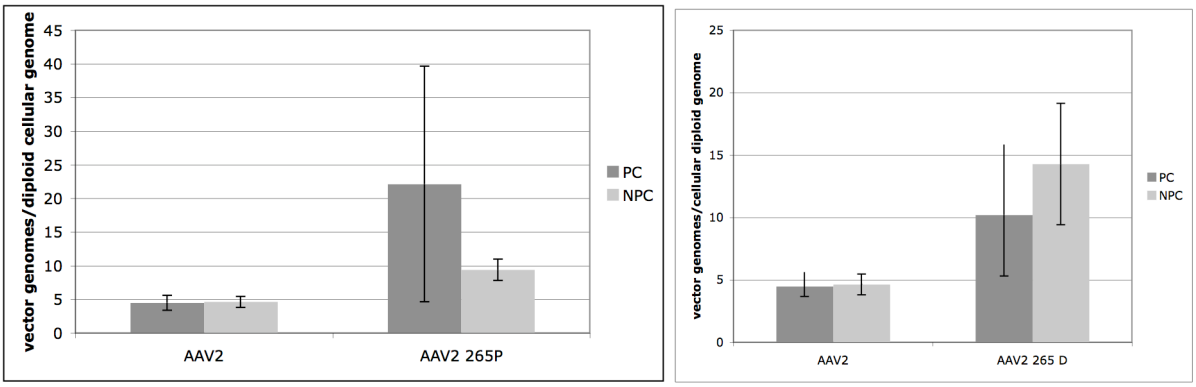

B.

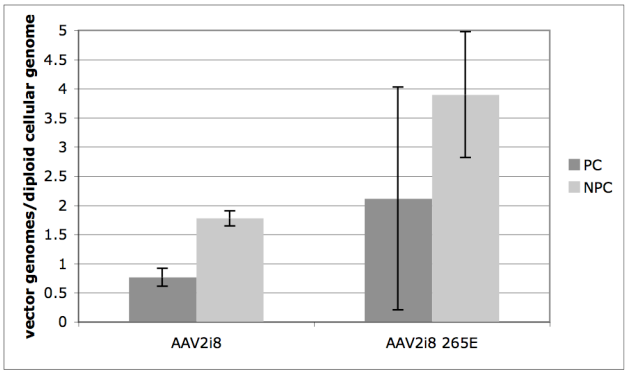

Figure 8. AAV 265 insertion mutants infect PCs and NPC efficiently. (A and B) Mice were injected with AAV 265 mutants at a dose of 1E10 vector genome containing particles. Two weeks post injection the livers were harvested and separated into PC and NPC fractions via differential centrifugation. DNA was isolated via DNeasy purification (Qiagen) and genome copies were quantified in each fraction via q-PCR with primers specific to the luciferase transgene and mouse lamin gene.

Figure 9. Surface roadmaps of AAV2 265 insertion mutants.

AAV1

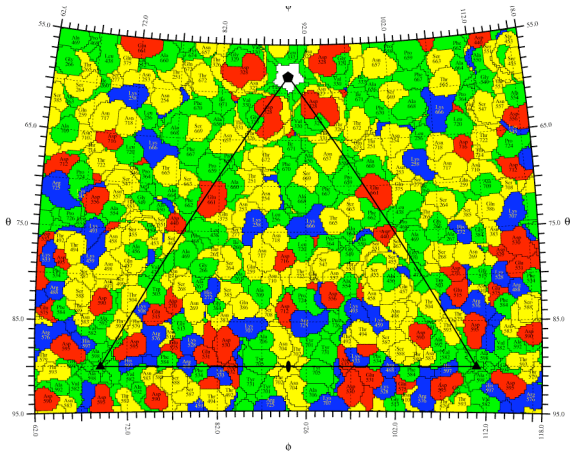

AAV2

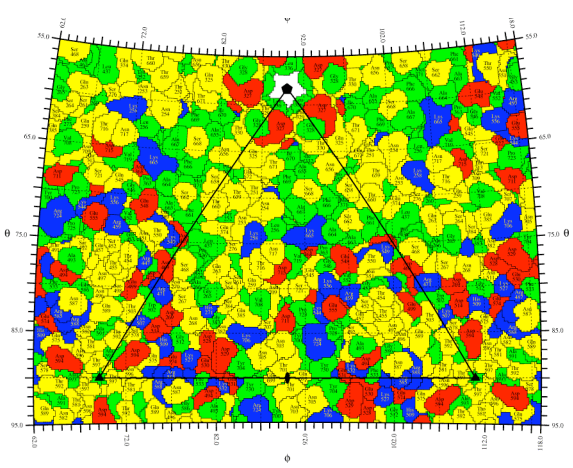

AAV2 265D

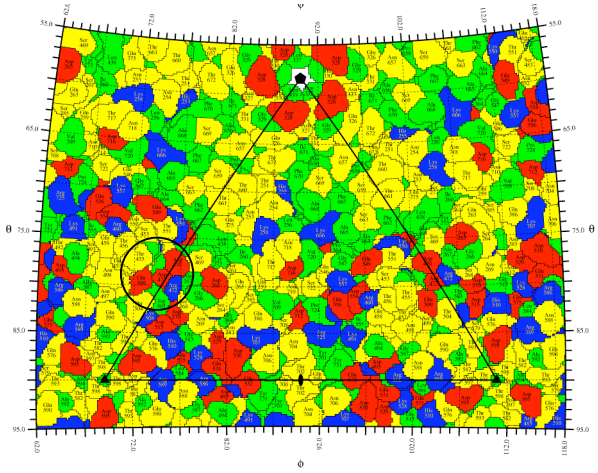

AAV2 265E

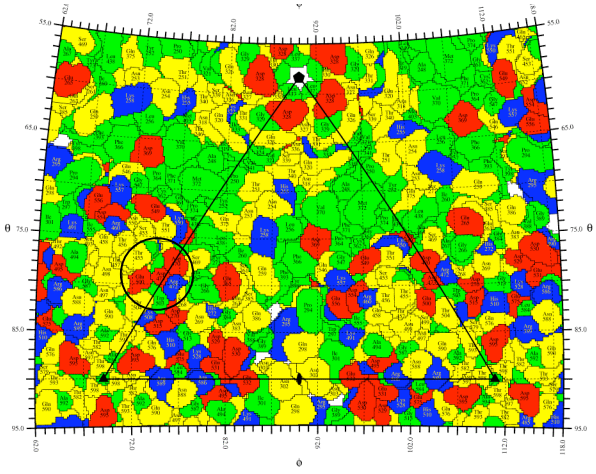

AAV2 265F

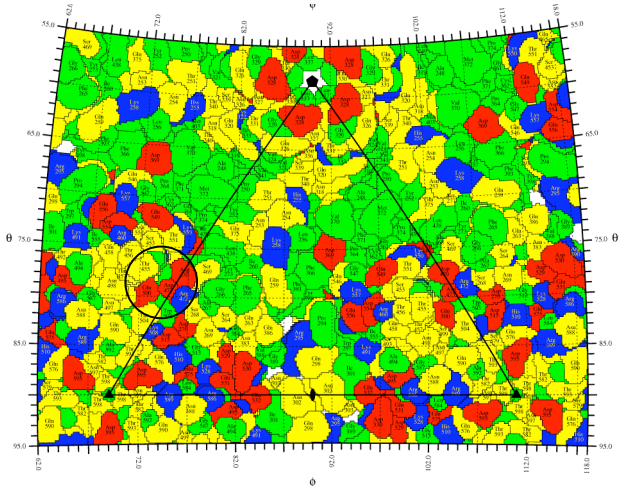

Figure 9. Surface roadmaps of AAV2 265 insertion mutants. Surface roadmaps were generated with RIVEM to determine the local and global effects of the AAV2 265 insertion mutants. Circled in black are amino acids D470, D473 and E500. The color representations are green-hydrophobic, yellow-hydrophilic/neutral, red-acidic, blue-basic. The black lined triangle connects the axes of symmetry with the pentagon being the five-fold, the triangles being the three-folds, and the oval the two-fold.

CHAPTER V

Synopsis and Future Directions

In this dissertation multiple surface loops on the AAV capsid surface were characterized using a battery of assays, ranging from basic biochemical to *in vivo* characterization. Each study performed displays important implications for future application in gene therapy, however, there are still many questions to be answered and more research to be performed.

Surface loop dynamics in AAV capsid assembly

In this study, via capsid domain swapping and further mutagenesis we identified a domain that is necessary for viral capsid assembly. The HI loop was studied in order to determine its role in the virus life cycle due to it being a prominent region on the five-fold that surrounds the pore, determined to be necessary for viral genome packaging, potentially Rep protein binding and VP1 externalization. In this thesis, viral genome packaging was discussed. For instance, via AAV2 HI loop removal and glycine loop substitution it was determined that the HI loop is necessary for viral protein assembly and viral genome packaging, respectively. However, the ablation of viral genome packaging may be due to an inability of the Rep protein to interact with the capsid properly upon mutagenesis of the HI loop. Similarly, upon replacement of the AAV2 HI loop with AAV4, there is a tenfold decrease in titer (Figure 4A), and based on previous work, AAV2/4 chimeras display a decrease in packaging capabilities (107). Based on preliminary data from immunoprecipitations, there does not appear to be a reduction in Rep protein binding to the particles that cannot package the viral genome efficiently, such as with AAV2 poly-glycine and AAV2 HI4 (data not shown). If anything, there appears to be an increase in Rep protein binding as seen with AAV2 432 packaging mutant examined by Bleker et al. (9). However, more experiments would have to be performed to determine if the HI loop is a potential site

for Rep protein binding, such as immunoprecipitations with HI loop packaging defect mutants, and transfections where the Rep protein is supplied in trans. For instance, when producing AAV2 HI4, the AAV4 Rep protein should be supplied to see if that would rescue the defect in packaging capabilities. Furthermore, viral genome packaging was not the only capsid phenotype affected by mutagenesis of the HI loop. Additionally, upon swapping the AAV2 HI loop with multiple serotypes specifically with the HI loop of AAV4, it was apparent that the HI loop plays a role in viral capsid stability, with the HI loop of AAV4 increasing AAV2 capsid resistance to heat treatment (Figure 4B).

Along these lines, the decrease in packaging capability may be related to the increase in particle stability observed with AAV2 HI4, possibly alluding to the fact that the capsid has to be amenable to conformational change during packaging, such as capsid expansion. This is a phenomenon that bacteriophage use to increase capsid capacity prior to genome packaging (56). The ability of the AAV capsid to expand during this stage in the viral life cycle should be explored via cryo-EM analysis and image reconstruction.

Not only was the HI loop swapped with other serotypes, but also substituted with targeting ligands, specifically peptides directed towards vascular endothelial cells (149) and RGD domains towards integrins on cancer cells (120). Our mutants with targeting ligands do not show an increase in transduction capabilities *in vitro*, however, these mutants should be tested *in vivo* to determine if they can retarget transduction. Based on work in Chapter III and the ability of a hexa-histidine motif within the HI loop to interact with nickel, it stands to reason that another targeting ligand in this position may allow for the redirection of viral tropism.

However, from these substitutions, more was learnt about the viral life cycle. From the targeting ligands that spanned a conserved F661 within the HI loop, further site mutagenesis and molecular modeling studies, it was determined that F661 interacts specifically with a proline in the neighboring underlying subunit crucial for maintaining proper viral protein assembly. Disruption of this hydrophobic amino acid interaction generates virus particles with a cleaved form of VP1 incorporated during capsid assembly into the intact particle, affecting viral infectivity. Further work may be performed in order to determine the exact site of VP1 cleavage, including mutagenesis to potentially inhibit this from occurring, along with potentially inhibiting proteases during viral production in order to prevent their actions on the viral protein.

This study was the first published work elucidating key functions of surface domains in virus assembly. Based on this work, there is a greater understanding of AAV capsid assembly and the importance of surface domains in this key stage of the virus life cycle.

From this research we have gained great insight as to locations amenable to manipulations for other purposes. We uncovered key amino acid contacts necessary for VP assembly and therefore located others that were malleable. Due to the plasticity of this region we were able to further utilize it as discussed in the second aim as a novel site for peptide insertion, specifically a hexa-histidine motif. Additionally, determining the amino acids that are necessary for viral protein assembly, allowed for further utilization by another researcher, Chengwen Li. He has substituted the HI loop with an immunodomain as a means to study the immunogenic pathway of AAV.

Apart from this, knowing the AAV2-heparan sulfate complex cryo-EM analysis and image reconstruction has added some insight as to potential biological functions of the HI

loop besides being necessary for proper assembly. For instance, it was demonstrated that this region might change conformation upon primary receptor recognition, and be important for priming the capsid for downstream stages such as VP1 extrusion and viral capsid uncoating. More research has to be performed in order to determine if the HI loop is participating in this aspect of the viral life cycle. If this is the case, the HI loop has the potential to play a role in multiple stages of the virus life cycle.

Multifunctional capsids: Site-specific incorporation of a hexa-histidine motif

Due to the characterization of the HI loop, it was clear which amino acids could be altered in this region of the capsid for application purposes. Therefore a portion of the HI loop was substituted with a hexa-histidine motif in order to use the nickel affinity properties of hexa-histidine peptides. In this case, we hoped to develop a universal purification method for the multiple AAV serotypes and many various isolates.

Upon substitution of the HI loop with the hexa-histidine motif we are able to utilize the vector for multiple functions. AAV2 and AAV9 with the hexa-histidine motif present on all sixty subunits gain the ability to be purified via a nickel column, resulting in pure peak fractions as determined through further biochemical analysis. The reagents developed and characterization performed opened many possibilities for future work. With the utilization of the hexa-histidine motif as a tag for universal purification, it allows for purification of the viral capsid via a uniform method that can be applied to multiple or all serotypes. In order to advance this technology, it will be beneficial to substitute the HI loop of all serotypes with the hexa-histidine motif, produce tagged virus in large quantities, and purify via the nickel column. Additionally, enlarging the His-Trap column size may increase the amount of virus

that can be purified and recovered. Altering the flow rate and the imidazole concentration in the elution buffers could uncover preferred conditions for purification via this method. However, this technique is powerful and shows potential for further development. Additionally this reagent is being further expanded to study capsid-protein interactions whether they are on the cell surface, cytosol or serum via pull-down with nickel conjugated NTA beads. Therefore, this reagent may become beneficial in elucidating key stages in the virus life cycle through protein-protein interactions.

Additionally, the hexa-histidine motif can be utilized as a site for nanogold conjugation for potential future EM applications. There may be many applications for this reagent. For instance, there have been minimal studies uncovering the pathway of virus trafficking. Being able to nanogold label the virus particle may prove to be a powerful tool in the understanding of virus trafficking. Additionally, these particles may be utilized for histological purposes post infection, which may be ideal for analyzing patient samples and locating virus capsids post infection. One other aspect that may prove beneficial is generating virus with the hexa-histidine tag present solely in VP1. Little is known about VP1 with regards to its position in the virus capsid post viral assembly since the crystal structure is based on VP3 subunits. Therefore, the presence of the hexa-histidine motif in the VP1 subunit may allow for further understanding on the role of the individual viral protein subunits.

Post *in vitro* validation, the vectors were injected *in vivo* for further characterization. Even though the vectors maintain the ability to infect cells *in vitro* similar to wildtype, they display a decrease in muscle transduction and an ablation of liver transduction *in vivo*. Interestingly, substituting the HI loop with the hexa-histidine peptide does not disrupt the

heparin-binding site, the location of primary receptor recognition. Therefore ablation of primary receptor interactions is not the reason for the decrease in liver transduction capabilities. It appears as if only sixty copies of the tag completely diminish transduction capabilities. Based on studies involving hepatocyte binding and capsid stability in the presence of mouse blood (Figure 7), it was determined that these particles may be less stable in the bloodstream, leading to the less efficient liver targeting, however, more experiments need to be performed in order to confirm that, such as determining the number of protected and unprotected genomes in the bloodstream over time post intravenous injection with AAV2 HI6xHis in addition to determining if fewer copies of the hexa-histidine motif on the capsid surface increases stability.

However, due to the liver detargeting phenotype, and depending on the mechanism behind it, another location such as the three-fold loop remains available for peptide insertions for retargeting of the virus capsid to specific tissues. Therefore, experiments should be performed where the AAV2 HI6xHis mutant contains a targeting ligand at position 585 to determine if tropism can be redirected post systemic injection, assuming the particle is not completely destabilized in the bloodstream.

Nonetheless, by altering the number of hexa-histidines on the capsid surface, we can modulate muscle and liver transduction. For instance, in the case of muscular dystrophy, it may be beneficial to have a vector with decreased liver transduction, while maintaining the ability to transduce other organs in the body including the skeletal muscle, as seen with AAV9 HI6xHis. Additionally, in the case of AAV2 HI6xHis, we may be able to generate a vector containing the hexa-histidine motif, but also carrying a targeting peptide that may direct it to another tissue of interest, specifically in the three-fold loop, the site of primary

receptor recognition. Therefore, this reagent may develop into a more powerful tool with multiple capabilities and functions for future uses in virology and vectorology. However, as mentioned previously, by altering the ratio of hexa-histidines on the capsid surface, we were able to maintain the ability to purify the AAV histidine mutants and fully and partially rescue muscle and liver transduction, respectively.

Redefining the dead zone

Based on my previous research, characterizing another loop on the capsid surface was an obvious transition. Surface loop I in the dead zone, a region thought to not be responsible in receptor binding, displayed a potential role in infectivity based on research in the literature. Additionally, previous work in the lab alluded to this region as being important for viral infectivity. Through further characterization of this domain some insight was gained on an alternative aspect of the virus life cycle, infectivity.

Specifically, amino acid position 265 on the capsid surface was characterized, being a prominent region, exposed for potential interactions with proteins or cell surfaces. Upon amino acid insertion at position 265 in the AAV2 capsid, an increase in muscle transduction was observed *in vivo*, specifically with aspartic acid, glutamic acid and phenylalanine insertions. Additionally, when the corresponding mutation was generated in AAV1, the same increase in muscle transduction was observed post mouse intramuscular injection, whether an amino acid was substituted or deleted in this position. It became apparent that mutating this loop greatly affected viral transduction *in vivo*. Additionally, AAV2 265 insertion mutants display an increase in liver transduction post intravenous administration, similar to the observed increase in muscle. Post genome quantification, it was determined

that more vector genomes of the 265 insertion mutants enter the liver as compared to the wildtype AAV2 virus particles.

To further validate this observed phenotype we chose to utilize a previously characterized vector in Dr. Aravind Asokan's laboratory as our next backbone. This unique vector AAV2i8 transduces entire mouse skeletal muscle via loss of heparan sulfate binding capabilities. Due to the loss in heparin binding, this mutant is also deficient in transducing the liver based on vector genomes and transgene expression. As a result, this vector became an obvious candidate for the 265 positional insertional mutagenesis, hoping to increase transduction and/or regain transduction in the liver.

Upon mutation of the AAV2i8 265 position on the capsid surface, an interesting phenotype was observed. Inserting a phenylalanine, aspartic acid, glutamic acid, or glutamine results in a remarkable increase in viral transduction *in vivo*. All AAV2i8 265 mutants regain liver transduction capabilities post systemic injection, being a gain of function or ability to infect a region that the mutant was unable to prior to mutagenesis based on animal imaging and vector genome quantification.

This observed mechanism may not be universal. For instance, the 265 insertion in the AAV2 backbone may be affecting the capsid in a completely different manner than in AAV1 or AAV2i8. This being said, based on further *in vitro* studies, it appears as if the AAV2 265 mutants gain the ability to infect endothelial cells in tissue culture, whereas AAV2 could not. Presumably, these mutants gain a tropism for this cell type in a tissue culture setting.

Based on this further studies have to be performed in order to confirm such effects. For instance, the AAV 265 mutants may gain the ability to bind to specific cell surfaces via receptor mediated interactions that they were unable to before. In order validate this

hypothesis, capsid pull-down studies would have to be performed to identify interacting partners. This could be executed via capsid biotinylation or utilizing the hexa-histidine tag as a means to purify the AAV 265 mutants since the primary antibodies do not recognize these mutants. Curiously, based on modeling of the capsid surface via roadmap analysis using RIVEM (Agbandje-McKenna), it appears as if mutation of the 265 position may result in the exposure of more negatively charged residues on the capsid surface near the two-fold axis of symmetry as compared to AAV1 and AAV2. This phenotypic alteration may be a consequence of a gross conformational change allowing for the interaction with variant receptors on cell surfaces. This avenue has to be explored further but provides interest in the possibility of relating AAV capsid structure to function.

Along these lines, it would be beneficial to determine if a change in this position in all serotypes results in this effect. It is quite possible that this may be a universal phenotype that would aid in the development of more efficient vectors for gene therapy applications. Specifically, the AAV2 265 mutants could be developed for gene therapy studies including hemophilia with our vector carrying secretable Factor IX post intramuscular injection (13). AAV2i8 265 mutants, could also be utilized in the clinic due to the approval of AAV2 vectors for trial and their ability to transduce systemically similar to AAV8 and AAV9.

Additionally, studies with this loop may take a completely different path. Recently, the AAV2 265 substitution mutants were injected into the brain, and there is evidence that they outperform the parent serotype on number and type of neuronal cells transduced. This further substantiates the gain of tropism phenotype, however, more experiments are being performed in order to characterize this phenomenon. Additionally, there is preliminary evidence that these mutants may generate low antibody titers or have a weak affinity for

neutralizing antibody interactions thereby opening the possibility for the development of vectors that can escape the immune response. Also this site may be utilized as a location for peptide insertion or substitution similar to what has been executed with the HI loop at the five-fold discussed in the first aim of this dissertation. This location on the capsid surface appears to tolerate changes and therefore may be explored for that purpose down the road. Overall, this dissertation research has opened many possibilities for future development in understanding the virus and the vector.

APPENDIX I

In addition to interests involving the AAV2 capsid with regards to surface domains involved in the virus life cycle, AAV4 arose as an interesting candidate for studies on structure-function dynamics. Stemming from the finding that the presence of the AAV4 HI loop on the AAV2 capsid increased capsid stability, the AAV4 axes warrant further in order to understand the structural domains on the capsid surface and their functional attributes. Therefore a collection of mutants was generated to aid in the study of AAV4 capsid structure-function.

AAV4 three-fold

After noting that the HI loop may be involved in capsid stability based on heat treatment analysis (Chapter II). We decided to study another region of the AAV4 capsid, the three-fold. On the three-fold axis of symmetry resides the three-fold spikes, similar to AAV2 but blunted topologically in comparison (97, 160, 163). Therefore, we targeted the surface tyrosines for two reasons, one being that they can hydrogen bond and interact with partners and two specific surface tyrosines on the AAV2 capsid may be phosphorylated (168), potentially contributing to specific stages in the virus life cycle.

Therefore, the AAV4 YKIPA surface domain that is present in both AAV4 and AAV11 spanning amino acid positions 491-495 was mutated (Figure 1). This domain was of interest based on its presence in two serotypes, it being on the surface of the three-fold containing a tyrosine residue, and matching potential receptor internalization domains.

Upon removal of this domain, AAV4-YKIPA was unable to infect cos-7 cells *in vitro* (Figure 2A). This observation may have been due to a change in receptor binding or a

downstream stage in the virus life cycle. Therefore we analyzed the cell surface binding capabilities of this mutant. Interestingly, AAV4-YKIPA was able to bind the cos-7 cell surface similarly to AAV4 based on vector genome quantification via densitometry analysis. However, when vector genomes were quantified post virus internalization in the cytoplasmic, membrane and nuclear subcellular fractions, there were less genomes present inside of the cell as compared to wildtype AAV4 genomes (Figure 2B). To determine if the inability to transduce cos-7 cells was due to a change in capsid stability we performed a heat treatment analysis, and observed the instability of AAV4-YKIPA initiating capsid dissociation at 59 degrees, whereas the AAV4 capsid maintaining stability until 75 degrees Celsius as detected with A1 and ADK4 primary antibodies to detect dissociated and intact capsid particles, respectively (Figure 2C).

This region remained intriguing due to it being exposed on the capsid surface and deleting the entire domain altered capsid stability. Therefore YK (491) and KY(504) based on further structural analysis were mutated to AA (Figure 1). Conformationally, these residues assemble in close proximity to possibly form a hypothesized nonlinear internalization motif. AAV4 YK-AA and KY-AA were unable to infect Cos-7 cells similar to the AAV4-YKIPA profile (Figure 3A). However, these mutants were able to bind mucin, confirming the lack of participation in cell surface recognition (Figure 3B). To determine if the observed decrease in transduction was due to capsid stability, we performed heat treatment analysis, which revealed the same phenotype as AAV4-YKIPA, with an ability to dissociate at 65C whereas AAV4 can withstand heat treatment up to 75C and potentially beyond (Figure 3C). Therefore, it was apparent that this region of the capsid is playing a

crucial role in capsid stability even though the side chains appear vulnerable to potential interactions with partners based on the crystal structure.

Therefore, to maintain capsid stability, instead of domain removal and alanine mutagenesis, we chose to solely mutate the tyrosines on the surface of the three-fold to phenylalanines to ensure unaltered hydrophobic interactions with the side chain ring structure (Figure 1). Mutation of the phenylalanines alone did not affect capsid stability based on heat treatment analysis (Figure 4B), nor did they affect viral transduction in cos-7 cells (Figure 4A), therefore the tyrosines on the surface of the three-fold are necessary for maintenance of viral capsid stability. Additionally, these mutants were injected systemically into mice and determined that altering the surface tyrosine did not affect tropism and transduction unlike what is observed with mutation of specific surface tyrosines on the AAV2 capsid.

AAV4 two-fold

Post analysis of what was thought to be a key domain on the three-fold axis, determining that it was necessary for AAV4 capsid stability, we decided to analyze the two-fold axis with a collection of mutant constructs generated by Joe Rabinowitz. The two-fold mutants were chimeras between AAV4 and AAV2, where small amino acid stretches of AAV4 were replaced with the corresponding AAV2 amino acids (Figure 5A). Originally, these constructs were generated in order to determine if altering the two-fold of AAV4 would alter capsid uncoating since it is believed that AAV4 may uncoat more slowly than AAV2 based on *in vivo* data (169).

Amino acids 253-267, 369-385, 694-705 in the AAV4 capsid were substituted with those from AAV2 in separate constructs and virus was produced. More chimeras were generated by cotransfecting all three constructs, which would completely replace the two-

fold, or just the AAV4/2 253-267 and AAV4/2 694-705 constructs to replace the surface and inner capsid regions of the two-fold axis. All mutants generated virus except for AAV4/2 369-385 based on dot blot analysis against the viral transgene (data not shown).

Additionally a western dot blot was performed on all viral preparations, and ADK4, the AAV4 primary antibody against intact particles was unable to recognize AAV4/2 253-276 (data not shown). Therefore, we may have determined one of the conformational epitopes necessary for primary antibody recognition. Next viral infectivity was examined on 293 and cos-7 cells to determine if the presence of the AAV2 domains on the capsid surface would rescue the inability of AAV4 to transduce or ablate AAV4 transduction, respectively (Figure 5B). The AAV4/2 chimeras were unable to transduce both cell types, therefore, the presence of AAV2 amino acids on the AAV4 capsid did not increase AAV4's ability to infect 293 cells and actually rendered the AAV4 capsid noninfectious in cos-7 cells.

Contrary to what was determined with the removal of the AAV4 YKIPA domain, all of these two-fold mutants maintained stability during heat treatment analysis similar to AAV4 wildtype particles based on the ability to protect the viral transgene post DNase treatment (Figure 5C).

Even though these mutants were not playing a role in capsid stability they may be playing a role in other aspects of the AAV4 life cycle. For instance, AAV4/2 253-267 was undetectable by primary antibody ADK4 against the intact particle, which potentially implicates this region as an epitope for antibody recognition or upon mutation conformationally changes the capsid elsewhere ablating antibody recognition. Additionally, AAV4/2 694-705 was unable to bind a mucin column (Figure 5D), containing the sialic acid residues established to be necessary for AAV4 primary receptor binding. Therefore the C-

terminal portion of the AAV4 capsid may be partly responsible for primary receptor recognition. Additionally, this mutant was injected IV along with AAV4 wildtype capsids as a control (Figure 6A). AAV4 transduces the lung and heart post systemic injection, however AAV4/2 694-705 was unable to transduce the heart and lung based on relative light units and vector genome quantification, and instead seemed to transduce the abdominal muscle more efficiently than other tissue types (Figure 6B). To further validate the lack of ability to bind sialic acid AAV4 was injected IV post systemic injection of sialidase ablating the ability of AAV4 to transduce *in vivo* (Figure 6C). Therefore, the AAV4/2 694-705 chimera may be a variant of AAV4 not affecting capsid stability, but potentially AAV4 tropism by ablation of sialic acid binding properties.

Conclusions and future work

In this study a series of mutants were generated in order to uncover more about the AAV4 capsid structure-function relationship. In doing so, we stumbled across what may develop to be important findings about multiple regions of the capsid and their contributions to functionality.

The AAV4 capsid topologically is extremely different than the AAV2 capsid, specifically in the loop regions. AAV4 has rounder more blunt three-fold spikes with narrower valleys and a deeper two-fold depression than observed with the AAV2 capsid structure.

There has not been much research performed on the AAV4 capsid with regards to understanding capsid domains. However it has been well established with the AAV2 capsid that specific domains, for example the three-fold loops are responsible for primary and co-

receptor binding as well as immune system stimulation (5, 64, 156). The 265 loop in the dead zone also plays a role in primary antibody recognition, where upon mutation A20 is unable to recognize the intact particle (79) (Bowles/DiPrimio unpublished). Interestingly, we chose to study multiple regions of the capsid, assuming these regions might be playing similar roles as in AAV2 but surprisingly observed varying results.

With regards to the three-fold axis, we characterized what was thought to be potentially a domain, YKIPA, for cell surface interactions based on the topology and amino acid sequence conservation with AAV11. Upon removal it was apparent that this domain was not involved in receptor recognition based on the ability of AAV4-YKIPA to bind cell surfaces. However, when vector genomes were quantified post internalization, AAV4-YKIPA infected cells contained fewer vector genomes as compared to AAV4. It was quite possible that this domain was necessary for virus internalization since multiple receptors utilize tyrosine driven internalization domains such as YXXhydrophobic (150), NPXY (26), YXRF (16), and YKYSKV (60). Not only did we think that YKIPA could be a linear domain, but conformationally, the AAV4 capsid forms a potential Y(491)KKY(594) motif on the capsid surface that warranted further characterization.

In order to determine if this domain was truly a tyrosine driven internalization motif, the tyrosines were mutated to phenylalanines to retain structural integrity. AAV4 Y491F and Y594F behaved similarly to AAV4, disproving the theory that the YKIPA domain was necessary for virus internalization. What was determined was that this region of the three-fold is necessary for capsid stability, since based on heat treatment analysis, AAV4-YKIPA was less stable than AAV4, being an extremely stable particle, maintaining integrity at 75°C. Therefore, we believe that between the binding and internalization stages of AAV4, the

capsid particle is destabilized and releases the genome externally, or prematurely internally allowing for DNA degradation. The three-fold axis, originally based on the AAV2 capsid structure is the most interdigitated region with the highest amino acid contact energies (163). Therefore the AAV4 data further validates the necessity to maintain contacts at this region for proper capsid stability. Additionally, these data eliminated the possibility that the surface tyrosines at the three-fold axis are playing a role in capsid phosphorylation dissimilar to what is observed with the AAV2 capsid in the literature (168).

In addition, the two-fold axis of symmetry was analyzed with a series of AAV4/2 chimeras. The reason behind the generation of these mutants by Joe Rabinowitz (unpublished) was based on the assumption that AAV4 is slower to uncoat and release the genome when compared to other serotypes, and the two-fold axis is the weakest part of the capsid so by altering it, may allow for an earlier onset of genome release. However, in the literature there is little proof of the two-fold axis being the site of virus uncoating (71), and AAV2 does not necessarily have a faster onset of expression that AAV4. Based on data in this appendix, AAV4 transduces the heart at least one week post injection which is similar to AAV2 transduction in the liver from previous research, so it may be more beneficial to replace this region with amino acids from another serotype (131). However, for the purpose of this study, we found these mutants interesting due to the possibility of uncovering other unknown phenotypic properties of the AAV4 capsid.

As predicted, domains for faster uncoating were not detected based on *in vitro* and *in vivo* studies. However, in generating these viruses, we have potentially located a domain for primary ADK4 (72) antibody recognition or a region that induces a gross conformational change ablating antibody recognition with AAV4/2 253-276. Antibody recognition epitopes

with respect to AAV2 have been determined by epitope mapping via phage display (153) or mutagenesis of the capsid (79) so with further analysis, we may be able to concretely identify epitopes on the AAV4 capsid surface.

Additionally, even though in the case of AAV2 and AAV5 (Agbandje-McKenna unpublished), the three-fold is the site of primary receptor and co-receptor binding it is possible that other serotypes utilize the two-fold as seen with the ablation of sialic acid binding based on mucin studies with AAV4/2 694-705 (61, 141). Substitution of this region of AAV4 with AAV2 amino acids may be affecting capsid gross conformation ablating receptor interactions, or this could actually be the site of primary receptor attachment. It has also been reported that MVM utilizes another region of the capsid, the two-fold depression for receptor recognition (91). With regards to sialic acid binding Dr. Agbandje-McKenna has determined the residues for AAV5 sialic acid recognition via co-crystallization as well as MVM (personal communication), so potentially further biochemical and structural analysis may allow for the determination of AAV4 sialic acid binding residues as well. Additionally, our treatment of mice with sialidase may be expanded as a model to study virus targeting *in vivo* in order to determine if mutants can enter tissues without using sialic acid, or heparin post heparinase treatment. Therefore these studies have opened possibilities for multiple projects involving AAV4 and mutant derivatives.

Figure 1. Mutagenesis of the AAV4 YKIPA three-fold domain

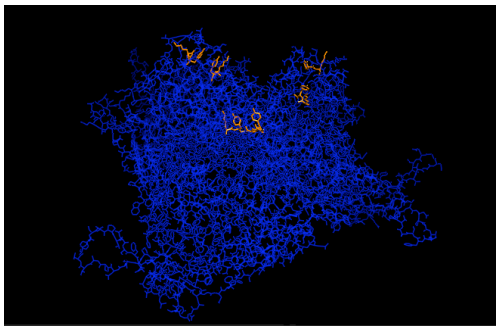

```
AAV2 (492)          SADN-----NNSE
AAV4 (487)          ANQNYKIPATGSD
AAV4-YKIPA (487)    ANQN-----TGSD

AAV4 YK-AA (487)    ANQNAAIPATGSD
AAV4 Y491F (487)    ANQNFKIPATGSD

AAV4 (497)          GSDSLIKYETHS
AAV4 KY-AA (497)    GSDSLIAAETHS
AAV4 Y504F (497)    GSDSLIKFETHS
```

Figure 1. Mutagenesis of the AAV4 YKIPA three-fold domain. A model of the AAV4 three-fold axis in blue with the YKIPA domain highlighted in pink is shown on top. Below the model are sequence alignments of the YKIPA region of the capsid and the deletion, phenylalanine and alanine mutants generated.

Figure 2. Removal of the AAV4 YKIPA region affects capsid stability.

A.

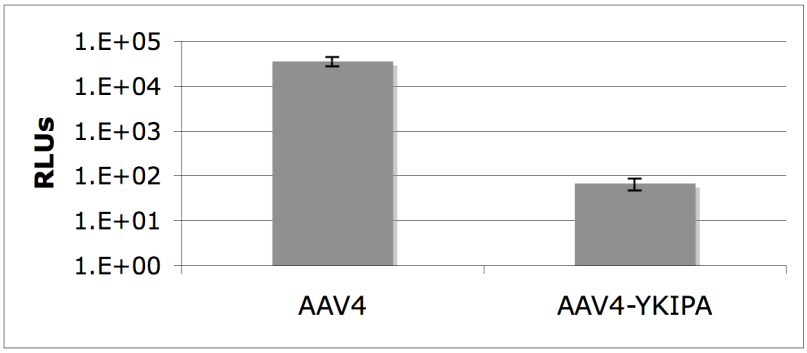

B.

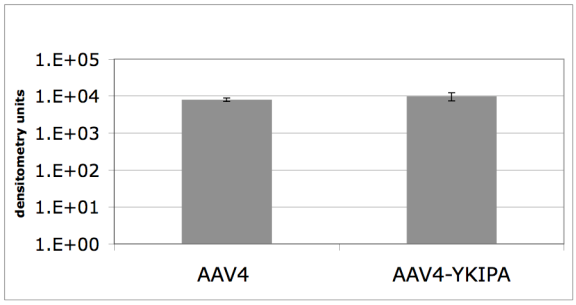

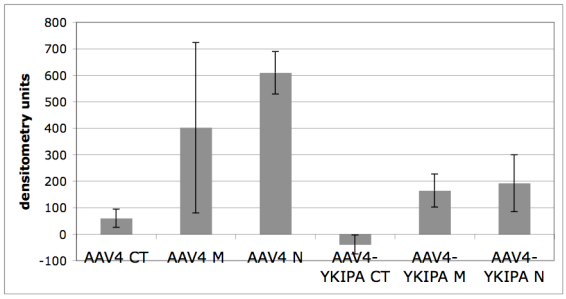

C.

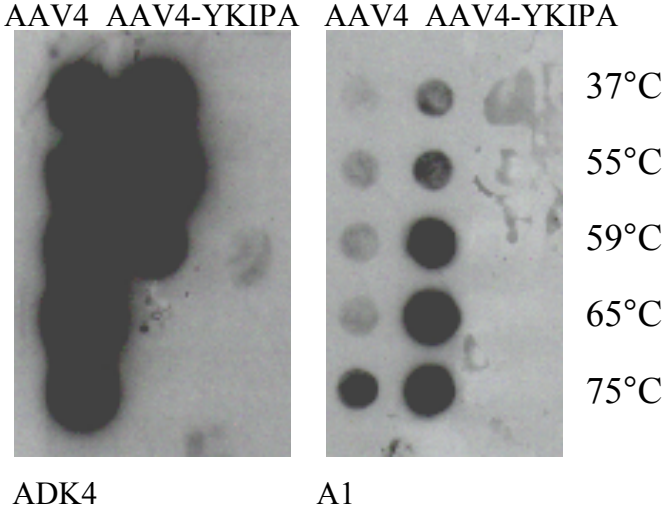

Figure 2. Removal of the AAV4 YKIPA region affects capsid stability. (A) Cos-7 cells were infected with 3000 vector genome containing particles/cell of AAV4 and AAV4-YKIPA carrying the luciferase transgene. Viral infectivity was quantified via luciferase assay of cos-7 cells as previously mentioned (Promega). (B) AAV4 cell surface binding and internalization was quantified. Cos-7 cells were incubated in suspension with AAV4 and AAV4-YKIPA (5000 vector genome containing particles/cell) at 4°C for 1 hour to facilitate binding. Cells were kept on ice, pelleted and washed three times with 1XPBS. Bound genomes (density units) were quantified via dot blot analysis (left panel). Cells in suspension with AAV4 and AAV4-YKIPA were incubated at 4°C to facilitate binding and then at 37°C for internalization. 2hours post internalization the Cos-7 cells were fractionated into the cytoplasmic, membranous and nuclear fractions (BioVision FractioPREP Cell Fractionation System). For viral genome quantification via DNA dot blot analysis (right panel). SD=black bars N=3 (C) 1E9 AAV4 and AAV4-YKIPA vector genome containing particles were incubated at varying temperatures and blotted on nitrocellulose membrane. The membrane was blotted with primary ADK4 antibody (undiluted) against intact particles, or A1 (1:20) to detect VP1 exposed particles.

Figure 3. Alanine mutagenesis of three-fold residues yields unstable particles.
A.
AAV4 (487) ANQNYKIPATGSDSLIKY
AAV4 (487) ANQNAAIPATGSDSLIAA

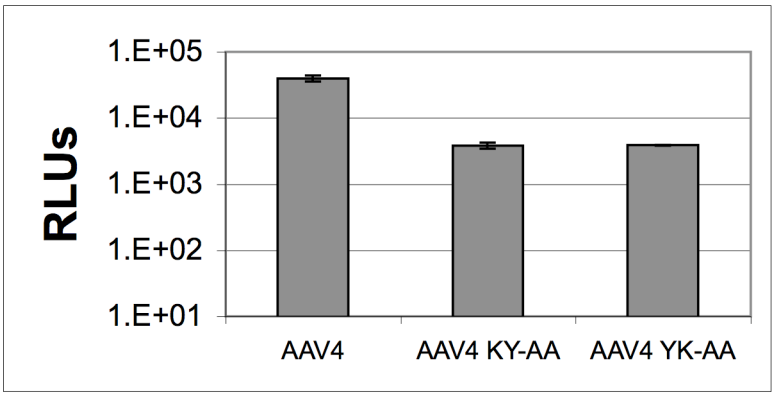

B.

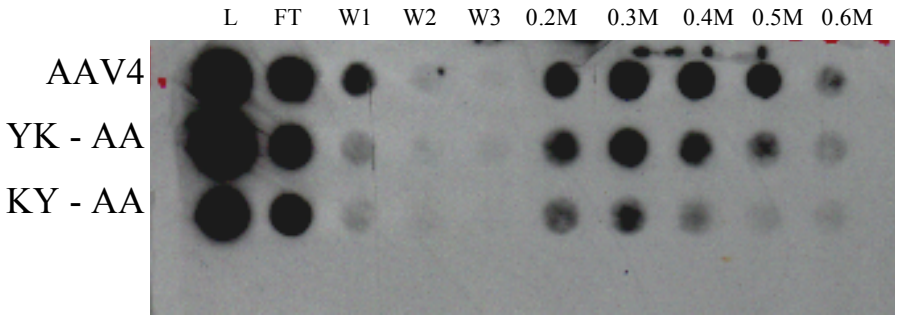

C.

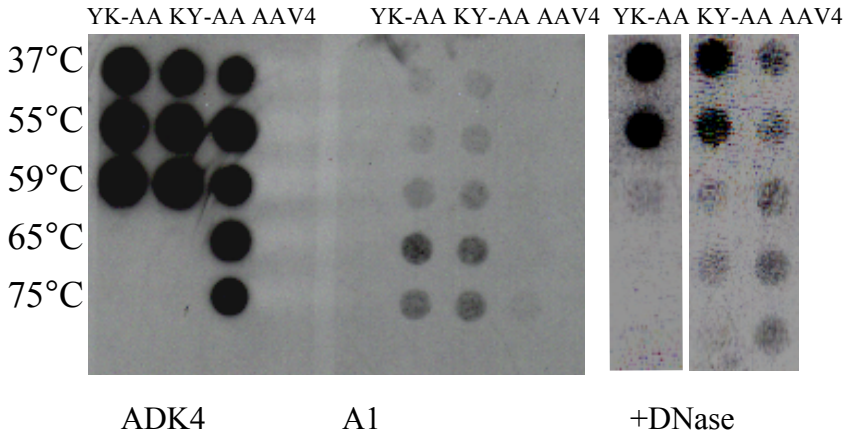

Figure 3. Alanine mutagenesis of three-fold residues yields unstable particles. (A) Cos-7 cells were infected with 3000 vector genome containing particles/cell of AAV4 KY-AA, AAV4 YK-AA and AAV4 and infectivity was quantified via luciferase assay as previously mentioned. (B) 2E9 AAV4, AAV4 YK-AA and AAV4 KY-AA were incubated with mucin

beads and eluted with increasing concentrations of salt. Fractions were blotted on a nitrocellulose membrane and stained with primary antibody ADK4 against intact capsids. (C) 6E8 AAV4, AAV4 YK-AA and AAV4 KY-AA particles were incubated at increasing temperatures, blotted on a nitrocellulose membrane and stained as previously mentioned. Additionally these heat-treated capsids were treated with DNase, blotted on a Hybond XL membrane, and genomes were detected with a radioactively labeled probed against the transgene.

Figure 4. Mutagenesis of three-fold tyrosines to phenylalanines rescues capsid stability
A.

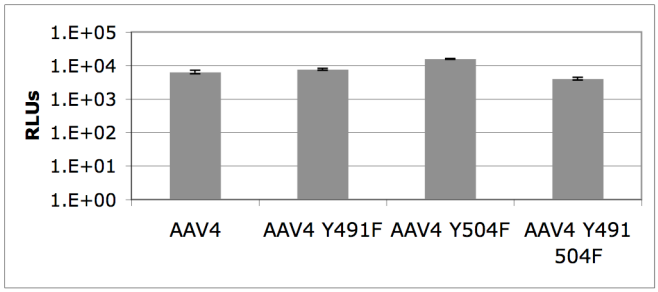

B.

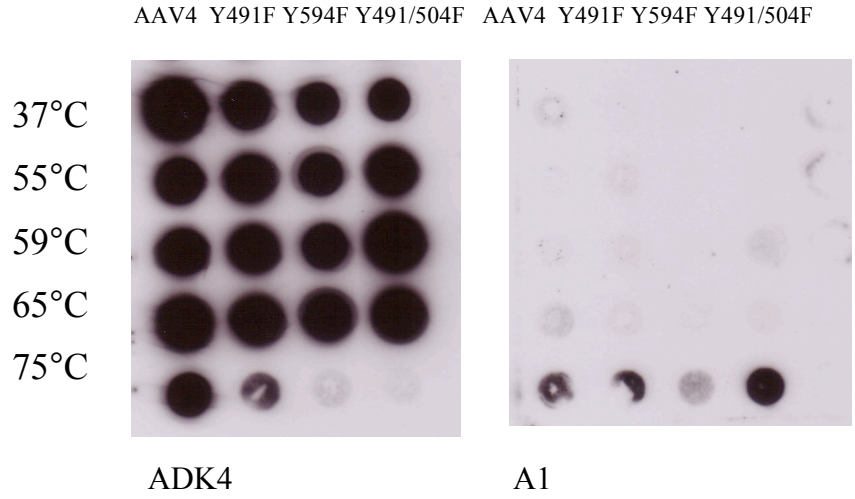

Figure 4. Mutagenesis of three-fold tyrosines to phenylalanines rescues capsid stability. (A) 3000 vector genome containing AAV4 Y491F, Y504F and Y491/504F particles/cell were incubated with Cos-7 cells, and infectivity was quantified via luciferase assay. (B) 6E8 vector genome containing particles of the aforementioned mutants were heat treated, blotted and stained as mentioned above.

Figure 5. AAV4/2 chimeras yield phenotypic alterations.
A.

AAV4	**(247) NNHLYKRLG---ESLQSNTYNGFSTP**
AAV4/2 253-276	**(247) NNHLYKQISSGSGASNDNHYFGFSTP**
AAV4(364)	**(364) PQYGYCGLVTGNTSQQQTDRNAFYCLEY**
AAV4/2 369-385	**(364) PQYGYLTLNNG---SQAVGRSSFYCLEY**
AAV4(690)	**(690) TSNYGQQNSLLWAPDAAGKYTEPRA**
AAV4/2 694-705	**(690) TSNYNKSVNVDFTVDTNGVYTEPRA**

B. Cos-7 and 293 cell transduction
C.

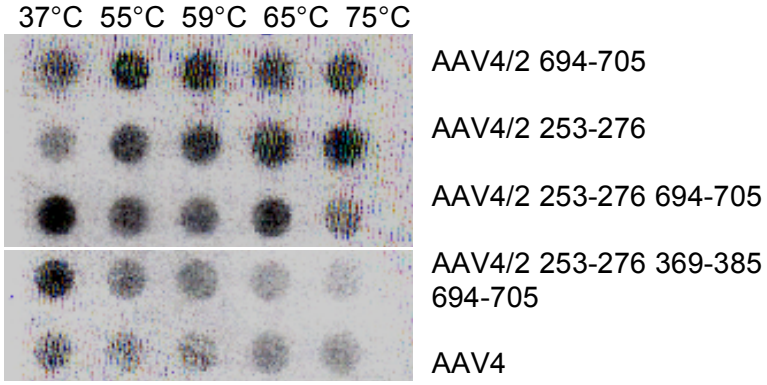

D.

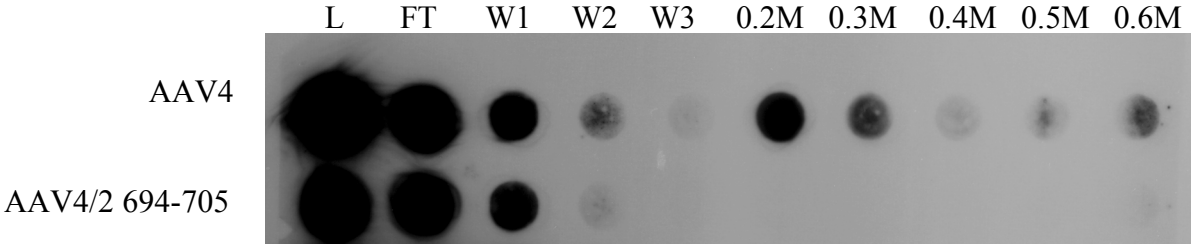

Figure 5. AAV4/2 chimeras yield phenotypic alterations. (A) Listed are sequence alignments of the AAV4 capsid regions replaced with AAV2. (B) Cos-7 cells and 293 cells were infected with 3000 vg containing particles/cell and quantified via luciferase assay as described previously. (C) AAV4/2 chimeras (6E8 vector genome containing particles) were incubated at increasing temperatures and treated with DNase to digest any exposed viral DNA. The treatments were blotted on a membrane and analyzed via DNA dot blot against the luciferase transgene. (D) AAV4 and AAV4/2 694-705 were incubated with mucin beads in a MicroBioSpin column (BioRad) and eluted with increasing concentrations of salt.

Figure 6. AAV4/2 694-705 particles are unable to transduce tissue *in vivo*.
A.

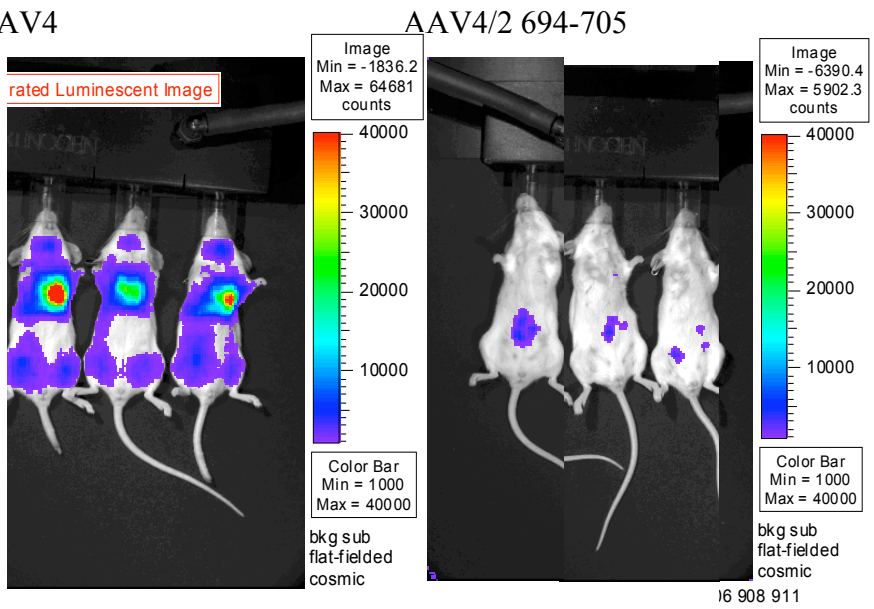

B.

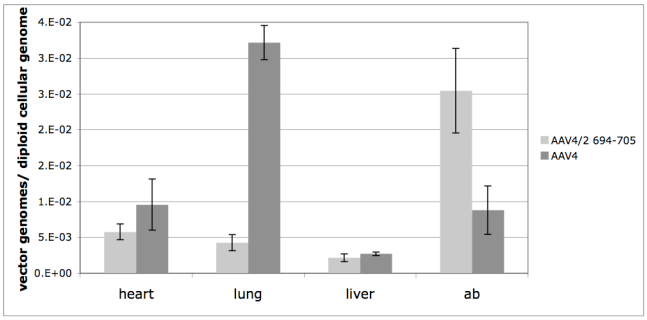

C.

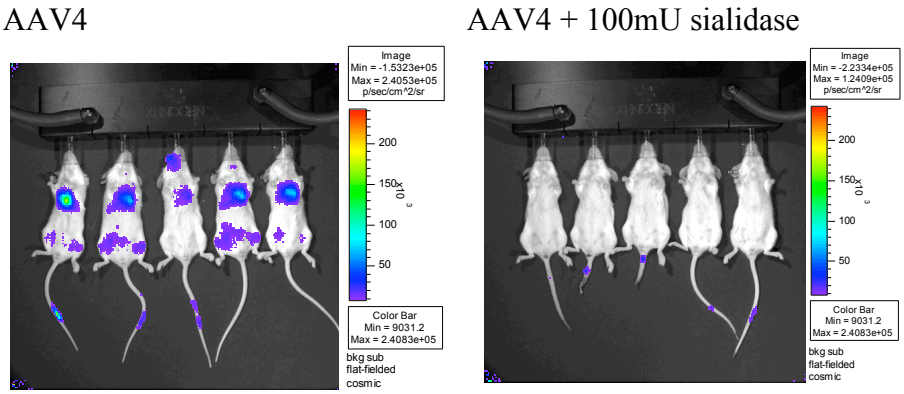

Figure 6. AAV4/2 694-705 particles are unable to transduce *in vivo*. (A) 1E11 vg containing particles of AAV4 and AAV4/2 694-705 were injected into mice via tail vein, and imaged 1week post injection with the IVIS Xenogen Imaging system (5min exposure). (B) Tissues were harvested 2weeks post injection and vector genomes were quantified via q-PCR of the luciferase transgene. (C) Mice were injected with 100mU sialidase and three hours post injection were injected with 1E11 vector genome containing particles of AAV4. Mice were imaged as previously mentioned.

REFERENCES

1. **Agbandje, M., R. McKenna, M. G. Rossmann, M. L. Strassheim, and C. R. Parrish.** 1993. Structure determination of feline panleukopenia virus empty particles. Proteins **16:**155-71.

2. **Agbandje-McKenna, M., A. L. Llamas-Saiz, F. Wang, P. Tattersall, and M. G. Rossmann.** 1998. Functional implications of the structure of the murine parvovirus, minute virus of mice. Structure **6:**1369-81.

3. **Akache, B., D. Grimm, K. Pandey, S. R. Yant, H. Xu, and M. A. Kay.** 2006. The 37/67-kilodalton laminin receptor is a receptor for adeno-associated virus serotypes 8, 2, 3, and 9. J Virol **80:**9831-6.

4. **Allocca, M., M. Doria, M. Petrillo, P. Colella, M. Garcia-Hoyos, D. Gibbs, S. R. Kim, A. Maguire, T. S. Rex, U. Di Vicino, L. Cutillo, J. R. Sparrow, D. S. Williams, J. Bennett, and A. Auricchio.** 2008. Serotype-dependent packaging of large genes in adeno-associated viral vectors results in effective gene delivery in mice. J Clin Invest **118:**1955-64.

5. **Asokan, A., J. B. Hamra, L. Govindasamy, M. Agbandje-McKenna, and R. J. Samulski.** 2006. Adeno-associated virus type 2 contains an integrin alpha5beta1 binding domain essential for viral cell entry. J Virol **80:**8961-9.

6. **Bantel-Schaal, U., B. Hub, and J. Kartenbeck.** 2002. Endocytosis of adeno-associated virus type 5 leads to accumulation of virus particles in the Golgi compartment. J Virol **76:**2340-9.

7. **Bartlett, J. S., R. Wilcher, and R. J. Samulski.** 2000. Infectious entry pathway of adeno-associated virus and adeno-associated virus vectors. J Virol **74:**2777-85.

8. **Berns, K. I., and R. M. Linden.** 1995. The cryptic life style of adeno-associated virus. Bioessays **17:**237-45.

9. **Bleker, S., M. Pawlita, and J. A. Kleinschmidt.** 2006. Impact of capsid conformation and Rep-capsid interactions on adeno-associated virus type 2 genome packaging. J Virol **80:**810-20.

10. **Bleker, S., F. Sonntag, and J. A. Kleinschmidt.** 2005. Mutational analysis of narrow pores at the fivefold symmetry axes of adeno-associated virus type 2 capsids reveals a dual role in genome packaging and activation of phospholipase A2 activity. J Virol **79:**2528-40.

11. **Brown, K. J., and C. R. Parish.** 1994. Histidine-rich glycoprotein and platelet factor 4 mask heparan sulfate proteoglycans recognized by acidic and basic fibroblast growth factor. Biochemistry **33:**13918-27.

12. **Chang, N. S., R. W. Leu, J. A. Rummage, J. K. Anderson, and J. E. Mole.** 1992. Regulation of complement functional efficiency by histidine-rich glycoprotein. Blood **79:**2973-80.

13. **Chao, H., P. E. Monahan, Y. Liu, R. J. Samulski, and C. E. Walsh.** 2001. Sustained and complete phenotype correction of hemophilia B mice following intramuscular injection of AAV1 serotype vectors. Mol Ther **4:**217-22.

14. **Chuah, M. K., and T. Vandendriessche.** 2007. Gene therapy for haemophilia "A" and "B": efficacy, safety and immune consequences. Bull Mem Acad R Med Belg **162:**357-61.

15. **Clement, N., B. Avalosse, K. El Bakkouri, T. Velu, and A. Brandenburger.** 2001. Cloning and sequencing of defective particles derived from the autonomous parvovirus minute virus of mice for the construction of vectors with minimal cis-acting sequences. J Virol **75:**1284-93.

16. **Collawn, J. F., M. Stangel, L. A. Kuhn, V. Esekogwu, S. Q. Jing, I. S. Trowbridge, and J. A. Tainer.** 1990. Transferrin receptor internalization sequence YXRF implicates a tight turn as the structural recognition motif for endocytosis. Cell **63:**1061-72.

17. **Colonno, R. J., J. H. Condra, S. Mizutani, P. L. Callahan, M. E. Davies, and M. A. Murcko.** 1988. Evidence for the direct involvement of the rhinovirus canyon in receptor binding. Proc Natl Acad Sci U S A **85:**5449-53.

18. **Crespo, M. D., G. W. Platt, R. Bofill, and M. S. Searle.** 2004. Context-dependent effects of proline residues on the stability and folding pathway of ubiquitin. Eur J Biochem **271:**4474-84.

19. **Davidson, B. L., C. S. Stein, J. A. Heth, I. Martins, R. M. Kotin, T. A. Derksen, J. Zabner, A. Ghodsi, and J. A. Chiorini.** 2000. Recombinant adeno-associated virus type 2, 4, and 5 vectors: transduction of variant cell types and regions in the mammalian central nervous system. Proc Natl Acad Sci U S A **97:**3428-32.

20. **Di Pasquale, G., B. L. Davidson, C. S. Stein, I. Martins, D. Scudiero, A. Monks, and J. A. Chiorini.** 2003. Identification of PDGFR as a receptor for AAV-5 transduction. Nat Med **9:**1306-12.

21. **Diaz-Avalos, R., and D. L. Caspar.** 1998. Structure of the stacked disk aggregate of tobacco mosaic virus protein. Biophys J **74:**595-603.

22. **DiMattia, M., L. Govindasamy, H. C. Levy, B. Gurda-Whitaker, A. Kalina, E. Kohlbrenner, J. A. Chiorini, R. McKenna, N. Muzyczka, S. Zolotukhin, and M. Agbandje-McKenna.** 2005. Production, purification, crystallization and preliminary

X-ray structural studies of adeno-associated virus serotype 5. Acta Crystallograph Sect F Struct Biol Cryst Commun **61:**917-21.

23. **Ding, W., L. Zhang, Z. Yan, and J. F. Engelhardt.** 2005. Intracellular trafficking of adeno-associated viral vectors. Gene Ther **12:**873-80.

24. **DiPrimio, N., A. Asokan, L. Govindasamy, M. Agbandje-McKenna, and R. J. Samulski.** 2008. Surface loop dynamics in adeno-associated virus capsid assembly. J Virol **82:**5178-89.

25. **Douar, A. M., K. Poulard, D. Stockholm, and O. Danos.** 2001. Intracellular trafficking of adeno-associated virus vectors: routing to the late endosomal compartment and proteasome degradation. J Virol **75:**1824-33.

26. **Eto, D. S., H. B. Gordon, B. K. Dhakal, T. A. Jones, and M. A. Mulvey.** 2008. Clathrin, AP-2, and the NPXY-binding subset of alternate endocytic adaptors facilitate FimH-mediated bacterial invasion of host cells. Cell Microbiol **10:**2553-67.

27. **Farr, G. A., L. G. Zhang, and P. Tattersall.** 2005. Parvoviral virions deploy a capsid-tethered lipolytic enzyme to breach the endosomal membrane during cell entry. Proc Natl Acad Sci U S A **102:**17148-53.

28. **Ferrari, F. K., T. Samulski, T. Shenk, and R. J. Samulski.** 1996. Second-strand synthesis is a rate-limiting step for efficient transduction by recombinant adeno-associated virus vectors. J Virol **70:**3227-34.

29. **Flotte, T. R., P. L. Zeitlin, T. C. Reynolds, A. E. Heald, P. Pedersen, S. Beck, C. K. Conrad, L. Brass-Ernst, M. Humphries, K. Sullivan, R. Wetzel, G. Taylor, B. J. Carter, and W. B. Guggino.** 2003. Phase I trial of intranasal and endobronchial administration of a recombinant adeno-associated virus serotype 2 (rAAV2)-CFTR vector in adult cystic fibrosis patients: a two-part clinical study. Hum Gene Ther **14:**1079-88.

30. **Fukuchi, K., K. Tahara, H. D. Kim, J. A. Maxwell, T. L. Lewis, M. A. Accavitti-Loper, H. Kim, S. Ponnazhagan, and R. Lalonde.** 2006. Anti-Abeta single-chain antibody delivery via adeno-associated virus for treatment of Alzheimer's disease. Neurobiol Dis **23:**502-11.

31. **Gao, G., Y. Lu, R. Calcedo, R. L. Grant, P. Bell, L. Wang, J. Figueredo, M. Lock, and J. M. Wilson.** 2006. Biology of AAV serotype vectors in liver-directed gene transfer to nonhuman primates. Mol Ther **13:**77-87.

32. **Gao, G., L. H. Vandenberghe, M. R. Alvira, Y. Lu, R. Calcedo, X. Zhou, and J. M. Wilson.** 2004. Clades of Adeno-associated viruses are widely disseminated in human tissues. J Virol **78:**6381-8.

33. **Geoffroy, M. C., and A. Salvetti.** 2005. Helper functions required for wild type and recombinant adeno-associated virus growth. Curr Gene Ther **5:**265-71.

34. **Giraud, C., E. Winocour, and K. I. Berns.** 1995. Recombinant junctions formed by site-specific integration of adeno-associated virus into an episome. J Virol **69:**6917-24.

35. **Girod, A., M. Ried, C. Wobus, H. Lahm, K. Leike, J. Kleinschmidt, G. Deleage, and M. Hallek.** 1999. Genetic capsid modifications allow efficient re-targeting of adeno-associated virus type 2. Nat Med **5:**1052-6.

36. **Girod, A., C. E. Wobus, Z. Zadori, M. Ried, K. Leike, P. Tijssen, J. A. Kleinschmidt, and M. Hallek.** 2002. The VP1 capsid protein of adeno-associated virus type 2 is carrying a phospholipase A2 domain required for virus infectivity. J Gen Virol **83:**973-8.

37. **Gorgani, N. N., C. R. Parish, S. B. Easterbrook Smith, and J. G. Altin.** 1997. Histidine-rich glycoprotein binds to human IgG and C1q and inhibits the formation of insoluble immune complexes. Biochemistry **36:**6653-62.

38. **Govindasamy, L., E. Padron, R. McKenna, N. Muzyczka, N. Kaludov, J. A. Chiorini, and M. Agbandje-McKenna.** 2006. Structurally mapping the diverse phenotype of adeno-associated virus serotype 4. J Virol **80:**11556-70.

39. **Grieger, J. C., V. W. Choi, and R. J. Samulski.** 2006. Production and characterization of adeno-associated viral vectors. Nat Protoc **1:**1412-28.

40. **Grieger, J. C., J. S. Johnson, B. Gurda-Whitaker, M. Agbandje-McKenna, and R. J. Samulski.** 2007. Surface-exposed adeno-associated virus Vp1-NLS capsid fusion protein rescues infectivity of noninfectious wild-type Vp2/Vp3 and Vp3-only capsids but not that of fivefold pore mutant virions. J Virol **81:**7833-43.

41. **Grieger, J. C., and R. J. Samulski.** 2005. Packaging capacity of adeno-associated virus serotypes: impact of larger genomes on infectivity and postentry steps. J Virol **79:**9933-44.

42. **Grieger, J. C., S. Snowdy, and R. J. Samulski.** 2006. Separate basic region motifs within the adeno-associated virus capsid proteins are essential for infectivity and assembly. J Virol **80:**5199-210.

43. **Grifman, M., M. Trepel, P. Speece, L. B. Gilbert, W. Arap, R. Pasqualini, and M. D. Weitzman.** 2001. Incorporation of tumor-targeting peptides into recombinant adeno-associated virus capsids. Mol Ther **3:**964-75.

44. **Hajjar, R. J., and K. Zsebo.** 2007. AAV vectors and cardiovascular disease: targeting TNF receptor in the heart: clue to way forward with AAV? Gene Ther **14:**1611-2.

45. **Hamilton, H., J. Gomos, K. I. Berns, and E. Falck-Pedersen.** 2004. Adeno-associated virus site-specific integration and AAVS1 disruption. J Virol **78:**7874-82.

46. **Hauck, B., and W. Xiao.** 2003. Characterization of tissue tropism determinants of adeno-associated virus type 1. J Virol **77:**2768-74.

47. **He, Y., V. D. Bowman, S. Mueller, C. M. Bator, J. Bella, X. Peng, T. S. Baker, E. Wimmer, R. J. Kuhn, and M. G. Rossmann.** 2000. Interaction of the poliovirus receptor with poliovirus. Proc Natl Acad Sci U S A **97:**79-84.

48. **Herzog, R. W.** 2007. Immune responses to AAV capsid: are mice not humans after all? Mol Ther **15:**649-50.

49. **Hickman, A. B., D. R. Ronning, R. M. Kotin, and F. Dyda.** 2002. Structural unity among viral origin binding proteins: crystal structure of the nuclease domain of adeno-associated virus Rep. Mol Cell **10:**327-37.

50. **Horn, N. M., and A. L. Thomas.** 1996. Interactions between the histidine stimulation of cadmium and zinc influx into human erythrocytes. J Physiol **496 (Pt 3):**711-8.

51. **Howard, D. B., K. Powers, Y. Wang, and B. K. Harvey.** 2008. Tropism and toxicity of adeno-associated viral vector serotypes 1, 2, 5, 6, 7, 8, and 9 in rat neurons and glia in vitro. Virology **372:**24-34.

52. **Hunter, L. A., and R. J. Samulski.** 1992. Colocalization of adeno-associated virus Rep and capsid proteins in the nuclei of infected cells. J Virol **66:**317-24.

53. **Huttner, N. A., A. Girod, L. Perabo, D. Edbauer, J. A. Kleinschmidt, H. Buning, and M. Hallek.** 2003. Genetic modifications of the adeno-associated virus type 2 capsid reduce the affinity and the neutralizing effects of human serum antibodies. Gene Ther **10:**2139-47.

54. **Inagaki, K., S. Fuess, T. A. Storm, G. A. Gibson, C. F. McTiernan, M. A. Kay, and H. Nakai.** 2006. Robust systemic transduction with AAV9 vectors in mice: efficient global cardiac gene transfer superior to that of AAV8. Mol Ther **14:**45-53.

55. **Janson, C., S. McPhee, L. Bilaniuk, J. Haselgrove, M. Testaiuti, A. Freese, D. J. Wang, D. Shera, P. Hurh, J. Rupin, E. Saslow, O. Goldfarb, M. Goldberg, G. Larijani, W. Sharrar, L. Liouterman, A. Camp, E. Kolodny, J. Samulski, and P. Leone.** 2002. Clinical protocol. Gene therapy of Canavan disease: AAV-2 vector for neurosurgical delivery of aspartoacylase gene (ASPA) to the human brain. Hum Gene Ther **13:**1391-412.

56. **Jardine, P. J., and D. H. Coombs.** 1998. Capsid expansion follows the initiation of DNA packaging in bacteriophage T4. J Mol Biol **284:**661-72.

57. **Jayandharan, G. R., L. Zhong, B. Li, B. Kachniarz, and A. Srivastava.** 2008. Strategies for improving the transduction efficiency of single-stranded adeno-associated virus vectors in vitro and in vivo. Gene Ther **15:**1287-93.

58. **Jiang, H., L. B. Couto, S. Patarroyo-White, T. Liu, D. Nagy, J. A. Vargas, S. Zhou, C. D. Scallan, J. Sommer, S. Vijay, F. Mingozzi, K. A. High, and G. F. Pierce.** 2006. Effects of transient immunosuppression on adenoassociated, virus-mediated, liver-directed gene transfer in rhesus macaques and implications for human gene therapy. Blood **108:**3321-8.

59. **Johnson, J. S., and R. J. Samulski.** 2009. Enhancement of AAV infection by mobilizing capsids into and out of the nucleolus. J Virol **83:**2632-44.

60. **Juuti-Uusitalo, K., K. J. Airenne, A. Laukkanen, E. L. Punnonen, V. M. Olkkonen, J. Gruenberg, M. Kulomaa, and V. Marjomaki.** 2000. Selective targeting of avidin/mannose 6-phosphate receptor chimeras to early or late endosomes. Eur J Cell Biol **79:**458-68.

61. **Kaludov, N., K. E. Brown, R. W. Walters, J. Zabner, and J. A. Chiorini.** 2001. Adeno-associated virus serotype 4 (AAV4) and AAV5 both require sialic acid binding for hemagglutination and efficient transduction but differ in sialic acid linkage specificity. J Virol **75:**6884-93.

62. **Kashiwakura, Y., K. Tamayose, K. Iwabuchi, Y. Hirai, T. Shimada, K. Matsumoto, T. Nakamura, M. Watanabe, K. Oshimi, and H. Daida.** 2005. Hepatocyte growth factor receptor is a coreceptor for adeno-associated virus type 2 infection. J Virol **79:**609-14.

63. **Kaufmann, B., A. A. Simpson, and M. G. Rossmann.** 2004. The structure of human parvovirus B19. Proc Natl Acad Sci U S A **101:**11628-33.

64. **Kern, A., K. Schmidt, C. Leder, O. J. Muller, C. E. Wobus, K. Bettinger, C. W. Von der Lieth, J. A. King, and J. A. Kleinschmidt.** 2003. Identification of a heparin-binding motif on adeno-associated virus type 2 capsids. J Virol **77:**11072-81.

65. **Kim, E., D. W. Shin, C. S. Hong, D. Jeong, D. H. Kim, and W. J. Park.** 2003. Increased Ca2+ storage capacity in the sarcoplasmic reticulum by overexpression of HRC (histidine-rich Ca2+ binding protein). Biochem Biophys Res Commun **300:**192-6.

66. **King, J. A., R. Dubielzig, D. Grimm, and J. A. Kleinschmidt.** 2001. DNA helicase-mediated packaging of adeno-associated virus type 2 genomes into preformed capsids. Embo J **20:**3282-91.

67. **Koerber, J. T., J. H. Jang, and D. V. Schaffer.** 2008. DNA shuffling of adeno-associated virus yields functionally diverse viral progeny. Mol Ther **16:**1703-9.

68. **Koerber, J. T., J. H. Jang, J. H. Yu, R. S. Kane, and D. V. Schaffer.** 2007. Engineering adeno-associated virus for one-step purification via immobilized metal affinity chromatography. Hum Gene Ther **18:**367-78.

69. **Kohlbrenner, E., G. Aslanidi, K. Nash, S. Shklyaev, M. Campbell-Thompson, B. J. Byrne, R. O. Snyder, N. Muzyczka, K. H. Warrington, Jr., and S. Zolotukhin.** 2005. Successful production of pseudotyped rAAV vectors using a modified baculovirus expression system. Mol Ther **12:**1217-25.

70. **Koivunen, E., D. A. Gay, and E. Ruoslahti.** 1993. Selection of peptides binding to the alpha 5 beta 1 integrin from phage display library. J Biol Chem **268:**20205-10.

71. **Kronenberg, S., B. Bottcher, C. W. von der Lieth, S. Bleker, and J. A. Kleinschmidt.** 2005. A conformational change in the adeno-associated virus type 2 capsid leads to the exposure of hidden VP1 N termini. J Virol **79:**5296-303.

72. **Kuck, D., A. Kern, and J. A. Kleinschmidt.** 2007. Development of AAV serotype-specific ELISAs using novel monoclonal antibodies. J Virol Methods **140:**17-24.

73. **Lai, Y., D. Li, Y. Yue, and D. Duan.** 2008. Design of trans-splicing adeno-associated viral vectors for Duchenne muscular dystrophy gene therapy. Methods Mol Biol **433:**259-75.

74. **Leung, L. L., R. L. Nachman, and P. C. Harpel.** 1984. Complex formation of platelet thrombospondin with histidine-rich glycoprotein. J Clin Invest **73:**5-12.

75. **Levy, H. C., V. D. Bowman, L. Govindasamy, R. McKenna, K. Nash, K. Warrington, W. Chen, N. Muzyczka, X. Yan, T. S. Baker, and M. Agbandje-McKenna.** 2009. Heparin binding induces conformational changes in Adeno-associated virus serotype 2. J Struct Biol **165:**146-56.

76. **Li, W., A. Asokan, Z. Wu, T. Van Dyke, N. DiPrimio, J. S. Johnson, L. Govindaswamy, M. Agbandje-McKenna, S. Leichtle, D. E. Redmond, Jr., T. J. McCown, K. B. Petermann, N. E. Sharpless, and R. J. Samulski.** 2008. Engineering and selection of shuffled AAV genomes: a new strategy for producing targeted biological nanoparticles. Mol Ther **16:**1252-60.

77. **Liu, G., I. H. Martins, J. A. Chiorini, and B. L. Davidson.** 2005. Adeno-associated virus type 4 (AAV4) targets ependyma and astrocytes in the subventricular zone and RMS. Gene Ther **12:**1503-8.

78. **Llamas-Saiz, A. L., M. Agbandje-McKenna, W. R. Wikoff, J. Bratton, P. Tattersall, and M. G. Rossmann.** 1997. Structure determination of minute virus of mice. Acta Crystallogr D Biol Crystallogr **53:**93-102.

79. **Lochrie, M. A., G. P. Tatsuno, B. Christie, J. W. McDonnell, S. Zhou, R. Surosky, G. F. Pierce, and P. Colosi.** 2006. Mutations on the external surfaces of adeno-associated virus type 2 capsids that affect transduction and neutralization. J Virol **80:**821-34.

80. **Lotery, A. J., G. S. Yang, R. F. Mullins, S. R. Russell, M. Schmidt, E. M. Stone, J. D. Lindbloom, J. A. Chiorini, R. M. Kotin, and B. L. Davidson.** 2003. Adeno-associated virus type 5: transduction efficiency and cell-type specificity in the primate retina. Hum Gene Ther **14:**1663-71.

81. **Maguire, A. M., F. Simonelli, E. A. Pierce, E. N. Pugh, Jr., F. Mingozzi, J. Bennicelli, S. Banfi, K. A. Marshall, F. Testa, E. M. Surace, S. Rossi, A. Lyubarsky, V. R. Arruda, B. Konkle, E. Stone, J. Sun, J. Jacobs, L. Dell'Osso, R. Hertle, J. X. Ma, T. M. Redmond, X. Zhu, B. Hauck, O. Zelenaia, K. S. Shindler, M. G. Maguire, J. F. Wright, N. J. Volpe, J. W. McDonnell, A. Auricchio, K. A. High, and J. Bennett.** 2008. Safety and efficacy of gene transfer for Leber's congenital amaurosis. N Engl J Med **358:**2240-8.

82. **McPhee, S. W., C. G. Janson, C. Li, R. J. Samulski, A. S. Camp, J. Francis, D. Shera, L. Lioutermann, M. Feely, A. Freese, and P. Leone.** 2006. Immune responses to AAV in a phase I study for Canavan disease. J Gene Med **8:**577-88.

83. **McTiernan, C. F., M. A. Mathier, X. Zhu, X. Xiao, E. Klein, C. H. Swan, H. Mehdi, G. Gibson, A. M. Trichel, J. C. Glorioso, A. M. Feldman, K. R. McCurry, and B. London.** 2007. Myocarditis following adeno-associated viral gene expression of human soluble TNF receptor (TNFRII-Fc) in baboon hearts. Gene Ther **14:**1613-22.

84. **Miller, E. B., B. Gurda-Whitaker, L. Govindasamy, R. McKenna, S. Zolotukhin, N. Muzyczka, and M. Agbandje-McKenna.** 2006. Production, purification and preliminary X-ray crystallographic studies of adeno-associated virus serotype 1. Acta Crystallogr Sect F Struct Biol Cryst Commun **62:**1271-4.

85. **Miyazawa, N., P. L. Leopold, N. R. Hackett, B. Ferris, S. Worgall, E. Falck-Pedersen, and R. G. Crystal.** 1999. Fiber swap between adenovirus subgroups B and C alters intracellular trafficking of adenovirus gene transfer vectors. J Virol **73:**6056-65.

86. **Morgan, W. T., V. Deaciuc, and J. P. Riehm.** 1989. A heme- and metal-binding hexapeptide from the sequence of rabbit plasma histidine-rich glycoprotein. J Mol Recognit **2:**122-6.

87. **Moss, R. B., D. Rodman, L. T. Spencer, M. L. Aitken, P. L. Zeitlin, D. Waltz, C. Milla, A. S. Brody, J. P. Clancy, B. Ramsey, N. Hamblett, and A. E. Heald.** 2004. Repeated adeno-associated virus serotype 2 aerosol-mediated cystic fibrosis transmembrane regulator gene transfer to the lungs of patients with cystic fibrosis: a multicenter, double-blind, placebo-controlled trial. Chest **125:**509-21.

88. **Muller, O. J., F. Kaul, M. D. Weitzman, R. Pasqualini, W. Arap, J. A. Kleinschmidt, and M. Trepel.** 2003. Random peptide libraries displayed on adeno-associated virus to select for targeted gene therapy vectors. Nat Biotechnol **21:**1040-6.

89. **Murphy, S. L., H. Li, S. Zhou, A. Schlachterman, and K. A. High.** 2008. Prolonged susceptibility to antibody-mediated neutralization for adeno-associated vectors targeted to the liver. Mol Ther **16:**138-45.

90. **Musatov, S., J. Roberts, D. Pfaff, and M. Kaplitt.** 2002. A cis-acting element that directs circular adeno-associated virus replication and packaging. J Virol **76:**12792-802.

91. **Nam, H. J., B. Gurda-Whitaker, W. Y. Gan, S. Ilaria, R. McKenna, P. Mehta, R. A. Alvarez, and M. Agbandje-McKenna.** 2006. Identification of the sialic acid structures recognized by minute virus of mice and the role of binding affinity in virulence adaptation. J Biol Chem **281:**25670-7.

92. **Nam, H. J., M. D. Lane, E. Padron, B. Gurda, R. McKenna, E. Kohlbrenner, G. Aslanidi, B. Byrne, N. Muzyczka, S. Zolotukhin, and M. Agbandje-McKenna.** 2007. Structure of adeno-associated virus serotype 8, a gene therapy vector. J Virol **81:**12260-71.

93. **Needham, P. G., J. M. Casper, V. Kalman-Maltese, K. Verrill, J. D. Dignam, and J. P. Trempe.** 2006. Adeno-associated virus rep protein-mediated inhibition of transcription of the adenovirus major late promoter in vitro. J Virol **80:**6207-17.

94. **O'Donnell, J., K. A. Taylor, and M. S. Chapman.** 2009. Adeno-associated virus-2 and its primary cellular receptor-Cryo-EM structure of a heparin complex. Virology **385:**434-43.

95. **Opella, S. J., A. C. Zeri, and S. H. Park.** 2008. Structure, dynamics, and assembly of filamentous bacteriophages by nuclear magnetic resonance spectroscopy. Annu Rev Phys Chem **59:**635-57.

96. **Opie, S. R., K. H. Warrington, Jr., M. Agbandje-McKenna, S. Zolotukhin, and N. Muzyczka.** 2003. Identification of amino acid residues in the capsid proteins of adeno-associated virus type 2 that contribute to heparan sulfate proteoglycan binding. J Virol **77:**6995-7006.

97. **Padron, E., V. Bowman, N. Kaludov, L. Govindasamy, H. Levy, P. Nick, R. McKenna, N. Muzyczka, J. A. Chiorini, T. S. Baker, and M. Agbandje-McKenna.** 2005. Structure of adeno-associated virus type 4. J Virol **79:**5047-58.

98. **Pajusola, K., M. Gruchala, H. Joch, T. F. Luscher, S. Yla-Herttuala, and H. Bueler.** 2002. Cell-type-specific characteristics modulate the transduction efficiency of adeno-associated virus type 2 and restrain infection of endothelial cells. J Virol **76:**11530-40.

99. **Parrish, C. R.** 1991. Mapping specific functions in the capsid structure of canine parvovirus and feline panleukopenia virus using infectious plasmid clones. Virology **183:**195-205.

100. **Paul, I., J. Cui, and E. L. Maynard.** 2006. Zinc binding to the HCCH motif of HIV-1 virion infectivity factor induces a conformational change that mediates protein-protein interactions. Proc Natl Acad Sci U S A **103:**18475-80.

101. **Perabo, L., D. Goldnau, K. White, J. Endell, J. Boucas, S. Humme, L. M. Work, H. Janicki, M. Hallek, A. H. Baker, and H. Buning.** 2006. Heparan sulfate proteoglycan binding properties of adeno-associated virus retargeting mutants and consequences for their in vivo tropism. J Virol **80:**7265-9.

102. **Petrella, J., C. J. Cohen, J. Gaetz, and J. M. Bergelson.** 2002. A zebrafish coxsackievirus and adenovirus receptor homologue interacts with coxsackie B virus and adenovirus. J Virol **76:**10503-6.

103. **Philpott, N. J., C. Giraud-Wali, C. Dupuis, J. Gomos, H. Hamilton, K. I. Berns, and E. Falck-Pedersen.** 2002. Efficient integration of recombinant adeno-associated virus DNA vectors requires a p5-rep sequence in cis. J Virol **76:**5411-21.

104. **Philpott, N. J., J. Gomos, and E. Falck-Pedersen.** 2004. Transgene expression after rep-mediated site-specific integration into chromosome 19. Hum Gene Ther **15:**47-61.

105. **Qing, K., C. Mah, J. Hansen, S. Zhou, V. Dwarki, and A. Srivastava.** 1999. Human fibroblast growth factor receptor 1 is a co-receptor for infection by adeno-associated virus 2. Nat Med **5:**71-7.

106. **Qu, G., J. Bahr-Davidson, J. Prado, A. Tai, F. Cataniag, J. McDonnell, J. Zhou, B. Hauck, J. Luna, J. M. Sommer, P. Smith, S. Zhou, P. Colosi, K. A. High, G. F. Pierce, and J. F. Wright.** 2007. Separation of adeno-associated virus type 2 empty

particles from genome containing vectors by anion-exchange column chromatography. J Virol Methods **140:**183-92.

107. **Rabinowitz, J. E., D. E. Bowles, S. M. Faust, J. G. Ledford, S. E. Cunningham, and R. J. Samulski.** 2004. Cross-dressing the virion: the transcapsidation of adeno-associated virus serotypes functionally defines subgroups. J Virol **78:**4421-32.

108. **Rabinowitz, J. E., F. Rolling, C. Li, H. Conrath, W. Xiao, X. Xiao, and R. J. Samulski.** 2002. Cross-packaging of a single adeno-associated virus (AAV) type 2 vector genome into multiple AAV serotypes enables transduction with broad specificity. J Virol **76:**791-801.

109. **Ranz, A. I., J. J. Manclus, E. Diaz-Aroca, and J. I. Casal.** 1989. Porcine parvovirus: DNA sequence and genome organization. J Gen Virol **70 (Pt 10):**2541-53.

110. **Reddy, V. S., P. Natarajan, B. Okerberg, K. Li, K. V. Damodaran, R. T. Morton, C. L. Brooks, 3rd, and J. E. Johnson.** 2001. Virus Particle Explorer (VIPER), a website for virus capsid structures and their computational analyses. J Virol **75:**11943-7.

111. **Remond, M., P. Boireau, and F. Lebreton.** 1992. Partial DNA cloning and sequencing of a canine parvovirus vaccine strain: application of nucleic acid hybridization to the diagnosis of canine parvovirus disease. Arch Virol **127:**257-69.

112. **Rose, J. A., J. V. Maizel, Jr., J. K. Inman, and A. J. Shatkin.** 1971. Structural proteins of adenovirus-associated viruses. J Virol **8:**766-70.

113. **Sacchetto, R., E. Damiani, F. Turcato, A. Nori, and A. Margreth.** 2001. Ca(2+)-dependent interaction of triadin with histidine-rich Ca(2+)-binding protein carboxyl-terminal region. Biochem Biophys Res Commun **289:**1125-34.

114. **Samulski, R. J., K. I. Berns, M. Tan, and N. Muzyczka.** 1982. Cloning of adeno-associated virus into pBR322: rescue of intact virus from the recombinant plasmid in human cells. Proc Natl Acad Sci U S A **79:**2077-81.

115. **Sanlioglu, S., P. K. Benson, J. Yang, E. M. Atkinson, T. Reynolds, and J. F. Engelhardt.** 2000. Endocytosis and nuclear trafficking of adeno-associated virus type 2 are controlled by rac1 and phosphatidylinositol-3 kinase activation. J Virol **74:**9184-96.

116. **Santos, K., and F. J. Medrano.** 2007. Expression, purification, and characterization of an aminopeptidase (Xac2987) with broad specificity from Xanthomonas axonopodis pv. citri. Protein Expr Purif **52:**117-22.

117. **Seiler, M. P., A. D. Miller, J. Zabner, and C. L. Halbert.** 2006. Adeno-associated virus types 5 and 6 use distinct receptors for cell entry. Hum Gene Ther **17:**10-9.

118. **Shen, X., T. Storm, and M. A. Kay.** 2007. Characterization of the Relationship of AAV Capsid Domain Swapping to Liver Transduction Efficiency. Mol Ther **15:**1955-62.

119. **Shi, W., G. S. Arnold, and J. S. Bartlett.** 2001. Insertional mutagenesis of the adeno-associated virus type 2 (AAV2) capsid gene and generation of AAV2 vectors targeted to alternative cell-surface receptors. Hum Gene Ther **12:**1697-711.

120. **Shi, W., and J. S. Bartlett.** 2003. RGD inclusion in VP3 provides adeno-associated virus type 2 (AAV2)-based vectors with a heparan sulfate-independent cell entry mechanism. Mol Ther **7:**515-25.

121. **Shi, X., G. Fang, W. Shi, and J. S. Bartlett.** 2006. Insertional mutagenesis at positions 520 and 584 of adeno-associated virus type 2 (AAV2) capsid gene and generation of AAV2 vectors with eliminated heparin- binding ability and introduced novel tropism. Hum Gene Ther **17:**353-61.

122. **Simpson, A. A., B. Hebert, G. M. Sullivan, C. R. Parrish, Z. Zadori, P. Tijssen, and M. G. Rossmann.** 2002. The structure of porcine parvovirus: comparison with related viruses. J Mol Biol **315:**1189-98.

123. **Smith, R. H., L. Yang, and R. M. Kotin.** 2008. Chromatography-based purification of adeno-associated virus. Methods Mol Biol **434:**37-54.

124. **Sollerbrant, K., J. Elmen, C. Wahlestedt, J. Acker, H. Leblois-Prehaud, M. Latta-Mahieu, P. Yeh, and M. Perricaudet.** 2001. A novel method using baculovirus-mediated gene transfer for production of recombinant adeno-associated virus vectors. J Gen Virol **82:**2051-60.

125. **Sonntag, F., S. Bleker, B. Leuchs, R. Fischer, and J. A. Kleinschmidt.** 2006. Adeno-associated virus type 2 capsids with externalized VP1/VP2 trafficking domains are generated prior to passage through the cytoplasm and are maintained until uncoating occurs in the nucleus. J Virol **80:**11040-54.

126. **Steinbach, S., A. Wistuba, T. Bock, and J. A. Kleinschmidt.** 1997. Assembly of adeno-associated virus type 2 capsids in vitro. J Gen Virol **78 (Pt 6):**1453-62.

127. **Stray, S. J., P. Ceres, and A. Zlotnick.** 2004. Zinc ions trigger conformational change and oligomerization of hepatitis B virus capsid protein. Biochemistry **43:**9989-98.

128. **Summerford, C., and R. J. Samulski.** 1998. Membrane-associated heparan sulfate proteoglycan is a receptor for adeno-associated virus type 2 virions. J Virol **72:**1438-45.

129. **Takeda, M., G. P. Leser, C. J. Russell, and R. A. Lamb.** 2003. Influenza virus hemagglutinin concentrates in lipid raft microdomains for efficient viral fusion. Proc Natl Acad Sci U S A **100:**14610-7.

130. **Terzi, D., and V. Zachariou.** 2008. Adeno-associated virus-mediated gene delivery approaches for the treatment of CNS disorders. Biotechnol J **3:**1555-63.

131. **Thomas, C. E., T. A. Storm, Z. Huang, and M. A. Kay.** 2004. Rapid uncoating of vector genomes is the key to efficient liver transduction with pseudotyped adeno-associated virus vectors. J Virol **78:**3110-22.

132. **Timpe, J., J. Bevington, J. Casper, J. D. Dignam, and J. P. Trempe.** 2005. Mechanisms of adeno-associated virus genome encapsidation. Curr Gene Ther **5:**273-84.

133. **Tratschin, J. D., I. L. Miller, and B. J. Carter.** 1984. Genetic analysis of adeno-associated virus: properties of deletion mutants constructed in vitro and evidence for an adeno-associated virus replication function. J Virol **51:**611-9.

134. **Tsuchida-Straeten, N., S. Ensslen, C. Schafer, M. Woltje, B. Denecke, M. Moser, S. Graber, S. Wakabayashi, T. Koide, and W. Jahnen-Dechent.** 2005. Enhanced blood coagulation and fibrinolysis in mice lacking histidine-rich glycoprotein (HRG). J Thromb Haemost **3:**865-72.

135. **Urabe, M., C. Ding, and R. M. Kotin.** 2002. Insect cells as a factory to produce adeno-associated virus type 2 vectors. Hum Gene Ther **13:**1935-43.

136. **Van der Geld, Y. M., M. L. Smook, M. G. Huitema, M. C. Harmsen, P. C. Limburg, and C. G. Kallenberg.** 2002. Expression of recombinant proteinase 3, the autoantigen in Wegener's granulomatosis, in insect cells. J Immunol Methods **264:**195-205.

137. **Vandenberghe, L. H., L. Wang, S. Somanathan, Y. Zhi, J. Figueredo, R. Calcedo, J. Sanmiguel, R. A. Desai, C. S. Chen, J. Johnston, R. L. Grant, G. Gao, and J. M. Wilson.** 2006. Heparin binding directs activation of T cells against adeno-associated virus serotype 2 capsid. Nat Med **12:**967-71.

138. **Vihinen-Ranta, M., D. Wang, W. S. Weichert, and C. R. Parrish.** 2002. The VP1 N-terminal sequence of canine parvovirus affects nuclear transport of capsids and efficient cell infection. J Virol **76:**1884-91.

139. **Wagner, J. A., A. H. Messner, M. L. Moran, R. Daifuku, K. Kouyama, J. K. Desch, S. Manley, A. M. Norbash, C. K. Conrad, S. Friborg, T. Reynolds, W. B. Guggino, R. B. Moss, B. J. Carter, J. J. Wine, T. R. Flotte, and P. Gardner.** 1999. Safety and biological efficacy of an adeno-associated virus vector-cystic fibrosis transmembrane regulator (AAV-CFTR) in the cystic fibrosis maxillary sinus. Laryngoscope **109:**266-74.

140. **Walters, R. W., M. Agbandje-McKenna, V. D. Bowman, T. O. Moninger, N. H. Olson, M. Seiler, J. A. Chiorini, T. S. Baker, and J. Zabner.** 2004. Structure of adeno-associated virus serotype 5. J Virol **78:**3361-71.

141. **Walters, R. W., J. M. Pilewski, J. A. Chiorini, and J. Zabner.** 2002. Secreted and transmembrane mucins inhibit gene transfer with AAV4 more efficiently than AAV5. J Biol Chem **277:**23709-13.

142. **Walters, R. W., S. M. Yi, S. Keshavjee, K. E. Brown, M. J. Welsh, J. A. Chiorini, and J. Zabner.** 2001. Binding of adeno-associated virus type 5 to 2,3-linked sialic acid is required for gene transfer. J Biol Chem **276:**20610-6.

143. **Wang, X. S., and A. Srivastava.** 1997. A novel terminal resolution-like site in the adeno-associated virus type 2 genome. J Virol **71:**1140-6.

144. **Warrington, K. H., Jr., O. S. Gorbatyuk, J. K. Harrison, S. R. Opie, S. Zolotukhin, and N. Muzyczka.** 2004. Adeno-associated virus type 2 VP2 capsid protein is nonessential and can tolerate large peptide insertions at its N terminus. J Virol **78:**6595-609.

145. **Warrington, K. H., Jr., and R. W. Herzog.** 2006. Treatment of human disease by adeno-associated viral gene transfer. Hum Genet **119:**571-603.

146. **Weger, S., A. Wistuba, D. Grimm, and J. A. Kleinschmidt.** 1997. Control of adeno-associated virus type 2 cap gene expression: relative influence of helper virus, terminal repeats, and Rep proteins. J Virol **71:**8437-47.

147. **Weitzman, M. D., K. J. Fisher, and J. M. Wilson.** 1996. Recruitment of wild-type and recombinant adeno-associated virus into adenovirus replication centers. J Virol **70:**1845-54.

148. **White, A. F., M. Mazur, E. J. Sorscher, K. Zinn, and S. Ponnazhagan.** 2008. Genetic modification of AAV2 capsid enhances gene transfer efficiency in polarized human airway epithelial cells. Hum Gene Ther.

149. **White, S. J., S. A. Nicklin, H. Buning, M. J. Brosnan, K. Leike, E. D. Papadakis, M. Hallek, and A. H. Baker.** 2004. Targeted gene delivery to vascular tissue in vivo by tropism-modified adeno-associated virus vectors. Circulation **109:**513-9.

150. **Wilde, A., C. Dempsey, and G. Banting.** 1994. The tyrosine-containing internalization motif in the cytoplasmic domain of TGN38/41 lies within a nascent helix. J Biol Chem **269:**7131-6.

151. **Wistuba, A., A. Kern, S. Weger, D. Grimm, and J. A. Kleinschmidt.** 1997. Subcellular compartmentalization of adeno-associated virus type 2 assembly. J Virol **71:**1341-52.

152. **Wistuba, A., S. Weger, A. Kern, and J. A. Kleinschmidt.** 1995. Intermediates of adeno-associated virus type 2 assembly: identification of soluble complexes containing Rep and Cap proteins. J Virol **69:**5311-9.

153. **Wobus, C. E., B. Hugle-Dorr, A. Girod, G. Petersen, M. Hallek, and J. A. Kleinschmidt.** 2000. Monoclonal antibodies against the adeno-associated virus type 2 (AAV-2) capsid: epitope mapping and identification of capsid domains involved in AAV-2-cell interaction and neutralization of AAV-2 infection. J Virol **74:**9281-93.

154. **Work, L. M., H. Buning, E. Hunt, S. A. Nicklin, L. Denby, N. Britton, K. Leike, M. Odenthal, U. Drebber, M. Hallek, and A. H. Baker.** 2006. Vascular bed-targeted in vivo gene delivery using tropism-modified adeno-associated viruses. Mol Ther **13:**683-93.

155. **Wu, E., L. Pache, D. J. Von Seggern, T. M. Mullen, Y. Mikyas, P. L. Stewart, and G. R. Nemerow.** 2003. Flexibility of the adenovirus fiber is required for efficient receptor interaction. J Virol **77:**7225-35.

156. **Wu, P., W. Xiao, T. Conlon, J. Hughes, M. Agbandje-McKenna, T. Ferkol, T. Flotte, and N. Muzyczka.** 2000. Mutational analysis of the adeno-associated virus type 2 (AAV2) capsid gene and construction of AAV2 vectors with altered tropism. J Virol **74:**8635-47.

157. **Wu, Z., A. Asokan, J. C. Grieger, L. Govindasamy, M. Agbandje-McKenna, and R. J. Samulski.** 2006. Single amino acid changes can influence titer, heparin binding, and tissue tropism in different adeno-associated virus serotypes. J Virol **80:**11393-7.

158. **Wu, Z., A. Asokan, and R. J. Samulski.** 2006. Adeno-associated virus serotypes: vector toolkit for human gene therapy. Mol Ther **14:**316-27.

159. **Xiao, X., J. Li, and R. J. Samulski.** 1998. Production of high-titer recombinant adeno-associated virus vectors in the absence of helper adenovirus. J Virol **72:**2224-32.

160. **Xie, Q., W. Bu, S. Bhatia, J. Hare, T. Somasundaram, A. Azzi, and M. S. Chapman.** 2002. The atomic structure of adeno-associated virus (AAV-2), a vector for human gene therapy. Proc Natl Acad Sci U S A **99:**10405-10.

161. **Xie, Q., and M. S. Chapman.** 1996. Canine parvovirus capsid structure, analyzed at 2.9 A resolution. J Mol Biol **264:**497-520.

162. **Xie, Q., H. M. Ongley, J. Hare, and M. S. Chapman.** 2008. Crystallization and preliminary X-ray structural studies of adeno-associated virus serotype 6. Acta Crystallogr Sect F Struct Biol Cryst Commun **64:**1074-8.

163. **Xie, Q., T. Somasundaram, S. Bhatia, W. Bu, and M. S. Chapman.** 2003. Structure determination of adeno-associated virus 2: three complete virus particles per asymmetric unit. Acta Crystallogr D Biol Crystallogr **59:**959-70.

164. **Zaiss, A. K., and D. A. Muruve.** 2005. Immune responses to adeno-associated virus vectors. Curr Gene Ther **5:**323-31.

165. **Zhang, H. G., J. Xie, I. Dmitriev, E. Kashentseva, D. T. Curiel, H. C. Hsu, and J. D. Mountz.** 2002. Addition of six-His-tagged peptide to the C terminus of adeno-associated virus VP3 does not affect viral tropism or production. J Virol **76:**12023-31.

166. **Zhang, P., S. Mueller, M. C. Morais, C. M. Bator, V. D. Bowman, S. Hafenstein, E. Wimmer, and M. G. Rossmann.** 2008. Crystal structure of CD155 and electron microscopic studies of its complexes with polioviruses. Proc Natl Acad Sci U S A **105:**18284-9.

167. **Zhi, N., Z. Zadori, K. E. Brown, and P. Tijssen.** 2004. Construction and sequencing of an infectious clone of the human parvovirus B19. Virology **318:**142-52.

168. **Zhong, L., B. Li, G. Jayandharan, C. S. Mah, L. Govindasamy, M. Agbandje-McKenna, R. W. Herzog, K. A. Weigel-Van Aken, J. A. Hobbs, S. Zolotukhin, N. Muzyczka, and A. Srivastava.** 2008. Tyrosine-phosphorylation of AAV2 vectors and its consequences on viral intracellular trafficking and transgene expression. Virology **381:**194-202.

169. **Zincarelli, C., S. Soltys, G. Rengo, and J. E. Rabinowitz.** 2008. Analysis of AAV serotypes 1-9 mediated gene expression and tropism in mice after systemic injection. Mol Ther **16:**1073-80.